Space-time hybridizable discontinuous Galerkin methods for free-surface wave problems

by

Giselle Gabriela Sosa Jones

A thesis
presented to the University of Waterloo
in fulfillment of the
thesis requirement for the degree of
Doctor of Philosophy
in
Applied Mathematics

Waterloo, Ontario, Canada, 2020

Examining Committee Membership

The following served on the Examining Committee for this thesis. The decision of the Examining Committee is by majority vote.

External Examiner:	Yan Xu Professor, School of Mathematical Sciences, University of Science and Technology of China
Supervisor:	Sander Rhebergen Professor, Department of Applied Mathematics, University of Waterloo
Internal Members:	Francis Poulin Professor, Department of Applied Mathematics, University of Waterloo
	Lilia Krivodonova Professor, Department of Applied Mathematics, University of Waterloo
Internal-External Member:	Jean-Pierre Hickey Professor, Department of Mechanical and Mechatronics Engineering, University of Waterloo

Author's Declaration

This thesis consists of material all of which I authored or co-authored: see Statement of Contributions included in the thesis. This is a true copy of the thesis, including any required final revisions, as accepted by my examiners.

I understand that my thesis may be made electronically available to the public.

Statement of contributions

Giselle Gabriela Sosa Jones was the sole author for Chapters 1, 2 and 4, which were written under the supervision of Dr. Sander Rhebergen. Chapters 1 and 2 were not written for publication, while the research presented in Chapter 4 will soon be submitted for publication.

Chapter 3:

This research was conducted primarily by Giselle Gabriela Sosa Jones under the supervision of Dr. Sander Rhebergen and with the collaboration of Dr. Jeonghun Lee. Dr. Lee contributed in sections 3.3, 3.4 and 3.5, providing ideas and proofreading what Giselle worked on. Giselle Gabriela Sosa Jones drafted the manuscript and each author provided intellectual input on the draft. The research in this chapter has been submitted for publication and the preprint can be found at https://arxiv.org/abs/1910.07315.

Abstract

Free-surface problems arise in many real-world applications such as in the design of ships and offshore structures, modeling of tsunamis, and dam breaking. Mathematically, free-surface wave problems are described by a set of partial differential equations that govern the movement of the fluid together with certain boundary conditions that describe the free-surface. The numerical solution of such problems is challenging because the boundary of the computational domain depends on the solution of the problem. This implies that there is a strong coupling between the fluid and the free-surface, and the domain must be continuously updated to track the changes in the free-surface.

In this thesis we explore and develop space-time hybridizable discontinuous Galerkin (HDG) methods for free-surface problems. First, we focus on a linear free-surface problem in which the amplitude of the waves is assumed to be small enough so that the domain can remain fixed. We initially consider a traditional approach for the numerical discretization of time-dependent partial differential equations: we discretize in space using, in this case, an HDG method to obtain an ordinary differential equation. Then, we use a second order backward differentiation formula to discretize in time. We see that in comparison to an interior penalty discontinuous Galerkin discretization, this HDG discretization results in smaller linear systems (in general), and produces better approximations to the velocity of the fluid.

Next, we consider the solution of the same linear free-surface problem with a space-time hybridizable discontinuous Galerkin method. Unlike previous finite element discretizations of this problem, we consider a mixed formulation in which the velocity of the flow can be approximated with an optimal order of convergence. We develop a set of space-time analysis tools that allow us to obtain *a priori* error estimates in which the dependency on the spatial mesh size and the time step is explicit. This is in contrast to previous space-time error analyses in which the error bounds depend on the size of the space-time elements.

Finally, we move on to incompressible nonlinear free-surface flow. We consider the two-fluid (gas and liquid) Navier–Stokes equations and use a level set method in which the flow and the level set equations are solved subsequently until a certain stopping criterion has been met. The flow equations are solved with a space-time HDG method which is exactly mass conserving. Furthermore, a space-time embedded discontinuous Galerkin method is employed for the solution of the level set equation. This discretization possesses the same conservation and stability properties as discontinuous Galerkin methods, but produces a continuous approximation to the free-surface elevation. When a discontinuous approximation to the free-surface elevation is obtained, smoothing techniques have to be applied in

order to move the mesh and track the interface. It has been shown in the past that such techniques can lead to instabilities and stabilization terms have to be added to the discretization. Therefore, obtaining a continuous approximation to the free-surface elevation in our discretization is crucial: not only can the mesh be deformed in a straightforward manner, but it can also be done without introducing any potential sources of instabilities. We present two numerical results that demonstrate the capabilities of the method. In the first test case we compare against an analytical solution and we demonstrate how the mesh conforms to the interface between the two fluids. Finally, we present a simulation of waves generated by a submerged obstacle.

Acknowledgements

First and foremost, I would like to thank God Almighty for giving me the strength and courage I have needed to achieve all my goals, and for being with me every step of the way. He is my rock, my fortress and my savior.

I want to thank my advisor, Dr. Sander Rhebergen, for his guidance and patience during these four years. I will always be grateful for the invaluable opportunity of pursuing this Ph.D. degree. Thank you for being supportive, approachable and friendly, for genuinely caring about my well being, and for guiding me towards this big success in my life.

To Dr. Jeonghun (John) Lee for sharing all his knowledge in analysis of finite element methods with me, and for proofreading and providing feedback for my work.

Thank you to my committee members: Dr. Krivodonova, Dr. Poulin, Dr. Hickey and Dr. He for their valuable feedback to my work.

To Tamás Horváth for always being ready to help with MFEM, Linux and everything I needed. Also, for being a fantastic lunch, coffee and life partner, and for having the best bad jokes. Thank you for your infinite love and support, and for filling my life with laughter and happiness.

To my friend and teammate Keegan Kirk. I will never be able to express how lucky and grateful I feel to have you in my life. Thank you for all your help with analysis and English, for listening to my rants, for your friendship and for being with me during my hardest times.

During my doctoral studies I had the pleasure of being part of a team of wonderful people. Thank you Greg Wang for being my family in Canada, for your support, for caring so much about me and for always being ready to help and provide feedback for my work. To my office mate Abdullah Ali Sivas, thank you for so many weird and funny conversations (evil twins forever!) while we waited for our codes to run, for helping me with Linux and PETSc and for always being so generous.

I had the honor of being the instructor of Linear Algebra for Engineering during Fall 2019, and I want to thank Dr. Ryan Trelford for his guidance and support during this time, and for taking the time to provide me with feedback for my teaching.

I would like to thank all the administrative and academic members of the Applied Mathematics Department for their assistance and help throughout my degree.

When I got accepted to the University of Waterloo, many wonderful people who did not know me supported me financially so that I could come study in Canada. They believed

in me and in what I wanted to accomplish, and I would not be here without their kindness and generosity. My appreciation also goes to Carlos Contreras and Hugo Montesinos for their help with my move to Canada.

Finally, to my dad Germán Sosa, my uncle David Jones and my grandma Rosalina Mora, and the rest of my family and friends, thank you for your infinite support, love and understanding, and for always believing in me.

Dedication

To my mom, Glenys Jones, without whom I would not be the person I am today. I live every day hoping that I can make her proud and that I can honor her life and all the sacrifices she made for me. Her memory gives me the strength and resilience I need to keep on going. If you are looking down on me, I hope you can see how much I love you and miss you. This and all of my successes are for you, mom.

Table of Contents

List of Figures

List of Tables

List of Abbreviations

ALE Arbitrary Lagrangian–Eulerian 2, 3

BDF Backward differentiation formula 3, 14, 15, 19, 92

DG Discontinuous Galerkin xv, 1–3, 14, 15, 22, 25–28, 30, 92

DOFs Degrees-of-freedom xiii, 2

EDG Embedded discontinuous Galerkin 2, 4, 14, 72, 75, 80–82, 84, 92

GCL Geometric Conservation Law 3

HDG Hybridizable discontinuous Galerkin xiii, 2–4, 14, 30, 31, 34, 35, 44, 56, 57, 66, 72, 75, 77, 79–82, 84, 85, 92

Chapter 1

Introduction

Free-surface waves are of great interest in various fields of applied mathematics and engineering. In addition to having many relevant real-life applications, such as in the modeling of ships and offshore structures, free-surface wave problems are challenging and compelling from the mathematical point of view as well.

Numerical modeling of free-surface waves involves the solution of a system of partial differential equations that govern the movement of the fluid, coupled with a set of free-surface boundary conditions that describe the free-surface. In these problems, the shape of the domain where the partial differential equations are solved depends on the position of the free-surface which leads to a strong coupling between the flow equations and the free-surface. In order to effectively track the free-surface, we require an accurate discretization technique that can handle moving domains. Moreover, it is desirable that the numerical method is stable under mesh movement.

This thesis is concerned with the accurate numerical solution of free-surface problems with space-time finite element methods, in particular, with space-time hybridizable discontinuous Galerkin methods, which are reviewed next.

Hybridizable discontinuous Galerkin methods. DG methods are a class of finite element methods where the approximate solution is allowed to be discontinuous between elements. These methods offer great conservation and stability properties, in particular for convection-dominated flows where classic finite element methods usually fail. DG methods have been criticized, however, because of the increase in the number of degrees-of-freedom caused by the discontinuous nature of the approximate solution. This implies that the linear system associated to DG methods is larger than for continuous finite element methods on the same mesh, and therefore, are computationally more expensive.

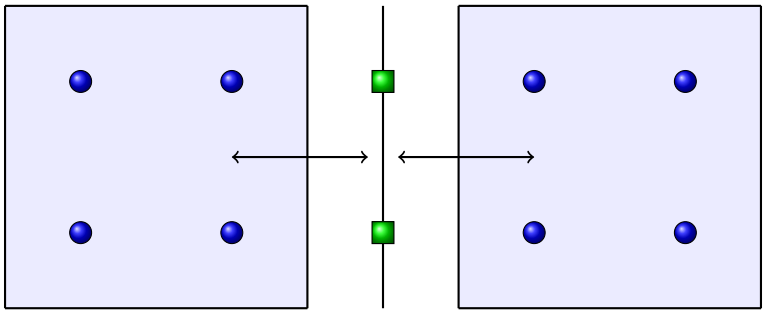

Figure 1.1: HDG DOFs for polynomials of total degree 1 on quadrilateral elements. The blue circles denote the element DOFs, while the green squares denote the facet DOFs.

HDG methods are a class of DG methods that allow for static condensation. HDG methods were introduced in [18] with the purpose of alleviating the computational load of DG methods while maintaining all its desirable properties. Somewhat paradoxically, this is achieved by introducing a variable that is defined on the facets of the mesh. The numerical fluxes are chosen in such a way that the only communication between the element unknowns is through the facet variable. Figure 1.1 depicts the HDG DOFs for polynomials of total degree 1 on quadrilateral elements. The arrows indicate that there is no communication between elements, only between elements and facets.

Thanks to the choice of numerical fluxes in HDG methods, static condensation can be performed: the element unknowns are locally eliminated which results in a linear system for the facet variables only [18]. This system is significantly smaller than the one corresponding to DG methods, and, in some cases, comparable in size to the one obtained by a continuous finite element method [44, 90]. Once the facet solution has been determined, the element solution can be computed locally using the facet solution. The number of globally coupled degrees-of-freedom can be further reduced by imposing that the facet variables are continuous between facets, resulting in the Embedded discontinuous Galerkin (EDG) method [20, 36].

Space-time hybridizable discontinuous Galerkin methods. For the discretization of time-dependent problems, the traditional approach is to first discretize in space using, for example, a (H)DG method, and then discretize the resulting ordinary differential equations using an appropriate time stepping method. For problems where the domain is time-dependent, however, such an approach is not possible since the approximate solution at a given time level might not be well defined on the next time level because of the changes in the domain. Arbitrary Lagrangian–Eulerian (ALE) methods can handle moving domains

by mapping the physical domain to a reference domain. The equations are solved on the reference domain using an approach like the one described above, and then mapped back onto the physical domain. ALE methods however do not automatically satisfy the Geometric Conservation Law (GCL) which states that a uniform flow on a dynamic mesh remains uniform. The GCL has proven to be essential for the accuracy of the solution [34, 51].

An alternative to ALE methods is to use a DG (or HDG) method both in space and time. These space-time methods, in addition to achieving high order accuracy in both space and time, can easily handle time-dependent domains. Moreover, space-time methods automatically satisfy the GCL. In [37], a space-time HDG method that is locally conservative and energy stable, and that produces point-wise divergence-free and $H(\mathrm{div})$-conforming velocity fields was presented. For incompressible flows, we can also refer to [64, 77, 78, 81, 37].

Space-time DG and HDG methods have also been applied to compressible flows [47, 83], two-fluid flows [71, 10] and nonlinear free-surface problems [84, 31, 56]. When a space-time (H)DG method is applied to free-surface flow, a discontinuous approximation to the free-surface elevation is obtained. This implies that the boundary of the domain is not well defined and a smoothing technique has to be applied. In [2] it was shown that this smoothing process may lead to instabilities unless extra stabilization terms are added to the discretization.

Level set methods. Since a free-surface problem can be viewed as a two-fluid flow problem, level set methods can be used for their discretization. Level set methods were first introduced in [62] and have since then been used for multiphase flows [14, 76], and for free-surface flows [33, 53, 54]. In the level set method, the fluid equations are solved in a domain that contains both water and air phases. A level set function, which satisfies an advection equation where the advection field is the velocity of the fluid, is defined such that it is positive in one of the fluids and negative in the other. The zero level set then corresponds to the interface between the two fluids. By solving the time-dependent advection equation for the level set function we are able to track the movement of the interface.

Objectives. The first objective of this research is to provide a theoretical and practical foundation of space-time hybridizable discontinuous Galerkin methods for free-surface problems. To achieve this, we consider a linear water wave model, which is first discretized with an HDG method combined with a second order Backward differentiation formula (BDF). Then, we consider a space-time HDG discretization for a mixed formulation of the linear free-surface problem. This formulation allows us to obtain optimal rates of conver-

gence for the velocity of the fluid. In contrast to other space-time error analyses, we obtain anisotropic *a priori* error bounds. To achieve this, we first develop a set of analysis tools that allow us to separate the dependency on the spatial mesh size and the time step.

The second objective of this thesis is to develop a space-time hybridizable/embedded discontinuous Galerkin method for incompressible free-surface flows. We propose an interface-tracking method where the domain can be updated in a straightforward manner without appealing to smoothing techniques that could potentially lead to instabilities. We consider a level set approach in which the two-fluid Navier–Stokes equations are solved with an exactly mass conserving space-time HDG method. The time-dependent advection equation for the level set function is discretized using a space-time EDG method so that the free-surface elevation is continuous. The mesh can then be updated without any smoothing.

In order to describe the problem, we first review some basic concepts in fluid mechanics.

1.1 Governing equations and basic concepts in fluid mechanics

In this section, we will show the equation of mass conservation and various equations of motion depending on the assumptions made on the flow. For a complete derivation of these equations, see, e.g., [49].

In the following, we denote the velocity of the fluid by $\boldsymbol{u} \equiv (u, v, w)$, where u, v, w are the velocity components in the x, y and z direction, respectively. We denote the fluid density by ρ and the fluid pressure by p. We will assume that $\boldsymbol{u}$, ρ and p are continuous functions, which is usually known as the continuum hypothesis [49].

Given a scalar function f, the material derivative of f denotes the rate of change of f with respect to time in a reference frame that is moving with velocity $\boldsymbol{u}$. This operator is defined as

$$\frac{D}{Dt} \coloneqq \frac{\partial}{\partial t} + \boldsymbol{u} \cdot \nabla. \tag{1.1}$$

1.1.1 Equation of mass conservation

Assume a fluid occupies a volume V bounded by a surface S. The principle of mass conservation states that mass is neither created nor destroyed in the fluid, i.e., mass remains

constant over time. This means that the rate of change of mass in V is equal to the rate of mass flowing into V across S. Mathematically, we express this principle in the form

$$\partial_t \rho + \nabla \cdot \big(\rho \boldsymbol{u}\big) = 0. \tag{1.2}$$

Expanding equation eq. (1.2) and using the definition of material derivative, equation eq. (1.2) can be written as

$$\frac{D\rho}{Dt} + \rho \nabla \cdot \boldsymbol{u} = 0.$$

For the study of water waves, we will assume that the fluid is incompressible, meaning,

$$\nabla \cdot \boldsymbol{u} = 0. \tag{1.3}$$

1.1.2 Incompressible Navier–Stokes equations

The incompressible Navier–Stokes equations describe the movement of a viscous fluid which is assumed to be incompressible. Assuming that the density ρ is constant, and using the material derivative, the incompressible Navier–Stokes equations are given by

$$\rho \frac{D\boldsymbol{u}}{Dt} - \nabla \cdot \boldsymbol{\sigma}(\boldsymbol{u}, p) = \boldsymbol{F}, \tag{1.4}$$

where $\boldsymbol{F} = (F_1, F_2, F_3)$ is the vector of external forces and $\boldsymbol{\sigma}(\boldsymbol{u}, p)$ is the viscous stress tensor defined as

$$\boldsymbol{\sigma}(\boldsymbol{u}, p) = -p\mathbb{I} + \mu \nabla \boldsymbol{u}. \tag{1.5}$$

Here, $\mathbb{I}$ is the identity matrix and μ is the dynamic viscosity, which is assumed to be constant. The material derivative and the gradient operators are applied to each component of $\boldsymbol{u}$.

The Navier–Stokes equations are usually written together with the mass conservation equation (1.3). Using the definition of the material derivative operator and the viscous stress tensor, and including the mass conservation equation, we obtain the classic form of the incompressible Navier–Stokes equations:

$$\rho \Big(\partial_t \boldsymbol{u} + \big(\boldsymbol{u} \cdot \nabla\big)\, \boldsymbol{u}\Big) + \nabla p - \mu \Delta \boldsymbol{u} = \boldsymbol{F}, \tag{1.6a}$$

$$\nabla \cdot \boldsymbol{u} = 0. \tag{1.6b}$$

Since eq. (1.6a) establishes that momentum is conserved, this equation is usually referred to as the momentum equation, while eq. (1.6b) is referred to as the continuity equation.

In this thesis we will consider two types of boundary conditions: Dirichlet and Neumann. On Dirichlet boundaries, we impose the value of the velocity, while on Neumann boundaries we impose the value of $\boldsymbol{\sigma}(\boldsymbol{u}, p)\boldsymbol{n}$.

1.1.3 Irrotational flow and the pressure equation

The *vorticity* of the fluid, $\boldsymbol{\omega}$, is defined as the curl of the velocity field, i.e.,

$$\boldsymbol{\omega} = \nabla \times \boldsymbol{u}. \tag{1.7}$$

The vorticity describes the local rotation of a fluid element. If $\boldsymbol{\omega} \equiv 0$, then the fluid is said to be *irrotational*. In the case of an irrotational flow, the velocity field can be expressed as the gradient of a potential function ϕ, i.e.,

$$\boldsymbol{u} = \nabla\phi. \tag{1.8}$$

An incompressible, irrotational flow is governed by Laplace's equation for ϕ:

$$\Delta\phi = 0. \tag{1.9}$$

For this problem, we consider Neumann boundary conditions, i.e., we impose the value of $\nabla\phi \cdot \boldsymbol{n}$ on the boundary.

There is a lot of theory particular to irrotational flows since they are easier to analyze than rotational flows and can be used to model many physical phenomena. For example, once ϕ has been determined by (1.9), it can be shown that, for unsteady flows, the pressure satisfies

$$\partial_t\phi + \frac{1}{2}\nabla\phi \cdot \nabla\phi + \frac{1}{\rho}p + \Psi = B(t), \tag{1.10}$$

where $B(t)$ is an arbitrary function and Ψ is such that $\boldsymbol{F} = -\nabla\Psi$, where $\boldsymbol{F}$ is the vector of external forces.

We are now ready to describe free-surface wave problems.

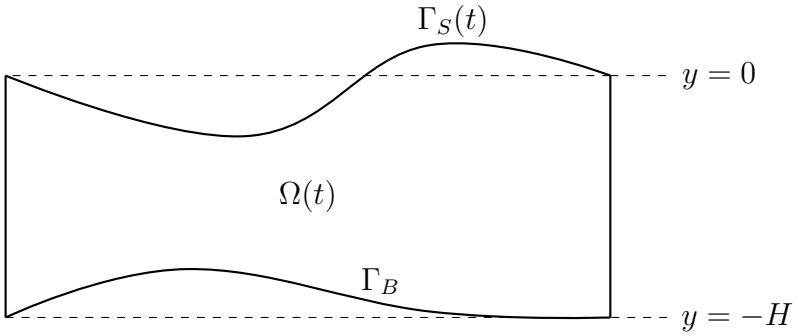

Figure 1.2: Depiction of the flow domain $\Omega(t) \subset \mathbb{R}^2$ for free-surface problems.

1.2 Free-surface wave problems

For simplicity, the following description is in two dimensions. The extension to three dimensions is straightforward. Let $\Omega(t) \subset \mathbb{R}^2$ denote the time-dependent computational domain which is bounded by a free-surface, a bottom boundary and two vertical boundaries. Choose a coordinate system so that the undisturbed free-surface is located at $y = 0$. We denote by $\zeta(x,t)$ the wave height, which in this thesis we define as the height of the fluid. The time-dependent free-surface boundary is defined as $\Gamma_S(t) \coloneqq \big\{(x,y) \in \Omega(t) : y = \zeta(x,t)\big\}$. On the other hand, the bottom boundary is defined as $\Gamma_B \coloneqq \big\{(x,y) \in \Omega(t) : y = b(x)\big\}$, where $b(x) = -H + h(x)$, H is the average water depth and $h(x)$ describes the topography of the bottom. See fig. 1.2 for a depiction of $\Omega(t)$.

Next, we present the kinematic and the dynamic free-surface boundary conditions in their general form as well as their linearizations.

1.2.1 Kinematic boundary condition

This condition establishes that if a particle of the fluid belongs to the free-surface, then it stays on the surface throughout the motion of the fluid. Notice that the free-surface can be defined as $f_S(x,y,t) = \zeta(x,t) - y = 0$ and that Df_S/Dt gives the rate of change of the free-surface with respect to the fluid. Therefore, if we impose that the free-surface moves with the fluid so that it always contains the same fluid particles, then the free-surface must satisfy

$$\frac{Df_S}{Dt} = 0. \tag{1.11}$$

This gives the kinematic boundary condition

$$\partial_t f_S + \boldsymbol{u} \cdot \nabla f_S = 0 \quad \text{on } y = \zeta(x,t). \tag{1.12}$$

Note that this equation implies that

$$v = \frac{D\zeta}{Dt} \quad \text{on } y = \zeta(x,t). \tag{1.13}$$

1.2.2 Dynamic boundary condition

The dynamic boundary condition states that the net force acting on a piece of the free-surface is zero, which is a consequence of that piece of surface having zero mass. If we neglect the effects of viscosity and surface tension, then the only force acting on the surface is the atmospheric pressure, p_a, which we will assume to be constant, and the pressure of the fluid, p. Then the dynamic boundary condition states that

$$p = p_a \quad \text{on } y = \zeta(x,t). \tag{1.14}$$

Alternatively, the dynamic boundary condition in its most general form can be written as

$$\boldsymbol{\sigma}(\boldsymbol{u}, p)\boldsymbol{n} = p_a \boldsymbol{n} \quad \text{on } y = \zeta(x,t). \tag{1.15}$$

If we assume that $p_a = 0$ and use the definition of $\boldsymbol{\sigma}$ eq. (1.5), then

$$\left(-p\mathbb{I} + \mu\nabla\boldsymbol{u}\right)\boldsymbol{n} = \boldsymbol{0} \quad \text{on } y = \zeta(x,t). \tag{1.16}$$

In this thesis we will use (1.16) as a dynamic boundary condition.

In the case of an incompressible, irrotational, unsteady flow, the pressure must satisfy (1.10). Setting $\Psi = gy$ in (1.10) (since in this case the only force acting on the fluid is gravity), we obtain

$$\partial_t \phi + \frac{1}{2}\nabla\phi \cdot \nabla\phi + \frac{1}{\rho}p + gy = B(t). \tag{1.17}$$

By redefining the velocity potential ϕ, we can take $B(t) = \frac{1}{\rho}p_a$. Then, since $p = p_a$ on $y = \zeta(x,t)$, we obtain the following dynamic boundary condition for the case of incompressible, irrotational, unsteady flow

$$\partial_t \phi + \frac{1}{2}\nabla\phi \cdot \nabla\phi + g\zeta = 0 \quad \text{on } y = \zeta(x,t). \tag{1.18}$$

When the effects of viscosity and surface tension are taken into account on the free-surface, an analogous condition can be derived, see, e.g., [43].

1.2.3 Linearized free-surface boundary conditions

The boundary conditions presented above can be linearized by assuming that the amplitude of the wave height and the velocity potential is small. In the case of an incompressible, irrotational and unsteady flow, the linearized kinematic boundary condition can be obtained from eq. (1.13) by dropping the nonlinear terms, to obtain

$$\nabla\phi \cdot \mathbf{n} = \partial_t \zeta \quad \text{on } y = 0. \tag{1.19}$$

and the linearized dynamic boundary condition is given by

$$\partial_t \phi + g\zeta = 0 \quad \text{on } y = 0. \tag{1.20}$$

This linearization is obtained by introducing a small amplitude parameter a through

$$\zeta = a\widetilde{\zeta}(x, t; a), \tag{1.21a}$$
$$\phi = a\widetilde{\phi}(x, y, t; a). \tag{1.21b}$$

These expressions are then substituted in eq. (1.12) and eq. (1.18), and the terms of $\mathcal{O}(a^2)$ and higher are dropped. The linearized free-surface problem is then given by

$$-\Delta\phi = 0 \qquad \text{in } \Omega, \tag{1.22a}$$
$$\nabla\phi \cdot \boldsymbol{n} = \partial_t \zeta \qquad \text{at } y = 0, \tag{1.22b}$$
$$\partial_t \phi + g\zeta = 0 \qquad \text{at } y = 0, \tag{1.22c}$$
$$\nabla\phi \cdot \boldsymbol{n} = 0 \qquad \text{at } y = -H + h(x), \tag{1.22d}$$

where we have dropped the tildes for simplicity. On the vertical boundaries of the domain we will consider periodic boundary conditions. Note that Ω is now considered to be fixed in time since the free-surface is located at $y = 0$.

This linearization significantly reduces the complexity of the free-surface boundary conditions not only because they are linear, but also because they are now applied at a fixed boundary, i.e., at $y = 0$.

This linearized problem has an analytical solution which will be derived next. We assume that $h(x) = 0$ for simplicity.

Since the equations in eq. (1.22) are all linear with constant coefficients, inspired by Fourier series, we guess a solution of the form

$$\zeta(x, t) = a \sin(\omega t - kx), \tag{1.23}$$

where k is the wave number and ω is the frequency of the wave. Noticing that $\boldsymbol{n} = (0, 1)$ on $y = 0$, eq. (1.22b) implies that

$$\partial_y \phi(x, 0, t) = a\omega \cos(\omega t - kx), \tag{1.24}$$

and eq. (1.22c) implies that

$$\partial_t \phi(x, 0, t) = -ag \sin(\omega t - kx). \tag{1.25}$$

Integrating with respect to time gives

$$\phi(x, 0, t) = \frac{a}{\omega} g \cos(\omega t - kx). \tag{1.26}$$

Since we are interested in periodic solutions in x, this integration does not introduce any function of integration that depends on x.

Guessing that the dependence on (x, t) of ϕ is of the form $\cos(\omega t - kx)$, we set

$$\phi(x, y, t) = a\omega f(y) \cos(\omega t - kx), \tag{1.27}$$

where f is a function that satisfies $f'(0) = 1$ (from eq. (1.22b)) and $f'(-H) = 0$ (from eq. (1.22d), noticing that $\boldsymbol{n} = (0, -1)$). From eq. (1.22a), we have that f must satisfy the following second order differential equation

$$f'' - k^2 f = 0, \tag{1.28}$$

so that

$$f(y) = C_1 \sinh(k(y + H)) + C_2 \cosh(k(y + H)). \tag{1.29}$$

Using $f'(-H) = 0$ we obtain $C_1 = 0$, and using $f'(0) = 1$ we obtain $C_2 = 1/k \sinh(kH)$. Thus,

$$\phi(x, y, t) = a \frac{\omega}{k \sinh(kH)} \cosh(k(y + H)) \cos(\omega t - kx). \tag{1.30}$$

Substituting eq. (1.23) and eq. (1.30) in eq. (1.22c), we obtain the dispersion relation

$$\omega = \pm \sqrt{gk \tanh(kH)}. \tag{1.31}$$

This dispersion relation gives the relation between the frequency ω and the wave number k for linear free-surface waves. In summary, the analytical solution for the linear-free surface problem eq. (1.22) in two dimensions with $h(x) = 0$ is

$$\phi(x, y, t) = a \frac{\omega}{k \sinh(kH)} \cosh(k(y + H)) \cos(\omega t - kx), \tag{1.32a}$$

$$\zeta(x, t) = a \sin(\omega t - kx). \tag{1.32b}$$

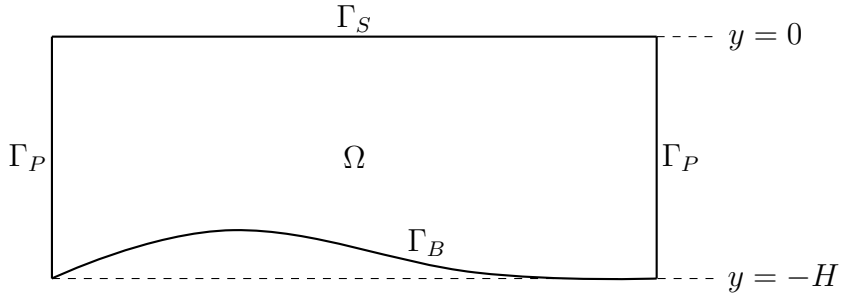

Figure 1.3: Depiction of the flow domain $\Omega \subset \mathbb{R}^2$ for the model eq. (1.33).

1.2.4 Free-surface wave models

In this thesis we will consider two different free-surface wave problems: a linear model and a nonlinear model. For the linear model we will assume that the flow is homogeneous, inviscid and irrotational. This model allows us to perform an extensive error analysis on the discretization and have a better understanding of the problem which will facilitate the design of the discretization of more complicated problems. On the other hand, for the nonlinear problem we will consider the incompressible Navier–Stokes equations with nonlinear free-surface boundary conditions. This is a very complex and general problem that will allow us to simulate more realistic applications. Below is the description of both models.

Model 1

The simplest model that we will consider is the case of irrotational, inviscid fluid with linearized free-surface boundary conditions. In this case, $\Omega \subset \mathbb{R}^2$ is a fixed domain that is bounded by the free-surface, Γ_S, a bottom surface, Γ_B, and a set of periodic boundaries, Γ_P, such that Γ_S, Γ_B and Γ_P do not overlap. Since we consider linearized free-surface boundary conditions, $\Gamma_S = \big\{(x, y) \in \Omega : y = 0\big\}$. See fig. 1.3 for a depiction of Ω in two dimensions.

Thus, the problem is the following

$$-\Delta\phi = 0 \qquad \text{in } \Omega, \tag{1.33a}$$
$$\nabla\phi \cdot \boldsymbol{n} = \partial_t \zeta \qquad \text{on } \Gamma_S, \tag{1.33b}$$
$$\partial_t \phi + \zeta = 0 \qquad \text{on } \Gamma_S, \tag{1.33c}$$
$$\nabla\phi \cdot \mathbf{n} = 0 \qquad \text{on } \Gamma_B, \tag{1.33d}$$

with periodic boundary conditions on Γ_P. Additionally, an initial condition is given for ϕ and ζ.

Model 2

In this model we will consider the two-fluid Navier–Stokes equations. Let $\Omega_l(t), \Omega_g(t) \subset \mathbb{R}^2$ denote the liquid and gas domains, respectively.

The full computational domain Ω is defined as $\Omega = \Omega_l(t) \cup \Omega_g(t)$ and is assumed to be fixed in time, while both $\Omega_l(t)$ and $\Omega_g(t)$ are time-dependent. Let $\Gamma_S(t) = \partial\Omega_l(t) \cap \partial\Omega_g(t)$ denote the interface between the two domains which can be defined as

$$\Gamma_S(t) := \left\{(x, y) \in \Omega : y = \zeta(x, t)\right\}, \tag{1.34}$$

where $\zeta(x, t)$ denotes the wave height. See fig. 1.4 for a depiction of Ω.

We introduce the level set function $\phi(x, y, t) = \zeta(x, t) - y$ and the Heaviside function $H(\phi)$ which is defined by

$$H(\phi) = \begin{cases} 1 & \text{if } \phi > 0, \\ 0 & \text{if } \phi < 0. \end{cases} \tag{1.35}$$

We note that the interface corresponds to the zero level set, $\phi = 0$.

Let k be a subscript to denote a liquid ($k = l$) or a gas ($k = g$) property. Then given the dynamic viscosities $\mu_k \in \mathbb{R}^+$, the constant densities $\rho_k \in \mathbb{R}^+$, and the constant acceleration due to gravity g, the two-fluid Navier–Stokes equations for the velocity $\boldsymbol{u} : \Omega \to \mathbb{R}^2$ and pressure $p : \Omega \to \mathbb{R}$ is given by

$$\rho\left(\partial_t \boldsymbol{u} + \boldsymbol{u} \cdot \nabla\boldsymbol{u}\right) + \nabla p - \mu\Delta\boldsymbol{u} = \rho\boldsymbol{g} \qquad \text{in } \Omega, \tag{1.36a}$$
$$\nabla \cdot \boldsymbol{u} = 0 \qquad \text{in } \Omega, \tag{1.36b}$$
$$\partial_t \phi + \boldsymbol{u} \cdot \nabla\phi = 0 \qquad \text{in } \Omega, \tag{1.36c}$$

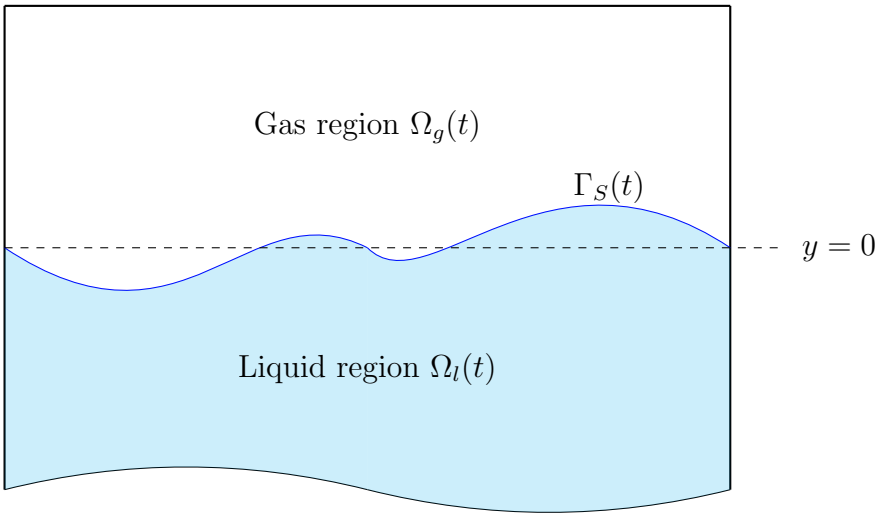

Figure 1.4: A description of the two-fluid flow domain $\Omega \subset \mathbb{R}^2$.

where $\boldsymbol{g} = [0, -g]^T$ and

$$\boldsymbol{u} = \boldsymbol{u}_g + (\boldsymbol{u}_l - \boldsymbol{u}_g)H(\phi), \qquad p = p_g + (p_l - p_g)H(\phi), \tag{1.37a}$$

$$\rho = \rho_g + (\rho_l - \rho_g)H(\phi), \qquad \mu = \mu_g + (\mu_l - \mu_g)H(\phi). \tag{1.37b}$$

We refer to eq. (1.36c) as the *level set equation*, which establishes that the flow moves together with the interface.

We assume that the boundary of Ω is partitioned into a Dirichlet part Γ_D and a Neumann part Γ_N such that there is no overlap between the two sets. Furthermore, we define the inflow boundary Γ^- as the portion of Γ_N where $\boldsymbol{u}\cdot\boldsymbol{n} < 0$, and the outflow boundary Γ^+ as the portion of Γ_N where $\boldsymbol{u}\cdot\boldsymbol{n} > 0$. We then prescribe the following boundary conditions

$$\boldsymbol{u} = 0 \qquad \text{on } \Gamma_D, \tag{1.38a}$$

$$\left[\boldsymbol{u}\cdot\boldsymbol{n} - \max\left(\boldsymbol{u}\cdot\boldsymbol{n}, 0\right)\right]\boldsymbol{u} + \left(p\mathbb{I} - \mu\nabla\boldsymbol{u}\right)\boldsymbol{n} = \boldsymbol{f} \qquad \text{on } \Gamma_N, \tag{1.38b}$$

$$-(\boldsymbol{u}\cdot\boldsymbol{n})\phi = r \qquad \text{on } \Gamma^-, \tag{1.38c}$$

where the boundary data $\boldsymbol{f} : \Gamma_N \to \mathbb{R}^2$ and $r : \Gamma^- \to \mathbb{R}$ are given. We furthermore prescribe an initial condition $\boldsymbol{u}_0 : \Omega \to \mathbb{R}^2$ for the velocity, and for the level set function $\phi_0(\boldsymbol{x}) := \zeta_0(x) - y$ with $\zeta_0(x)$ the given initial wave height. Note that eq. (1.38a) is a

standard no-slip boundary condition on a fixed wall, whereas eq. (1.38b) imposes the total momentum flux on the inflow portion ($\boldsymbol{u} \cdot \boldsymbol{n} < 0$) of Γ_N, and only the diffusive flux on the outflow portion ($\boldsymbol{u} \cdot \boldsymbol{n} > 0$) of Γ_N. Additionally, eq. (1.38c) is a standard inflow boundary condition.

We remark that the two-fluid problem assumes a no-slip and a dynamic boundary condition on the interface, i.e.,

$$\boldsymbol{u}_l = \boldsymbol{u}_g \qquad \text{on } \Gamma_S(t), \tag{1.39a}$$

$$(p_l \mathbb{I} - \mu_l \nabla \boldsymbol{u}_l)\, \boldsymbol{n}_S = (p_g \mathbb{I} - \mu_g \nabla \boldsymbol{u}_g)\, \boldsymbol{n}_S \qquad \text{on } \Gamma_S(t), \tag{1.39b}$$

respectively, where $\boldsymbol{n}_S$ is the normal vector on the interface $\Gamma_S(t)$ pointing outwards from $\Omega_l(t)$.

1.3 Outline

This thesis is structured as follows. In Chapter 2 we present an HDG discretization of eq. (1.33) with a second order BDF time stepper. We demonstrate how a mixed formulation results in an optimal approximation for the velocity of the fluid, in comparison to DG discretizations. In Chapter 3 we present a novel space-time HDG method for problem eq. (1.33). We show that the discrete formulation has a unique solution and perform an *a priori* error analysis in which the dependency in the spatial mesh size and the time step is explicit. This is in contrast to other *a priori* error estimates for space-time methods that depend on the size of the whole space-time element. An interface-tracking space-time hybridized/embedded DG method is introduced in Chapter 4 for the two-fluid Navier–Stokes problem eq. (1.36). We show how using this mixed HDG/EDG discretization results in a scheme that is exactly mass conserving and produces continuous approximations to the wave height. Finally, we draw conclusions in Chapter 5.

Chapter 2

A hybridizable discontinuous Galerkin method for the linear free-surface problem

In this chapter we extend the HDG method of [16] for elliptic problems to the linear free-surface problem eq. (1.33). For the time discretization, we use a second order BDF time stepper. We will consider a mixed formulation to obtain optimal rates for the approximation of the velocity of the fluid. We compare this discretization to the interior penalty DG method in [82].

2.1 Mixed formulation

We introduce a variable $\boldsymbol{q} = -\nabla\phi$, which is the negative velocity of the fluid, and combine eq. (1.33b) and eq. (1.33c) into one equation, to obtain the first order system

$$\boldsymbol{q} + \nabla\phi = 0 \qquad \text{in } \Omega, \tag{2.1a}$$
$$\nabla \cdot \boldsymbol{q} = 0 \qquad \text{in } \Omega, \tag{2.1b}$$
$$\boldsymbol{q} \cdot \boldsymbol{n} = \partial_t^2 \phi \qquad \text{on } \Gamma_S, \tag{2.1c}$$
$$\boldsymbol{q} \cdot \boldsymbol{n} = 0 \qquad \text{on } \Gamma_B. \tag{2.1d}$$

It has been shown that, for the advection-diffusion equation, the HDG method converges with order $p+1$ in the L^2-norm when polynomials of degree p are used to represent both the

scalar variable and its gradient. Notice that for this problem, this is particularly relevant since $\nabla\phi$ represents the velocity of the fluid, which will be approximated optimally, in contrast to, for example [82], where the velocity approximation converges suboptimally. Additionally, the HDG method allows for a local postprocessing of the scalar variable which results in *superconvergence* of the scalar variable, i.e., convergence of order $p+2$ in the L^2-norm [16].

2.2 The hybridizable discontinuous Galerkin method

Before deriving the discrete formulation, we introduce some useful notation.

2.2.1 Tessellation, function spaces and trace operators

Let $\mathcal{T}_h$ denote a tessellation of a polygonal domain $\Omega \subset \mathbb{R}^d$, with $d = 2, 3$, with quadrilateral elements K with maximum diameter h. Let $\mathcal{E}_h^0$ denote the set of interior faces of $\mathcal{T}_h$, $\mathcal{E}_h^\partial$ the set of boundary faces, and $\mathcal{E}_h = \mathcal{E}_h^0 \cup \mathcal{E}_h^\partial$. Moreover, we denote by $\mathcal{E}_h^S$ the set of faces that lie on the free-surface boundary and by $\mathcal{E}_h^B$ the set of faces that lie on the Neumann boundary.

Let $Q^p(D)$ denote the space of polynomials of degree at most p in each variable on a domain D. We define the following finite element spaces

$$W_h^p \coloneqq \left\{ w \in L^2(\Omega) \,:\, w|_K \in Q^p(K),\, \forall K \in \mathcal{T}_h \right\}, \tag{2.2a}$$

$$\boldsymbol{V}_h^p \coloneqq \left\{ \boldsymbol{v} \in \left[L^2(\Omega)\right]^d \,:\, \boldsymbol{v}|_K \in \left[Q^p(K)\right]^2,\, \forall K \in \mathcal{T}_h \right\}. \tag{2.2b}$$

We also introduce the trace finite element space

$$M_h^p \coloneqq \left\{ \mu \in L^2(\mathcal{E}_h) \,:\, \mu|_e \in Q^p(e),\, \forall e \in \mathcal{E}_h \right\}. \tag{2.3}$$

Let $e \in \mathcal{E}_h^0$ be an interior face shared by elements K_1 and K_2 in $\mathcal{T}_h$, and define the unit normal vectors $\boldsymbol{n}_1$ and $\boldsymbol{n}_2$ on e pointing exterior to K_1 and K_2, respectively. We denote by u_1 and u_2 the traces of $u \in W_h^p$, and $\boldsymbol{q}_1$ and $\boldsymbol{q}_2$ the traces $\boldsymbol{q} \in \boldsymbol{V}_h^p$. We define the jump operator $[\![\cdot]\!]$ as follows

$$[\![\boldsymbol{q} \cdot \boldsymbol{n}]\!] = \boldsymbol{q}_1 \cdot \boldsymbol{n}_1 + \boldsymbol{q}_2 \cdot \boldsymbol{n}_2, \qquad [\![u\boldsymbol{n}]\!] = u_1\boldsymbol{n}_1 + u_2\boldsymbol{n}_2. \tag{2.4}$$

For $e \in \mathcal{E}_h^\partial$ the set of boundary faces, the definition is as follows

$$[\![\boldsymbol{q}\cdot\boldsymbol{n}]\!] = \boldsymbol{q}\cdot\boldsymbol{n}, \qquad [\![u\boldsymbol{n}]\!] = u\boldsymbol{n}, \tag{2.5}$$

where $\boldsymbol{n}$ is the exterior unit normal to e. For single-valued functions, the jump is zero.

For functions $\boldsymbol{f}$ and $\boldsymbol{g}$ in $\left[L^2(D)\right]^d$, we denote $(\boldsymbol{f},\boldsymbol{g})_D = \int_D \boldsymbol{f}\cdot\boldsymbol{g}\,\mathrm{d}D$, where $D \subset \mathbb{R}^d$. If f and g are functions in $L^2(D)$, we denote $(f,g)_D = \int_D fg\,\mathrm{d}D$ if $D \subset \mathbb{R}^d$, and $\langle f,g\rangle_D = \int_D fg\,\mathrm{d}s$ if $D \subset \mathbb{R}^{d-1}$. We will use the following notation

$$(w,v)_{\mathcal{T}_h} = \sum_{K\in\mathcal{T}_h}(w,v)_K\,, \qquad \langle w,v\rangle_{\partial\mathcal{T}_h} = \sum_{K\in\mathcal{T}_h}\langle w,v\rangle_{\partial K}, \qquad \langle w,v\rangle_{\mathcal{E}_h} = \sum_{e\in\mathcal{E}_h}\langle w,v\rangle_e. \tag{2.6}$$

2.2.2 The finite element variational formulation

To obtain the discrete variational form, multiply eq. (2.1a) and eq. (2.1b) by test functions $\boldsymbol{v}_h \in \boldsymbol{V}_h^p$ and $w_h \in W_h^p$, respectively, integrate over an element $K \in \mathcal{T}_h$, replace $\boldsymbol{q}$ by $\boldsymbol{q}_h \in \boldsymbol{V}_h^p$ and ϕ by $\phi_h \in W_h^p$, and sum over all elements to find

$$\sum_{K\in\mathcal{T}_h}\int_K \boldsymbol{q}_h\cdot\boldsymbol{v}_h\,\mathrm{d}x\,\mathrm{d}y + \sum_{K\in\mathcal{T}_h}\int_K \nabla\phi_h\cdot\boldsymbol{v}_h\,\mathrm{d}x\,\mathrm{d}y = 0, \tag{2.7a}$$

$$\sum_{K\in\mathcal{T}_h}\int_K w_h\nabla\cdot\boldsymbol{q}_h\,\mathrm{d}x\,\mathrm{d}y = 0. \tag{2.7b}$$

Applying integration by parts,

$$\sum_{K\in\mathcal{T}_h}\int_K \boldsymbol{q}_h\cdot\boldsymbol{v}_h\,\mathrm{d}x\,\mathrm{d}y - \sum_{K\in\mathcal{T}_h}\int_K \phi_h\nabla\cdot\boldsymbol{v}_h\,\mathrm{d}x\,\mathrm{d}y + \sum_{K\in\mathcal{T}_h}\int_{\partial K}\widehat{\phi}_h\,\boldsymbol{v}_h\cdot\boldsymbol{n}\,\mathrm{d}s = 0, \tag{2.8a}$$

$$-\sum_{K\in\mathcal{T}_h}\int_K \nabla w_h\cdot\boldsymbol{q}_h\,\mathrm{d}x\,\mathrm{d}y + \sum_{K\in\mathcal{T}_h}\int_{\partial K} w_h\widehat{\boldsymbol{q}}_h\cdot\boldsymbol{n}\,\mathrm{d}s = 0. \tag{2.8b}$$

Since ϕ_h and $\boldsymbol{q}_h$ are allowed to be discontinuous across faces, we have introduced the numerical fluxes $\widehat{\phi}_h$ and $\widehat{\boldsymbol{q}}_h$ which are approximations to ϕ and $-\nabla\phi$, respectively, over ∂K. We consider the following form of the numerical flux

$$\widehat{\boldsymbol{q}}_h = \boldsymbol{q}_h + \tau\left(\phi_h - \widehat{\phi}_h\right)\boldsymbol{n}, \tag{2.9}$$

where $\tau > 0$ is a local stabilization parameter that penalizes the jump between ϕ_h and its numerical trace $\widehat{\phi}_h$. To obtain optimal rates of convergence, we take τ to be of order one, see [60].

In classic discontinuous Galerkin methods, the numerical flux $\widehat{\phi}_h$ on the boundary ∂K of an element K, would be a function of ϕ_h on the element K and on the neighboring element K^-. This means that the degrees-of-freedom associated with ϕ_h and $\boldsymbol{q}_h$ are coupled from one element to its neighbors. In HDG, we instead introduce a trace variable $\lambda_h \in M_h^p$, and express $\widehat{\phi}_h$ as

$$\widehat{\phi}_h = \lambda_h \quad \text{on } \mathcal{E}_h. \tag{2.10}$$

Substituting eq. (2.9) and eq. (2.10) into eq. (2.8a) and eq. (2.8b), we obtain

$$\left(\boldsymbol{q}_h, \boldsymbol{v}_h\right)_{\mathcal{T}_h} - \left(\phi_h, \nabla \cdot \boldsymbol{v}_h\right)_{\mathcal{T}_h} + \langle \lambda, \boldsymbol{v}_h \cdot \boldsymbol{n} \rangle_{\partial \mathcal{T}_h} = 0, \quad \forall \boldsymbol{v}_h \in \boldsymbol{V}_h^p, \tag{2.11a}$$

$$-\left(\nabla w_h, \boldsymbol{q}_h\right)_{\mathcal{T}_h} + \langle w_h, \boldsymbol{q}_h \cdot \boldsymbol{n} \rangle_{\partial \mathcal{T}_h} + \tau \langle w_h, \phi_h \rangle_{\partial \mathcal{T}_h} - \tau \langle w_h, \lambda_h \rangle_{\partial \mathcal{T}_h} = 0, \quad \forall w_h \in W_h^p. \tag{2.11b}$$

In addition to these two equations, we impose the following condition to ensure continuity of the numerical flux $\widehat{\boldsymbol{q}}_h$ in the normal direction across faces:

$$\langle [\![\widehat{\boldsymbol{q}}_h \cdot \boldsymbol{n}]\!], \mu_h \rangle_{\mathcal{E}_h} = \langle \partial_t^2 \phi_h, \mu_h \rangle_{\mathcal{E}_h^S}, \quad \forall \mu_h \in M_h^p, \tag{2.12}$$

where we have also used the boundary condition eq. (2.1c).

Note that this equation states that $\widehat{\boldsymbol{q}}_h \cdot \boldsymbol{n} = 0$ on Γ_B and $\widehat{\boldsymbol{q}}_h \cdot \boldsymbol{n} = \partial_t^2 \phi_h$ on Γ_S. Furthermore, over interior faces, we have the following identity

$$\langle [\![\widehat{\boldsymbol{q}}_h \cdot \boldsymbol{n}]\!], \mu_h \rangle_{\mathcal{E}_h^0} = 0, \quad \forall \mu_h \in M_h^p. \tag{2.13}$$

Since $[\![\widehat{\boldsymbol{q}}_h \cdot \boldsymbol{n}]\!] \in M_h^p$, we can take $\mu_h = [\![\widehat{\boldsymbol{q}}_h \cdot \boldsymbol{n}]\!]$ in eq. (2.13) to conclude that $[\![\widehat{\boldsymbol{q}}_h \cdot \boldsymbol{n}]\!] = 0$ point-wise over interior faces. In other words, the numerical flux is single-valued in the normal direction across faces of the mesh. From a physical point of view, this equation states that the numerical flux is conservative. Moreover, note that

$$\langle [\![\widehat{\boldsymbol{q}}_h \cdot \boldsymbol{n}]\!], \mu_h \rangle_{\mathcal{E}_h} = \langle \widehat{\boldsymbol{q}}_h \cdot \boldsymbol{n}, \mu_h \rangle_{\partial \mathcal{T}_h}. \tag{2.14}$$

We apply integration by parts to the first term in (2.11b) and multiply equations (2.11a) and (2.12) by -1, to obtain the following semidiscrete variational form: Find $\left(\boldsymbol{q}_h, \phi_h, \lambda_h\right) \in \boldsymbol{V}_h^p \times W_h^p \times M_h^p$ such that

$$-\left(\boldsymbol{q}_h, \boldsymbol{v}_h\right)_{\mathcal{T}_h} + \left(\phi_h, \nabla \cdot \boldsymbol{v}_h\right)_{\mathcal{T}_h} - \langle \lambda_h, \boldsymbol{v}_h \cdot \boldsymbol{n} \rangle_{\partial \mathcal{T}_h} = 0, \tag{2.15a}$$

$$\left(w_h, \nabla \cdot \boldsymbol{q}_h\right)_{\mathcal{T}_h} + \tau \langle w_h, \phi_h \rangle_{\partial \mathcal{T}_h} - \tau \langle w_h, \lambda_h \rangle_{\partial \mathcal{T}_h} = 0, \tag{2.15b}$$

$$-\langle \boldsymbol{q}_h \cdot \boldsymbol{n}, \mu_h \rangle_{\mathcal{E}_h} - \tau \langle \phi_h, \mu_h \rangle_{\mathcal{E}_h} + \tau \langle \lambda_h, \mu_h \rangle_{\mathcal{E}_h} = -\langle \partial_t^2 \phi_h, \mu_h \rangle_{\mathcal{E}_h^S}, \tag{2.15c}$$

for all $\left(\boldsymbol{v}_h, w_h, \mu_h\right) \in \boldsymbol{V}_h^p \times W_h^p \times M_h^p$.

The discretization of the term $\partial_t^2 \phi_h$ will be described next.

2.3 Temporal discretization

We consider the time interval $[0, t_f]$ which is discretized using a time step Δt such that $t_0 = 0$ and $t_n = t_{n-1} + \Delta t$, $n \geq 1$. To approximate $\partial_t \phi_h$ at $t = t_n$, we employ a first order BDF for the first time step, and a second order BDF for the following time steps:

$$\partial_t \phi_h|_{t_1} \approx \sigma_h^1 \coloneqq \frac{1}{\Delta t}\left(\phi_h^1 - \phi_h^0\right), \tag{2.16a}$$

$$\partial_t \phi_h|_{t_n} \approx \sigma_h^n \coloneqq \frac{1}{\Delta t}\left(\frac{3}{2}\phi_h^n - 2\phi_h^{n-1} + \frac{1}{2}\phi_h^{n-2}\right) \qquad \text{for } n \geq 2, \tag{2.16b}$$

where $\phi_h^n = \phi_h|_{t_n}$, and ϕ_h^0 is the L^2-projection of the initial condition $\phi_0(x, y)$ onto W_h^p.

Using these expressions, we can then approximate $\partial_t^2 \phi_h$ as follows

$$\partial_t^2 \phi_h|_{t_1} \approx \frac{1}{\Delta t^2}\phi_h^1 - \frac{1}{\Delta t^2}\phi_h^0 - \frac{1}{\Delta t}\sigma_h^0, \tag{2.17a}$$

$$\partial_t^2 \phi_h|_{t_n} \approx \frac{9}{4\Delta t^2}\phi_h^n - \frac{3}{\Delta t^2}\phi_h^{n-1} + \frac{3}{4\Delta t^2}\phi_h^{n-2} - \frac{2}{\Delta t}\sigma_h^{n-1} + \frac{1}{2\Delta t}\sigma_h^{n-2} \quad \text{for } n \geq 2, \tag{2.17b}$$

where σ_h^0 is the L^2-projection of the initial condition $\sigma_0(x, y)$ onto W_h^p.

For the first time step, eq. (2.15c) can be written as

$$\begin{aligned} -\langle \boldsymbol{q}_h^1 \cdot \boldsymbol{n}, \mu_h\rangle_{\mathcal{E}_h} - \tau\langle \phi_h^1, \mu_h\rangle_{\mathcal{E}_h} + \tau\langle \lambda_h^1, \mu_h\rangle_{\mathcal{E}_h} + \frac{1}{\Delta t^2}\langle \phi_h^1, \mu_h\rangle_{\mathcal{E}_h^S} = \\ -\frac{1}{\Delta t^2}\langle \phi_h^0, \mu_h\rangle_{\mathcal{E}_h^S} + \frac{1}{\Delta t}\langle \sigma_h^0, \mu_h\rangle_{\mathcal{E}_h^S}, \qquad \forall \mu_h \in M_h^p. \end{aligned} \tag{2.18}$$

For $n \geq 2$, we approximate eq. (2.15c) by

$$\begin{aligned} -\langle \boldsymbol{q}_h^n \cdot \boldsymbol{n}, \mu_h\rangle_{\mathcal{E}_h} - \tau\langle \phi_h^n, \mu_h\rangle_{\mathcal{E}_h} + \tau\langle \lambda_h^n, \mu_h\rangle_{\mathcal{E}_h} + \frac{9}{4\Delta t^2}\langle \phi_h^n, \mu_h\rangle_{\mathcal{E}_h^S} = \\ \frac{3}{\Delta t^2}\langle \phi_h^{n-1}, \mu_h\rangle_{\mathcal{E}_h^S} - \frac{3}{4\Delta t^2}\langle \phi_h^{n-2}, \mu_h\rangle_{\mathcal{E}_h^S} \\ +\frac{2}{\Delta t}\langle \sigma_h^{n-1}, \mu_h\rangle_{\mathcal{E}_h^S} - \frac{1}{2\Delta t}\langle \sigma_h^{n-2}, \mu_h\rangle_{\mathcal{E}_h^S}, \qquad \forall \mu_h \in M_h^p. \end{aligned} \tag{2.19}$$

The fully discrete weak formulation becomes: find $(\phi_h^n,\, \boldsymbol{q}_h^n,\, \lambda_h^n) \in W_h^p \times \boldsymbol{V}_h^p \times M_h^p$ such that for all $(w_h,\, \boldsymbol{v}_h,\, \mu_h) \in W_h^p \times \boldsymbol{V}_h^p \times M_h^p$, the following relations are satisfied for $n = 1$

$$-\left(\boldsymbol{q}_h^1, \boldsymbol{v}_h\right)_{\mathcal{T}_h} + \left(\phi_h^1, \nabla\cdot\boldsymbol{v}_h\right)_{\mathcal{T}_h} - \langle\lambda_h^1, \boldsymbol{v}_h\cdot\boldsymbol{n}\rangle_{\partial\mathcal{T}_h} = 0, \tag{2.20a}$$

$$\left(w_h, \nabla\cdot\boldsymbol{q}_h^1\right)_{\mathcal{T}_h} + \tau\langle w_h, \phi_h^1\rangle_{\partial\mathcal{T}_h} - \tau\langle w_h, \lambda_h^1\rangle_{\partial\mathcal{T}_h} = 0, \tag{2.20b}$$

$$-\langle\boldsymbol{q}_h^1\cdot\boldsymbol{n}, \mu_h\rangle_{\mathcal{E}_h} - \tau\langle\phi_h^1, \mu_h\rangle_{\mathcal{E}_h} + \tau\langle\lambda_h^1, \mu_h\rangle_{\mathcal{E}_h} + \frac{1}{\Delta t^2}\langle\phi_h^1, \mu_h\rangle_{\mathcal{E}_h^S} = -\frac{1}{\Delta t^2}\langle\phi_h^0, \mu_h\rangle_{\mathcal{E}_h^S} + \frac{1}{\Delta t}\langle\sigma_h^0, \mu_h\rangle_{\mathcal{E}_h^S}, \tag{2.20c}$$

and for $n \geq 2$

$$-\left(\boldsymbol{q}_h^n, \boldsymbol{v}_h\right)_{\mathcal{T}_h} + \left(\phi_h^n, \nabla\cdot\boldsymbol{v}_h\right)_{\mathcal{T}_h} - \langle\lambda_h^n, \boldsymbol{v}_h\cdot\boldsymbol{n}\rangle_{\partial\mathcal{T}_h} = 0, \tag{2.21a}$$

$$\left(w_h, \nabla\cdot\boldsymbol{q}_h^n\right)_{\mathcal{T}_h} + \tau\langle w_h, \phi_h^n\rangle_{\partial\mathcal{T}_h} - \tau\langle w_h, \lambda_h^n\rangle_{\partial\mathcal{T}_h} = 0, \tag{2.21b}$$

$$-\langle\boldsymbol{q}_h^n\cdot\boldsymbol{n}, \mu_h\rangle_{\mathcal{E}_h} - \tau\langle\phi_h^n, \mu_h\rangle_{\mathcal{E}_h} + \tau\langle\lambda_h^n, \mu_h\rangle_{\mathcal{E}_h} + \frac{9}{4\Delta t^2}\langle\phi_h^n, \mu_h\rangle_{\mathcal{E}_h^S} = \frac{3}{\Delta t^2}\langle\phi_h^{n-1}, \mu_h\rangle_{\mathcal{E}_h^S} - \frac{3}{4\Delta t^2}\langle\phi_h^{n-2}, \mu_h\rangle_{\mathcal{E}_h^S} + \frac{2}{\Delta t}\langle\sigma_h^{n-1}, \mu_h\rangle_{\mathcal{E}_h^S} - \frac{1}{2\Delta t}\langle\sigma_h^{n-2}, \mu_h\rangle_{\mathcal{E}_h^S}. \tag{2.21c}$$

Note that ϕ_h^n is related to the wave height through equation (1.33c). Once ϕ_h^n has been obtained an approximation ζ_h^n to the wave height can be computed using eq. (2.16).

In [19], it was shown that this HDG method for convection-diffusion problems converges with order $p+1$ in both the scalar and vector variables. The free-surface problem considered here is slightly different since we have a free-surface boundary condition. However, we expect the rates of convergence in space to be similar.

2.4 Numerical results

Here we present some numerical results obtained when applying the HDG method described above to two different test cases. First, we consider a linear free surface problem in an unbounded domain where the analytical solution is known. We present rates of convergence for linear, quadratic and cubic polynomials. In addition to the HDG method described above, we show the results for the same case solved with an interior penalty discontinuous Galerkin method that recreates the results in [82]. The second test case that we present corresponds to the simulation of water waves generated by a wave maker. All the simulations were carried out using the Modular Finite Element Method (MFEM) library [25]. The stabilization parameter τ is chosen as $\tau = 5$.

2.4.1 Static condensation

As mentioned above, one of the most attractive features of HDG methods is that they allow for static condensation, which we describe next. Let $Q \in \mathbb{R}^{\dim \boldsymbol{V}_h^p}$, $\Phi \in \mathbb{R}^{\dim W_h^p}$ and $\Lambda \in \mathbb{R}^{\dim M_h^p}$ be the vectors that contain the coefficients of $\boldsymbol{q}_h$, ϕ_h and λ_h, respectively, with respect to the basis of their corresponding vector spaces. Then, $W = \begin{bmatrix} Q^T & \Phi^T \end{bmatrix}$ is the vector of all element degrees-of-freedom. At each time step, a linear system of the following structure must be solved

$$\begin{bmatrix} A & B \\ C & D \end{bmatrix} \begin{bmatrix} W \\ \Lambda \end{bmatrix} = \begin{bmatrix} 0 \\ F \end{bmatrix}. \tag{2.22}$$

Thanks to the definition of the numerical fluxes eq. (2.10) and eq. (2.9), A has a block-diagonal structure. Therefore, we can eliminate W by locally inverting A, to obtain the reduced linear system $\left(-CA^{-1}B + D\right)\Lambda = F$. To solve this reduced system, we use the direct solver of MUMPS [5, 4] through PETSc [8]. Once Λ has been computed, we can calculate W element-wise using $W = -A^{-1}B\Lambda$.

2.4.2 Postprocessing

Since in HDG methods $\boldsymbol{q}_h$ converges with optimal order, a local postprocessing can be performed, which results in a numerical solution $\phi_h^* \in W_h^{p+1}$ that converges to ϕ with order $p+2$ To construct a superconvergent solution, we use that the average of ϕ_h superconverges and that $\boldsymbol{q}_h$ converges optimally. Following [90], the new variable ϕ_h^* can then be computed as the solution to

$$\left(1, \phi_h^*\right)_K = \left(1, \phi_h\right)_K, \tag{2.23a}$$

$$\left(\nabla w_h^*, \nabla \phi_h^*\right)_K = -\left(\nabla w_h^*, \boldsymbol{q}_h\right)_K \qquad \forall w_h^* \in W_h^{p+1}. \tag{2.23b}$$

Note that this is a local problem, so it can be solved very efficiently.

2.4.3 Linear waves in an unbounded domain

In this example we consider time harmonic linear free-surface waves in an unbounded domain. We consider $\Omega = [-1, 1] \times [-1, 0]$ and apply periodic boundary conditions on $x = -1$ and $x = 1$. The analytical solution for this problem is given by

$$\phi(x, y, t) = A \cosh(k(y+1)) \cos(\omega t - kx), \tag{2.24}$$

where A denotes the amplitude of the velocity potential, k is the wave number, which is related to the wavelength λ_w by $k = 2\pi/\lambda_w$, and ω is the frequency of the oscillations, which satisfies the dispersion relation

$$\omega^2 = k \tanh(k). \tag{2.25}$$

This solution is obtained from the analytical solution in eq. (1.32) by setting $A = a/\omega \cosh(kH)$. The analytical wave height is then given by

$$\zeta(x,t) = -\partial_t \phi(x,0,t) = A\omega \cosh(k) \sin(\omega t - kx). \tag{2.26}$$

We take $\lambda_w = 1$, and A such that the maximum amplitude of the wave height is 0.05. For each method, we show the approximation errors and convergence rates for ϕ_h and ϕ_h^* at $t_f = 2.5$ for linear ($p = 1$) and quadratic ($p = 2$) polynomial approximations, and at $t_f = 0.2$ for cubic polynomials ($p = 3$). Note that for cubic polynomials the error in space is of order 4, whereas the error in time is of order 2, so we require a very small time step in order to make the spatial error dominant over the temporal one. This causes the method to be very expensive computationally. In order to alleviate this, we choose the final time for the cubic polynomials case to be smaller than for the linear and quadratic polynomials cases. The initial time step is $\Delta t = 0.05$ for linear polynomials, for quadratic polynomials it is $\Delta t = 0.01$ and for cubic polynomials it is $\Delta t = 0.004$. Table 2.1 shows the number of degrees-of-freedom (DOFs) for both the HDG method in section 2.2 and an interior penalty DG (IP-DG) method, the $L^2(\Omega)$-errors of ϕ_h and ϕ_h^* and the convergence rates for both methods. Next, we give a brief description of the IP-DG applied to the problem eq. (2.1). This method is similar to the one in [82].

Interior penalty discontinuous Galerkin method

We consider the same spaces W_h^p and $\boldsymbol{V}_h^p$ in eq. (2.2) and proceed as in section 2.2.2: multiply eq. (2.1a) and eq. (2.1b) by test functions $\boldsymbol{v}_h \in \boldsymbol{V}_h^p$ and $w_h \in W_h^p$, respectively, integrate over an element $K \in \mathcal{T}_h$, replace $\boldsymbol{q}$ by $\boldsymbol{q}_h \in \boldsymbol{V}_h^p$ and ϕ by $\phi_h \in W_h^p$, and sum over all elements to find

$$\sum_{K\in\mathcal{T}_h} \int_K \boldsymbol{q}_h \cdot \boldsymbol{v}_h \,\mathrm{d}x\,\mathrm{d}y + \sum_{K\in\mathcal{T}_h} \int_K \nabla\phi_h \cdot \boldsymbol{v}_h \,\mathrm{d}x\,\mathrm{d}y = 0, \tag{2.27a}$$

$$\sum_{K\in\mathcal{T}_h} \int_K w_h \nabla\cdot \boldsymbol{q}_h \,\mathrm{d}x\,\mathrm{d}y = 0. \tag{2.27b}$$

Applying integration by parts (twice for eq. (2.27a)),

$$\sum_{K\in\mathcal{T}_h}\int_K \boldsymbol{q}_h\cdot\boldsymbol{v}_h\,\mathrm{d}x\,\mathrm{d}y+\sum_{K\in\mathcal{T}_h}\int_K \nabla\phi_h\cdot\boldsymbol{v}_h\,\mathrm{d}x\,\mathrm{d}y+\sum_{K\in\mathcal{T}_h}\int_{\partial K}\left(\widehat{\phi}_h-\phi_h\right)\boldsymbol{v}_h\cdot\boldsymbol{n}\,\mathrm{d}s=0, \tag{2.28a}$$

$$-\sum_{K\in\mathcal{T}_h}\int_K \nabla w_h\cdot\boldsymbol{q}_h\,\mathrm{d}x\,\mathrm{d}y+\sum_{K\in\mathcal{T}_h}\int_{\partial K} w_h\widehat{\boldsymbol{q}}_h\cdot\boldsymbol{n}\,\mathrm{d}s=0. \tag{2.28b}$$

Next, we use the following relation [6]

$$\sum_{K\in\mathcal{T}_h}\int_{\partial K} w_h\boldsymbol{v}_h\cdot\boldsymbol{n}\,\mathrm{d}s=\sum_{F\in\mathcal{E}_h}\int_F[\![w_h\boldsymbol{n}]\!]\cdot\{\!\{\boldsymbol{v}_h\}\!\}\,\mathrm{d}s+\sum_{F\in\mathcal{E}_h^0}\int_F[\![\boldsymbol{v}_h\cdot\boldsymbol{n}]\!]\,\{\!\{w_h\}\!\}\,\mathrm{d}s, \tag{2.29}$$

for any $w_h\in W_h^p$ and $\boldsymbol{v}_h\in\boldsymbol{V}_h^p$, and where $\{\!\{\cdot\}\!\}$ denotes the average operator defined as follows for $F\in\mathcal{E}_h^0$

$$\{\!\{\boldsymbol{q}\}\!\}=\frac{1}{2}\left(\boldsymbol{q}_1+\boldsymbol{q}_2\right). \tag{2.30}$$

For $F\in\mathcal{E}_h^\partial$, the definition is as follows

$$\{\!\{\boldsymbol{q}\}\!\}=\boldsymbol{q}. \tag{2.31}$$

The definition of $\{\!\{\cdot\}\!\}$ for scalar functions is completely analogous. Using eq. (2.29) in eq. (2.28a) and eq. (2.28b), we obtain

$$\sum_{K\in\mathcal{T}_h}\int_K \boldsymbol{q}_h\cdot\boldsymbol{v}_h\,\mathrm{d}x\,\mathrm{d}y+\sum_{K\in\mathcal{T}_h}\int_K \nabla\phi_h\cdot\boldsymbol{v}_h\,\mathrm{d}x\,\mathrm{d}y \tag{2.32a}$$

$$+\sum_{F\in\mathcal{E}_h}\int_F\left[\!\!\left[\left(\widehat{\phi}_h-\phi_h\right)\boldsymbol{n}\right]\!\!\right]\cdot\{\!\{\boldsymbol{v}_h\}\!\}\,\mathrm{d}s+\sum_{F\in\mathcal{E}_h^0}\int_F[\![\boldsymbol{v}_h\cdot\boldsymbol{n}]\!]\,\{\!\{\widehat{\phi}_h-\phi_h\}\!\}\,\mathrm{d}s=0,$$

$$-\sum_{K\in\mathcal{T}_h}\int_K \nabla w_h\cdot\boldsymbol{q}_h\,\mathrm{d}x\,\mathrm{d}y+\sum_{F\in\mathcal{E}_h}\int_F[\![w_h\boldsymbol{n}]\!]\cdot\{\!\{\widehat{\boldsymbol{q}}_h\}\!\}\,\mathrm{d}s+\sum_{F\in\mathcal{E}_h^0}\int_F[\![\widehat{\boldsymbol{q}}_h\cdot\boldsymbol{n}]\!]\,\{\!\{w_h\}\!\}\,\mathrm{d}s=0. \tag{2.32b}$$

The IP-DG numerical fluxes are [6]

$$\widehat{\phi}_h=\{\!\{\phi_h\}\!\},\qquad \widehat{\boldsymbol{q}}_h=-\{\!\{\nabla\phi_h\}\!\}+\alpha h_F^{-1}[\![\phi_h\boldsymbol{n}]\!],\qquad F\in\mathcal{E}_h^0, \tag{2.33a}$$

$$\widehat{\phi}_h=\phi_h,\ \ F\in\mathcal{E}_h^\partial\qquad \widehat{\boldsymbol{q}}_h\cdot\boldsymbol{n}=\begin{cases}\partial_t^2\phi_h, & F\in\mathcal{E}_h^S\\ 0, & F\in\mathcal{E}_h^B\end{cases}, \tag{2.33b}$$

where h_F is the size of the face F and $\alpha > 0$ is a penalty parameter that has to be chosen large enough to ensure stability [6]. Substituting eq. (2.33) in eq. (2.32a) and eq. (2.32b), and using that $\widehat{\phi}_h$ and $\widehat{\boldsymbol{q}}_h$ are single-valued, we obtain

$$\sum_{K\in\mathcal{T}_h}\int_K \boldsymbol{q}_h\cdot\boldsymbol{v}_h\,\mathrm{d}x\,\mathrm{d}y+\sum_{K\in\mathcal{T}_h}\int_K \nabla\phi_h\cdot\boldsymbol{v}_h\,\mathrm{d}x\,\mathrm{d}y-\sum_{F\in\mathcal{E}_h^0}\int_F[\![\phi_h\boldsymbol{n}]\!]\cdot\{\!\{\boldsymbol{v}_h\}\!\}\,\mathrm{d}s=0, \tag{2.34a}$$

$$-\sum_{K\in\mathcal{T}_h}\int_K \nabla w_h\cdot\boldsymbol{q}_h\,\mathrm{d}x\,\mathrm{d}y-\sum_{F\in\mathcal{E}_h^0}\int_F[\![w_h\boldsymbol{n}]\!]\cdot\{\!\{\nabla\phi_h\}\!\}\,\mathrm{d}s \tag{2.34b}$$

$$+\sum_{F\in\mathcal{E}_h^0}\int_F \alpha h_F^{-1}[\![w_h\boldsymbol{n}]\!]\cdot[\![\phi_h\boldsymbol{n}]\!]\,\mathrm{d}s+\int_{\Gamma_S} w_h\partial_t^2\phi_h\,\mathrm{d}s=0.$$

Taking $\boldsymbol{v}_h=\nabla w_h$ in eq. (2.34a) and adding with eq. (2.34b), we obtain

$$\sum_{K\in\mathcal{T}_h}\int_K \nabla\phi_h\cdot\nabla w_h\,\mathrm{d}x\,\mathrm{d}y-\sum_{F\in\mathcal{E}_h^0}\int_F[\![\phi_h\boldsymbol{n}]\!]\cdot\{\!\{\nabla w_h\}\!\}\,\mathrm{d}s-\sum_{F\in\mathcal{E}_h^0}\int_F[\![w_h\boldsymbol{n}]\!]\cdot\{\!\{\nabla\phi_h\}\!\}\,\mathrm{d}s$$
$$+\sum_{F\in\mathcal{E}_h^0}\int_F \alpha h_F^{-1}[\![w_h\boldsymbol{n}]\!]\cdot[\![\phi_h\boldsymbol{n}]\!]\,\mathrm{d}s+\int_{\Gamma_S} w_h\partial_t^2\phi_h\,\mathrm{d}s=0. \tag{2.35}$$

The semi-discrete form is then given by: find $\phi_h\in W_h^p$ such that

$$\sum_{K\in\mathcal{T}_h}\int_K \nabla\phi_h\cdot\nabla w_h\,\mathrm{d}x\,\mathrm{d}y-\sum_{F\in\mathcal{E}_h^0}\int_F[\![\phi_h\boldsymbol{n}]\!]\cdot\{\!\{\nabla w_h\}\!\}\,\mathrm{d}s-\sum_{F\in\mathcal{E}_h^0}\int_F[\![w_h\boldsymbol{n}]\!]\cdot\{\!\{\nabla\phi_h\}\!\}\,\mathrm{d}s$$
$$+\sum_{F\in\mathcal{E}_h^0}\int_F \alpha h_F^{-1}[\![w_h\boldsymbol{n}]\!]\cdot[\![\phi_h\boldsymbol{n}]\!]\,\mathrm{d}s+\int_{\Gamma_S} w_h\partial_t^2\phi_h\,\mathrm{d}s=0, \tag{2.36}$$

for all $w_h\in W_h^p$. The fully discrete form is obtained in a similar fashion as in section 2.3.

Convergence rates

In table 2.2, we show the $L^2(\Omega)$-errors and convergence rates for $\boldsymbol{q}_h$ and the $L^2(\Gamma_S)$-errors and convergence rates for ζ_h.

Recall that the time stepping scheme used here is a second order method. Therefore, when using quadratic and cubic polynomials, even though the error in space is of order 3 and 4, respectively, the full discretization error in space and time will not necessarily be of

the same order as the one in space. This is why we see some loss in the rates of convergence in the quadratic and cubic cases. Despite this shortcoming, we see that both the velocity potential and the wave height converge at nearly optimal rates for both HDG and DG methods. We can also see that in general, the errors for HDG are lower than those for DG. In table 2.1, we can see that for quadratic and cubic approximations, the number of globally coupled degrees of freedom for HDG are lower than for DG. Additionally, thanks to the element-wise postprocessing in the HDG method, we obtain a variable ϕ_h^* that converges to ϕ with one order higher than ϕ_h.

We remark that the DG method in [82] and in section 2.4.3 is based on a primal formulation in which the only unknown is ϕ. The velocity of the fluid can be obtained from ϕ by calculating its gradient. If ϕ is approximated by polynomials of degree p, then its gradient will be a piecewise polynomial of degree $p-1$, meaning that it will converge, at best, with a rate of p. In the present discretization we introduce the unknown $\boldsymbol{q}$ which is the negative velocity of the fluid, and we approximate it with polynomials of degree p. We see in table 2.2 that the rate of convergence for $\boldsymbol{q}_h$ is $p+1$, which is superior to what we would obtain from a primal DG formulation. Therefore, our HDG discretization allows us to obtain a better approximation to the velocity of the fluid than using a DG method.

Thus, with the HDG method described in Chapter 2, we can approximate the wave height and the velocity of the fluid with order $p+1$, where p is the degree of the polynomials employed for the approximations. Moreover, by performing a simple element-by-element postprocessing, we obtain approximations for the velocity potential of order $p+2$. In contrast, the DG method in [82] only finds approximations for the velocity potential or order $p+1$.

Simulation of a wavemaker

In this example we investigate waves generated by a piston-type wave maker. This simulation is proposed in [82, 88]. In this case the domain is $\Omega = [0,\, 10] \times [-1,\, 0]$. We apply homogeneous Neumann boundary conditions (no-normal flow) on $x = 10$ and $y = -1$. The wave maker is located on the left side of the domain, i.e., at $x = 0$, where the boundary condition is

$$\nabla\phi \cdot \mathbf{n} = (y+1)T(t) \quad \text{at } x = 0, \tag{2.37}$$

Table 2.1: Convergence rates for ϕ_h and ϕ_h^* computed with the HDG method in Chapter 2 and the DG method in [82].

		HDG (ϕ_h)			HDG (ϕ_h^*)		DG (ϕ_h)		
	$nx \times ny$	DOFs	$L^2(\Omega)$-error	Order	$L^2(\Omega)$-error	Order	DOFs	$L^2(\Omega)$-error	Order
Q^1	3×3	42	8.18e-03	-	8.28e-03	-	36	5.52e-03	-
	6×6	156	2.03e-03	2.01	1.72e-03	2.27	144	3.62e-03	0.61
	12×12	600	3.74e-04	2.44	2.96e-04	2.54	576	1.01e-03	1.84
	24×24	2352	7.92e-05	2.24	4.56e-05	2.70	2304	2.55e-04	1.99
	48×48	9312	1.67e-05	2.25	6.05e-06	2.91	9216	6.38e-05	2.00
Q^2	3×3	63	1.90e-03	-	1.73e-03	-	81	2.68e-03	-
	6×6	234	2.76e-04	2.78	2.38e-04	2.86	324	3.98e-04	2.75
	12×12	900	2.27e-05	3.60	1.20e-05	4.31	1296	3.72e-05	3.42
	24×24	3528	2.70e-06	3.07	8.82e-07	3.77	5184	4.06e-06	3.19
	48×48	13968	3.37e-07	3.00	7.44e-08	3.57	20736	4.74e-07	3.10
Q^3	3×3	84	3.17e-04	-	2.22e-04	-	144	4.21e-04	-
	6×6	312	2.23e-05	3.83	1.10e-05	4.33	576	2.49e-05	4.08
	12×12	1200	1.41e-06	3.98	4.42e-07	4.64	2304	1.70e-06	3.87
	24×24	4704	8.90e-08	3.99	1.74e-08	4.67	9216	1.18e-07	3.85

Table 2.2: Convergence rates for $\boldsymbol{q}_h$ and ζ_h computed with the HDG method in Chapter 2 and the DG method in [82].

	$nx \times ny$	HDG ($\boldsymbol{q}_h$)		HDG (ζ_h)		DG (ζ_h)	
		$L^2(\Omega)$-error	Order	$L^2(\Gamma_S)$-error	Order	$L^2(\Gamma_S)$-error	Order
Q^1	3×3	7.44e-02	-	8.51e-02	-	7.51e-02	-
	6×6	2.36e-02	1.66	2.22e-02	1.94	3.86e-02	0.96
	12×12	5.00e-03	2.24	3.22e-03	2.79	1.05e-02	1.87
	24×24	1.47e-03	1.77	7.82e-04	2.04	2.23e-03	2.24
	48×48	3.72e-04	1.98	1.62e-04	2.27	5.65e-04	1.98
Q^2	3×3	2.03e-02	-	1.75e-02	-	2.49e-02	-
	6×6	4.20e-03	2.27	2.87e-03	2.61	8.84e-03	1.49
	12×12	4.97e-04	3.08	2.62e-04	3.45	1.29e-03	2.78
	24×24	7.37e-05	2.75	2.88e-05	3.19	2.53e-04	2.35
	48×48	1.15e-05	2.68	3.37e-06	3.10	5.73e-05	2.14
Q^3	3×3	4.00e-03	-	3.13e-03	-	5.22e-03	-
	6×6	3.60e-04	3.47	2.51e-04	3.64	1.25e-03	2.07
	12×12	2.75e-05	3.71	1.58e-05	3.99	4.54e-05	4.78
	24×24	1.91e-06	3.85	1.03e-06	3.94	3.59e-06	3.66

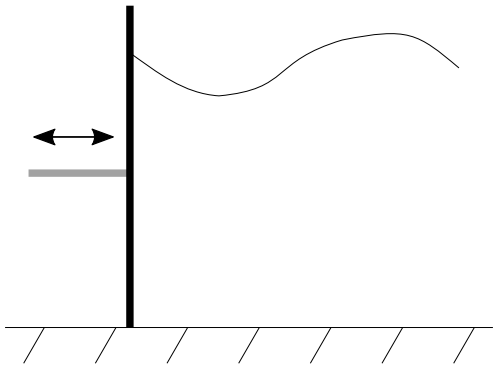

Figure 2.1: Piston-type wave maker used in section 2.4.3.

where

$$T(t) = a\sin(\omega_w t). \tag{2.38}$$

Here, a represents the amplitude of the wave and ω_w is the frequency of the wave. Figure 2.1 depicts the wavemaker.

The initial velocity potential and wave height are taken to be zero and we consider two meshes: one with 1024 elements and one with 4096 elements. Figure 2.2a, fig. 2.2b and fig. 2.2c show the free-surface elevation at $t = 18.4$, $t = 32.96$ and $t = 51.04$, respectively. For each of these times, we compute the approximate solution using linear and quadratic polynomials.

In fig. 2.2, we show the elevation of the free-surface at different times. At $t = 18.4$, before the wave generated by the wavemaker has reached the opposite wall $x = 10$. At time $t = 32.96$, the wave has just hit the opposite wall and is reflected back into the domain. For this time, we start to notice a discrepancy between the linear and quadratic polynomial cases on the mesh with 1024 elements. However, on the mesh with 4096 elements, the linear solution agrees with the quadratic one. When time is $t = 51.04$, the wave has already started to travel back into the domain affecting the waves generated by the wavemaker. Here we see that for linear polynomials, the solution is completely different than when using a quadratic polynomial approximation. Nevertheless, on the finer mesh, the solutions with $p = 1$ and $p = 2$ are very similar. The results obtained with the DG method in [82] are very similar to the ones obtained with the HDG method described in Chapter 2, and therefore they are not shown here.

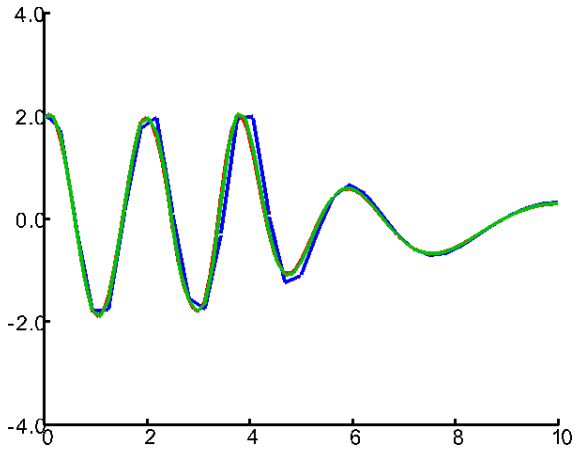

(a) Free-surface elevation at $t = 18.4$.

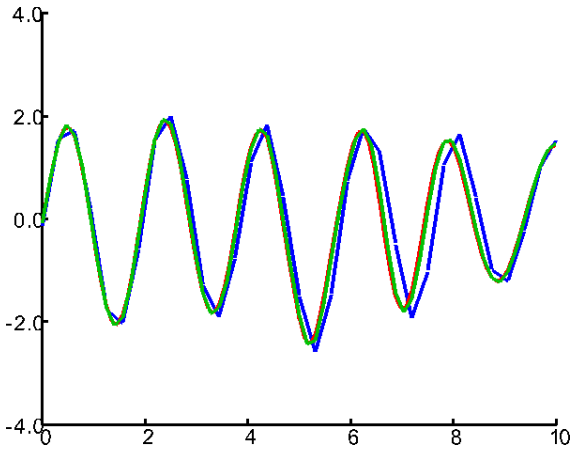

(b) Free-surface elevation at $t = 32.96$.

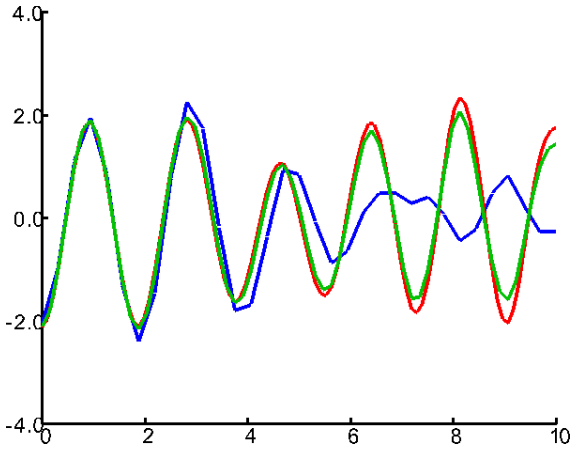

(c) Free-surface elevation at $t = 51.04$.

Figure 2.2: Simulation of water waves generated by a wavemaker, see section 2.4.3. The free-surface elevation (scaled by a factor of 50) at different time levels for polynomial degree $p = 1$, 1024 elements (blue line), $p = 2$, 1024 elements (red line), and $p = 1$, 4096 elements (green line).

Chapter 3

A space-time hybridizable discontinuous Galerkin method for the linear free-surface problem

In this chapter we introduce a space-time hybridizable discontinuous Galerkin method for the linear free-surface problem eq. (1.33). We consider a mixed formulation based on the splitting introduced originally for the wave equation in [73]. This is different from previous works on DG methods for free-surface problems in which the primal form of the problem is considered [82, 84]. The reason to consider the mixed formulation is that it allows us to immediately obtain the velocity of the fluid without post-processing. To the best of our knowledge, such a splitting has not been considered for inviscid, incompressible and irrotational free-surface flow problems. Furthermore, as opposed to standard discontinuous Galerkin discretizations, our space-time HDG formulation uses weighted inner-products. The idea of using weighted inner-products was previously applied in [27] to the wave equation. Here, we use weighted inner-products to prove well-posedness of the space-time HDG formulation of the linear free-surface waves problem.

The *a priori* error analysis in this chapter is projection based [19], but modified for weighted inner-products and space-time prismatic elements. Additionally, we derive scaling identities between the reference and physical space-time prisms that separate the spatial dimension from the temporal dimension. Such anisotropic scaling identities were previously derived in the context of anisotropic meshes in [32] and space-time meshes in [45, 75]. Furthermore, these scaling identities allow us to obtain *a priori* error estimates in which the dependence on the time step and the spatial mesh size is explicit. This is in contrast to

error bounds that depend on the space-time mesh size as derived, for example, for parabolic problems in [12].

3.1 Space-time setting

To introduce the space-time HDG method we first formulate the mixed space-time formulation of the linear free-surface problem eq. (1.33) in two spatial dimensions.

Space-time methods do not distinguish between temporal and spatial variables. A point at time $t = x_0$ with position vector $\boldsymbol{x} = (x_1, x_2)$ has Cartesian coordinates $(x_0, \boldsymbol{x})$. We therefore pose the linear free-surface problem eq. (1.33) on a space-time domain defined as $\mathcal{E} := \big\{(x_0, \boldsymbol{x}) \in \mathbb{R}^3 : \boldsymbol{x} \in \Omega,\, 0 < x_0 < T\big\}$. The boundary $\partial\mathcal{E}$ of the space-time domain $\mathcal{E}$ consists of $\Omega_0 := \big\{(x_0, \boldsymbol{x}) \in \partial\mathcal{E} : x_0 = 0\big\}$, $\Omega_N := \big\{(x_0, \boldsymbol{x}) \in \partial\mathcal{E} : x_0 = T\big\}$ and $\mathcal{Q}_\mathcal{E} := \big\{(x_0, \boldsymbol{x}) \in \partial\mathcal{E} : 0 < x_0 < T\big\}$. Furthermore, $\mathcal{Q}_\mathcal{E}$ is subdivided as $\mathcal{Q}_\mathcal{E} = \partial\mathcal{E}_\mathcal{S} \cup \partial\mathcal{E}_\mathcal{B} \cup \partial\mathcal{E}_\mathcal{P}$, where $\partial\mathcal{E}_\mathcal{S} := \big\{(x_0, \boldsymbol{x}) \in \partial\mathcal{E} : \boldsymbol{x} \in \Gamma_S, 0 < x_0 < T\big\}$, $\partial\mathcal{E}_\mathcal{B} := \{(x_0, \boldsymbol{x}) \in \partial\mathcal{E} : \boldsymbol{x} \in \Gamma_B, 0 < x_0 < T\}$, and $\partial\mathcal{E}_\mathcal{P} := \big\{(x_0, \boldsymbol{x}) \in \partial\mathcal{E} : \boldsymbol{x} \in \Gamma_P, 0 < x_0 < T\big\}$.

We next introduce two new variables, namely $\boldsymbol{q} = -\nabla\phi$ and $v = -\partial_t\phi$. A similar choice of variables was introduced in [61] for the wave equation. The linear free-surface problem eq. (1.33) on the space-time domain $\mathcal{E}$ can then be written as a mixed space-time formulation which is given by

$$\partial_t \boldsymbol{q} - \nabla v = 0 \qquad \text{in } \mathcal{E}, \tag{3.1a}$$
$$\nabla \cdot \boldsymbol{q} = 0 \qquad \text{in } \mathcal{E}, \tag{3.1b}$$
$$-\boldsymbol{q} \cdot \boldsymbol{n} = \partial_t v \qquad \text{on } \partial\mathcal{E}_\mathcal{S}, \tag{3.1c}$$
$$-\boldsymbol{q} \cdot \boldsymbol{n} = 0 \qquad \text{on } \partial\mathcal{E}_\mathcal{B}, \tag{3.1d}$$
$$\boldsymbol{q}(0, \boldsymbol{x}) = \boldsymbol{q}_0(\boldsymbol{x}) \qquad \text{on } \Omega_0, \tag{3.1e}$$
$$v(0, \boldsymbol{x}) = v_0(\boldsymbol{x}) \qquad \text{on } \Omega_0, \tag{3.1f}$$

where $\boldsymbol{q}_0(\boldsymbol{x})$ and $v_0(\boldsymbol{x})$ are given initial conditions.

Note that the wave height ζ will be the restriction of v to the free-surface Γ_S.

3.1.1 Space-time notation

Let $\mathcal{I} = [0, T]$ denote the time interval. We partition the time interval into time levels $0 = t_0 < t_1 < t_2 < \cdots < t_N = T$ and denote the n^{th} time interval by $I_n = (t_n, t_{n+1})$.

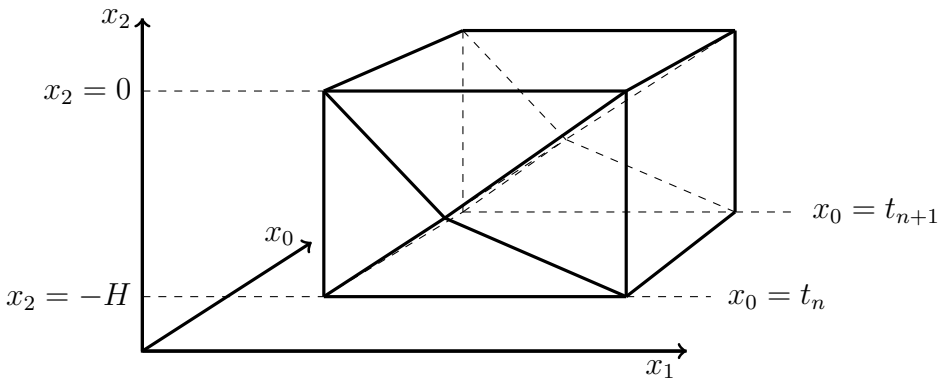

Figure 3.1: Depiction of a space-time slab $\mathcal{E}^n \subset \mathbb{R}^3$.

The length of each time interval is constant and is denoted by Δt. The n^{th} space-time slab is then defined as $\mathcal{E}^n := \mathcal{E} \cap \big(I_n \times \mathbb{R}^2\big)$. Define $\Omega_n := \big\{(x_0, \boldsymbol{x}) \in \mathcal{E} : x_0 = t_n\big\}$. The boundary of a space-time slab, $\partial\mathcal{E}^n$, can then be divided into Ω_n, Ω_{n+1} and $\mathcal{Q}_{\mathcal{E}}^n := \partial\mathcal{E}^n \backslash (\Omega_{n+1} \cup \Omega_n)$. We can further subdivide $\mathcal{Q}_{\mathcal{E}}^n$ as $\mathcal{Q}_{\mathcal{E}}^n = \partial\mathcal{E}_{\mathcal{S}}^n \cup \partial\mathcal{E}_{\mathcal{B}}^n \cup \partial\mathcal{E}_{\mathcal{P}}^n$, where $\partial\mathcal{E}_{\mathcal{S}}^n := \big\{(x_0, \boldsymbol{x}) \in \partial\mathcal{E} : \boldsymbol{x} \in \Gamma_S, t_n < x_0 < t_{n+1}\big\}$, $\partial\mathcal{E}_{\mathcal{B}}^n := \big\{(x_0, \boldsymbol{x}) \in \partial\mathcal{E} : \boldsymbol{x} \in \Gamma_B, t_n < x_0 < t_{n+1}\big\}$, and $\partial\mathcal{E}_{\mathcal{P}}^n := \big\{(x_0, \boldsymbol{x}) \in \partial\mathcal{E} : \boldsymbol{x} \in \Gamma_P, t_n < x_0 < t_{n+1}\big\}$.

For linear free-surface waves the spatial domain Ω does not change with time. We therefore introduce a space-time mesh as follows. We first introduce a triangulation $\mathcal{T} := \{K\}$ of the domain Ω_n, which is the same for all n. Each space-time element $\mathcal{K} \subset \mathcal{E}^n$ is constructed as $\mathcal{K} = K \times I_n$. The set of all space-time elements, $\mathcal{T}^n := \{\mathcal{K} : \mathcal{K} \subset \mathcal{E}^n\}$ is then a triangulation of the space-time slab $\mathcal{E}^n$. This is repeated for all n. See fig. 3.1 for an illustration of $\mathcal{E}^n$.

Consider a space-time element $\mathcal{K}_j^n \in \mathcal{T}^n$. Let $K_j^n := \{(x_0, \boldsymbol{x}) \in \partial\mathcal{K}_j^n : x_0 = t_n\} \in \mathcal{T}$. The boundary of a space-time element $\mathcal{K}_j^n \in \mathcal{T}^n$ is then composed of K_j^n, K_j^{n+1} and $\mathcal{Q}_{\mathcal{K}_j^n} := \partial\mathcal{K}_j^n \backslash \partial\mathcal{K}_0^n$ where $\partial\mathcal{K}_0^n := K_j^n \cup K_j^{n+1}$.

The outward unit space-time normal vector field on $\partial\mathcal{K}_j^n$ is denoted by $\hat{\boldsymbol{n}}_j^n = ((n_t)_j^n, \boldsymbol{n}_j^n)$, where $(n_t)_j^n$ and $\boldsymbol{n}_j^n$ are, respectively, the temporal and spatial parts of the space-time normal vector. Since the mesh does not change with time, $\hat{\boldsymbol{n}}_j^n = (1, \boldsymbol{0})$ on K_j^{n+1}, $\hat{\boldsymbol{n}}_j^n = (-1, \boldsymbol{0})$ on K_j^n, and $\hat{\boldsymbol{n}}_j^n = (0, \boldsymbol{n}_j^n)$ on $\mathcal{Q}_{\mathcal{K}_j^n}$.

In the remainder of this chapter we will omit the subscripts and superscripts when referring to space-time elements, their boundaries, and the normal vector wherever no confusion will occur.

In a space-time slab $\mathcal{E}^n$, the set and union of all faces in $\partial\mathcal{E}_S$ are denoted by $\mathcal{F}_S^n$ and Γ_S^n, respectively. Furthermore, the set of all interior and boundary faces in $\mathcal{E}^n$ that are not on $\Omega_n \cup \Omega_{n+1}$ is denoted by $\mathcal{F}_Q^n$, and the union of all interior and boundary faces in $\mathcal{E}^n$ that are not on $\Omega_n \cup \Omega_{n+1}$ is denoted by Γ_Q^n. On the other hand, faces on Ω_n and Ω_{n+1} are denoted by $\mathcal{F}_\Omega^n(t_n)$ and $\mathcal{F}_\Omega^n(t_{n+1})$, respectively. Finally, $\partial\mathcal{E}_S^n(t_n)$ denotes the set of edges $e \in \partial\mathcal{E}_S^n$ at $t = t_n$.

3.1.2 Finite element spaces

For triangular prismatic space-time elements we introduce the following local spaces:

$$W_h(\mathcal{K}) := P_p(K) \otimes P_p(I_n), \tag{3.2a}$$

$$\boldsymbol{V}_h(\mathcal{K}) := \left[P_p(K) \otimes P_p(I_n)\right]^2, \tag{3.2b}$$

$$M_h(\mathcal{F}) := Q_p(\mathcal{F}) \qquad \forall \mathcal{F} \subset \mathcal{Q}_\mathcal{K}, \tag{3.2c}$$

where $P_p(D)$ is the space of polynomials of degree at most p on a domain D and $Q_p(D)$ denotes the tensor-product polynomials of degree p. The global finite element spaces are then defined as:

$$W_h := \left\{w \in L^2(\mathcal{E}^n) \,:\, w|_\mathcal{K} \in W_h(\mathcal{K}),\, \forall \mathcal{K} \in \mathcal{T}^n\right\}, \tag{3.3a}$$

$$\boldsymbol{V}_h := \left\{\boldsymbol{v} \in \left[L^2(\mathcal{E}^n)\right]^2 \,:\, \boldsymbol{v}|_\mathcal{K} \in \boldsymbol{V}_h(\mathcal{K}),\, \forall \mathcal{K} \in \mathcal{T}^n\right\}, \tag{3.3b}$$

$$M_h := \left\{\mu \in L^2(\Gamma_Q^n) : \mu|_\mathcal{F} \in M_h(\mathcal{F}),\, \forall \mathcal{F} \in \mathcal{F}_Q^n\right\}. \tag{3.3c}$$

For scalar functions we introduce the following inner-products:

$$\begin{aligned} \big(v, w\big)_\mathcal{K} &= \int_\mathcal{K} vw \,\mathrm{d}\mathcal{K}, \quad \langle v, w\rangle_\mathcal{Q} = \int_\mathcal{Q} vw \,\mathrm{d}\mathcal{Q}, \quad \langle v, w\rangle_{K_j^n} = \int_{K_j^n} vw \,\mathrm{d}K, \\ \langle\!\langle v, w\rangle\!\rangle_e &= \int_e vw \,\mathrm{d}e, \qquad \langle v, w\rangle_\mathcal{F} = \int_\mathcal{F} vw \,\mathrm{d}\mathcal{F}, \end{aligned} \tag{3.4}$$

and

$$\begin{aligned} \big(v, w\big)_{\mathcal{T}^n} &= \sum_{\mathcal{K}\in\mathcal{T}^n} \big(v, w\big)_\mathcal{K}, \qquad \langle v, w\rangle_{\mathcal{F}_\mathcal{Q}^n} = \sum_{\mathcal{K}\in\mathcal{T}^n} \langle v, w\rangle_\mathcal{Q}, \\ \langle v, w\rangle_{\mathcal{F}_\Omega^n(t_n)} &= \sum_{\mathcal{K}\in\mathcal{T}^n} \langle v, w\rangle_{K_j^n}, \quad \langle\!\langle v, w\rangle\!\rangle_{\partial\mathcal{E}_S^n(t_n)} = \sum_{e\in\partial\mathcal{E}_S^n(t_n)} \langle\!\langle v, w\rangle\!\rangle_e, \\ \langle v, w\rangle_{\mathcal{F}_S^n} &= \sum_{\mathcal{F}\in\mathcal{F}_S^n} \langle v, w\rangle_\mathcal{F}. \end{aligned} \tag{3.5}$$

Similar notation is used for vector functions, for example,

$$\left(\boldsymbol{v},\boldsymbol{w}\right)_{\mathcal{K}} = \int_{\mathcal{K}} \boldsymbol{v}\cdot\boldsymbol{w}\,\mathrm{d}\mathcal{K} \qquad \text{and} \qquad \left(\boldsymbol{v},\boldsymbol{w}\right)_{\mathcal{T}^n} = \sum_{\mathcal{K}\in\mathcal{T}^n} \left(\boldsymbol{v},\boldsymbol{w}\right)_{\mathcal{K}}. \tag{3.6}$$

The L^2-norm of a function v on a domain D will be denoted by $\|v\|_D$.

3.2 The finite element variational formulation

In this section we derive the space-time HDG discretization for eq. (3.1) on a space-time slab $\mathcal{E}^n$. To be able to show existence and uniqueness of a solution to our discretization we use weighted inner products, as done originally for the wave equation in [27].

Let f_n be a weight function, depending only on time, which is defined as $f_n(t) = e^{-\alpha(t-t_n)}$, $\alpha > 0$. Multiply eq. (3.1a) by $\boldsymbol{r}_h f_n$, where $\boldsymbol{r}_h \in \boldsymbol{V}_h$ and eq. (3.1b) by $w_h f_n$, where $w_h \in W_h$. Integrate both equations over a space-time element $\mathcal{K} \in \mathcal{T}_h^n$ and replace $\boldsymbol{q}$ by $\boldsymbol{q}_h \in \boldsymbol{V}_h$ and v by $v_h \in W_h$. Sum over all space-time elements in $\mathcal{E}^n$ to obtain:

$$\left(\partial_t \boldsymbol{q}_h, \boldsymbol{r}_h f_n\right)_{\mathcal{T}_h^n} - \left(\nabla v_h, \boldsymbol{r}_h f_n\right)_{\mathcal{T}_h^n} = 0, \tag{3.7a}$$

$$\left(w_h f_n, \nabla\cdot\boldsymbol{q}_h\right)_{\mathcal{T}_h^n} = 0. \tag{3.7b}$$

Integrating by parts both equations in space-time we obtain

$$\begin{aligned} -\left(\boldsymbol{q}_h, f_n\partial_t \boldsymbol{r}_h\right)_{\mathcal{T}_h^n} - \left(\boldsymbol{q}_h, \boldsymbol{r}_h f_n'\right)_{\mathcal{T}_h^n} + \langle\widehat{\boldsymbol{q}}_h, \boldsymbol{r}_h f_n\rangle_{\mathcal{F}_\Omega^n(t_{n+1})} \\ - \langle\widehat{\boldsymbol{q}}_h, \boldsymbol{r}_h f_n\rangle_{\mathcal{F}_\Omega^n(t_n)} + \left(v_h, f_n\nabla\cdot\boldsymbol{r}_h\right)_{\mathcal{T}_h^n} - \langle\widehat{v}_h, \boldsymbol{r}_h\cdot\boldsymbol{n} f_n\rangle_{\mathcal{F}_\mathcal{Q}^n} = 0, \end{aligned} \tag{3.8a}$$

and

$$-\left(\boldsymbol{q}_h, f_n\nabla w_h\right)_{\mathcal{T}_h^n} + \langle\widehat{\boldsymbol{q}}_h\cdot\boldsymbol{n}, w_h f_n\rangle_{\mathcal{F}_\mathcal{Q}^n} = 0, \tag{3.8b}$$

where we used that $\hat{\boldsymbol{n}} = (1,0)$ on K_j^{n+1}, $\hat{\boldsymbol{n}} = (-1,0)$ on K_j^n and $\hat{\boldsymbol{n}} = (0,\boldsymbol{n})$ on $\mathcal{Q}$. The numerical traces $\widehat{v}_h$ and $\widehat{\boldsymbol{q}}_h$ introduced in eq. (3.8) are approximations to, respectively, v and $\boldsymbol{q}$ over $\partial\mathcal{K}$. They are defined as:

$$\widehat{v}_h = \lambda_h \qquad \text{on } \Gamma_\mathcal{Q}^n, \tag{3.9a}$$

$$\widehat{\boldsymbol{q}}_h = \boldsymbol{q}_h - \tau\left(v_h - \lambda_h\right)\boldsymbol{n} \qquad \text{on } \Gamma_\mathcal{Q}^n, \tag{3.9b}$$

$$\widehat{\boldsymbol{q}}_h = \boldsymbol{q}_h^- \qquad \text{on } K_j^n, \tag{3.9c}$$

$$\widehat{\boldsymbol{q}}_h = \boldsymbol{q}_h \qquad \text{on } K_j^{n+1}, \tag{3.9d}$$

where $\lambda_h \in M_h$ is the facet approximation to v, $\tau > 0$ is a stabilization parameter, and $\boldsymbol{q}_h^-$ denotes the trace of $\boldsymbol{q}_h$ at $x_0 = t_n$ from the previous space-time slab $\mathcal{E}^{n-1}$, or the initial condition if $n = 1$. Note that the numerical flux eq. (3.9b) is the same as in eq. (2.9), whereas eq. (3.9c) and eq. (3.9d) correspond to an upwind flux in time.

Normal continuity of the numerical flux $\widehat{\boldsymbol{q}}_h$ across element boundaries is ensured by imposing

$$\langle \mu_h f_n, \widehat{\boldsymbol{q}}_h \cdot \boldsymbol{n} \rangle_{\mathcal{F}_{\mathcal{Q}}^n} = -\langle \mu_h f_n, \partial_t \lambda_h \rangle_{\mathcal{F}_{\mathcal{S}}^n}, \quad \forall \mu_h \in M_h. \tag{3.10}$$

Substituting the expressions for the numerical traces eq. (3.9) into eq. (3.8) and eq. (3.10), integrating eq. (3.8b) by parts in space and eq. (3.10) by parts in time results in the space-time HDG method for the linear free-surface problem: Find $(\boldsymbol{q}_h, v_h, \lambda_h) \in \boldsymbol{V}_h \times W_h \times M_h$ such that for all $(\boldsymbol{r}_h, w_h, \mu_h) \in \boldsymbol{V}_h \times W_h \times M_h$ the following relations are satisfied:

$$\begin{aligned} -\left(\boldsymbol{q}_h, f_n \partial_t \boldsymbol{r}_h\right)_{\mathcal{T}_h^n} - \left(\boldsymbol{q}_h, \boldsymbol{r}_h f_n'\right)_{\mathcal{T}_h^n} + \langle \boldsymbol{q}_h, \boldsymbol{r}_h f_n \rangle_{\mathcal{F}_\Omega^n(t_{n+1})} \\ + \left(v_h, f_n \nabla \cdot \boldsymbol{r}_h\right)_{\mathcal{T}_h^n} - \langle \lambda_h, \boldsymbol{r}_h \cdot \boldsymbol{n} f_n \rangle_{\mathcal{F}_{\mathcal{Q}}^n} = \langle \boldsymbol{q}_h^-, \boldsymbol{r}_h f_n \rangle_{\mathcal{F}_\Omega^n(t_n)}, \end{aligned} \tag{3.11a}$$

$$-\left(w_h, f_n \nabla \cdot \boldsymbol{q}_h\right)_{\mathcal{T}_h^n} + \langle \tau \left(v_h - \lambda_h\right), w_h f_n \rangle_{\mathcal{F}_{\mathcal{Q}}^n} = 0, \tag{3.11b}$$

and

$$\begin{aligned} \langle \boldsymbol{q}_h \cdot \boldsymbol{n} - \tau \left(v_h - \lambda_h\right), \mu_h f_n \rangle_{\mathcal{F}_{\mathcal{Q}}^n} - \langle \lambda_h f_n, \partial_t \mu_h \rangle_{\mathcal{F}_{\mathcal{S}}^n} \\ - \langle \lambda_h, \mu_h f_n' \rangle_{\mathcal{F}_{\mathcal{S}}^n} + \langle\!\langle \lambda_h, \mu_h f_n \rangle\!\rangle_{\partial\mathcal{E}_{\mathcal{S}}^n(t_{n+1})} = \langle\!\langle \lambda_h^-, \mu_h f_n \rangle\!\rangle_{\partial\mathcal{E}_{\mathcal{S}}^n(t_n)}, \quad \forall \mu_h \in M_h, \end{aligned} \tag{3.11c}$$

where λ_h^- denotes the known value of v_h $(= \lambda_h)$ at $x_0 = t_n$ from the previous space–time slab $\mathcal{E}^{n-1}$, or the initial condition if $n = 0$.

3.2.1 Well posedness

We now show the existence of a unique solution to the space-time HDG method eq. (3.11).

Theorem 3.1 (Existence and uniqueness)**.** *A unique solution* $(\boldsymbol{q}_h, v_h, \lambda_h) \in \boldsymbol{V}_h \times W_h \times M_h$ *to eq.* (3.11) *exists if the stabilization parameter* τ *is positive.*

Proof. It is sufficient to show that if the data is equal to zero, the only solution to eq. (3.11) is the trivial one. We only need to show this for an arbitrary space-time slab $\mathcal{E}^n$ assuming $\lambda_h^- = 0$ and $\boldsymbol{q}_h^- = 0$.

Take $\boldsymbol{r}_h = \boldsymbol{q}_h$ in eq. (3.11a), $w_h = v_h$ in eq. (3.11b) and $\mu_h = \lambda_h$ in eq. (3.11c), and add the three equations together:

$$\begin{aligned} -\left(\boldsymbol{q}_h, f_n \partial_t \boldsymbol{q}_h\right)_{\mathcal{T}^n} - \left(|\boldsymbol{q}_h|^2, f_n'\right)_{\mathcal{T}^n} + \langle |\boldsymbol{q}_h|^2, f_n \rangle_{\mathcal{F}_\Omega^n(t_{n+1})} \\ + \langle \tau \left(v_h - \lambda_h\right)^2, f_n \rangle_{\mathcal{F}_\mathcal{Q}^n} - \langle \lambda_h f_n, \partial_t \lambda_h \rangle_{\mathcal{F}_\mathcal{S}^n} - \langle \lambda_h^2, f_n' \rangle_{\mathcal{F}_\mathcal{S}^n} \\ + \langle\!\langle \lambda_h^2, f_n \rangle\!\rangle_{\partial \mathcal{E}_\mathcal{S}^n(t_{n+1})} = 0. \end{aligned} \tag{3.12}$$

Note that since $\boldsymbol{q}_h \cdot \partial_t \boldsymbol{q}_h = \frac{1}{2}\partial_t(|\boldsymbol{q}_h|^2)$, we may write the first term on the left hand side, after integration by parts in time, as

$$-\left(\boldsymbol{q}_h, f_n \partial_t \boldsymbol{q}_h\right)_{\mathcal{T}^n} = \tfrac{1}{2}\left(|\boldsymbol{q}_h|^2, f_n'\right)_{\mathcal{T}^n} - \tfrac{1}{2}\langle |\boldsymbol{q}_h|^2, f_n \rangle_{\mathcal{F}_\Omega^n(t_{n+1})} + \tfrac{1}{2}\langle |\boldsymbol{q}_h|^2, f_n \rangle_{\mathcal{F}_\Omega^n(t_n)}. \tag{3.13}$$

Similarly, the fifth term on the left hand side of eq. (3.12) may be written as

$$-\langle \lambda_h f_n, \partial_t \lambda_h \rangle_{\mathcal{F}_\mathcal{S}^n} = \tfrac{1}{2}\langle \lambda_h^2, f_n' \rangle_{\mathcal{F}_\mathcal{S}^n} - \tfrac{1}{2}\langle\!\langle \lambda_h^2, f_n \rangle\!\rangle_{\partial \mathcal{E}_\mathcal{S}^n(t_{n+1})} + \tfrac{1}{2}\langle\!\langle \lambda_h^2, f_n \rangle\!\rangle_{\partial \mathcal{E}_\mathcal{S}^n(t_n)}. \tag{3.14}$$

Combining eq. (3.12)–eq. (3.14), we obtain

$$\begin{aligned} 0 = -\tfrac{1}{2}\left(|\boldsymbol{q}_h|^2, f_n'\right)_{\mathcal{T}^n} + \tfrac{1}{2}\langle |\boldsymbol{q}_h|^2, f_n \rangle_{\mathcal{F}_\Omega^n(t_{n+1})} \\ + \tfrac{1}{2}\langle |\boldsymbol{q}_h|^2, f_n \rangle_{\mathcal{F}_\Omega^n(t_n)} + \langle \tau \left(v_h - \lambda_h\right)^2, f_n \rangle_{\mathcal{F}_\mathcal{Q}^n} \\ - \tfrac{1}{2}\langle \lambda_h^2, f_n' \rangle_{\mathcal{F}_\mathcal{S}^n} + \tfrac{1}{2}\langle\!\langle \lambda_h^2, f_n \rangle\!\rangle_{\partial \mathcal{E}_\mathcal{S}^n(t_{n+1})} + \tfrac{1}{2}\langle\!\langle \lambda_h^2, f_n \rangle\!\rangle_{\partial \mathcal{E}_\mathcal{S}^n(t_n)}. \end{aligned} \tag{3.15}$$

Since $\tau > 0$, $f_n > 0, \forall t$, and $f_n' < 0, \forall t$, we conclude that $\boldsymbol{q}_h = 0$ in $\mathcal{E}^n$ and on $K_j^n \cup K_j^{n+1}$, $v_h = \lambda_h$ on $\Gamma_\mathcal{Q}^n$, and $\lambda_h = 0$ on $\Gamma_\mathcal{S}^n$ and on $\partial\mathcal{E}_\mathcal{S}^n(t_n) \cup \partial\mathcal{E}_\mathcal{S}^n(t_{n+1})$. Substituting into eq. (3.11a),

$$\begin{aligned} 0 &= \left(v_h, f_n \nabla \cdot \boldsymbol{r}_h\right)_{\mathcal{T}^n} - \langle \lambda_h, \boldsymbol{r}_h \cdot \boldsymbol{n} f_n \rangle_{\mathcal{F}_\mathcal{Q}^n} \\ &= -\left(\nabla v_h, f_n \boldsymbol{r}_h\right)_{\mathcal{T}^n} + \langle \left(v_h - \lambda_h\right), \boldsymbol{r}_h \cdot \boldsymbol{n} f_n \rangle_{\mathcal{F}_\mathcal{Q}^n} \\ &= -\left(\nabla v_h, f_n \boldsymbol{r}_h\right)_{\mathcal{T}^n}, \end{aligned} \tag{3.16}$$

which holds for all $\boldsymbol{r}_h \in \boldsymbol{V}_h$. Since $f_n > 0$ we conclude that $\nabla v_h = 0$ in $\mathcal{E}^n$, implying that v_h depends only on time. To show that $v_h = 0$ in $\mathcal{E}^n$, consider the following. Since v_h depends only on time, then v_h is constant on $\Omega \times \{t\}$, for all $t \in (t_n, t_{n+1})$. In addition, $v_h = \lambda_h = 0$ on $\Gamma_\mathcal{S}^n$, so $v_h = 0$ on $\mathcal{E}^n$. □

3.3 Analysis tools

In this section, we develop some of the tools needed to perform the error analysis in section 3.4.

3.3.1 Notation and anisotropic Sobolev spaces

Let the multi-index α be a vector of non-negative integers α_i and let $|\alpha|$ be defined as $|\alpha| = \sum_i \alpha_i$. By $D^\alpha v$ we denote the partial derivative of order $|\alpha|$ of v, i.e.,

$$D^\alpha v = \partial_{x_0}^{\alpha_0} \partial_{x_1}^{\alpha_1} \partial_{x_2}^{\alpha_2} v. \tag{3.17}$$

We define the Sobolev space $H^s(\Omega) = \left\{ v \in L^2(\Omega) : D^\alpha v \in L^2(\Omega) \text{ for } |\alpha| \leq s \right\}$. This space is equipped with the following norm and seminorm:

$$\|v\|_{H^s(\Omega)}^2 = \sum_{|\alpha| \leq s} \|D^\alpha v\|_{L^2(\Omega)}^2 \qquad \text{and} \qquad |v|_{H^s(\Omega)}^2 = \sum_{|\alpha| = s} \|D^\alpha v\|_{L^2(\Omega)}^2 . \tag{3.18}$$

For $\alpha_i \geq 0$, $i = 0, 1, 2$, we introduce the anisotropic Sobolev space of order (s_t, s_s) on $\mathcal{E} \subset \mathbb{R}^3$ by

$$H^{(s_t, s_s)}(\mathcal{E}) = \left\{ v \in L^2(\mathcal{E}) : D^{(\alpha_t, \alpha_s)} v \in L^2(\mathcal{E}) \text{ for } \alpha_t \leq s_t,\, |\alpha_s| \leq s_s \right\}, \tag{3.19}$$

where $\alpha_t = \alpha_0$ and $\alpha_s = (\alpha_1, \alpha_2)$ and $D^{(\alpha_t, \alpha_s)} v = \partial_{x_0}^{\alpha_t} \partial_{x_1}^{\alpha_1} \partial_{x_2}^{\alpha_2} v$. The anisotropic Sobolev norm and seminorm are given by, respectively,

$$\|v\|_{H^{(s_t, s_s)}(\mathcal{E})}^2 = \sum_{\substack{\alpha_t \leq s_t \\ |\alpha_s| \leq s_s}} \left\| D^{(\alpha_t, \alpha_s)} v \right\|_{L^2(\mathcal{E})}^2 \text{ and } |v|_{H^{(s_t, s_s)}(\mathcal{E})}^2 = \sum_{\substack{\alpha_t = s_t \\ |\alpha_s| = s_s}} \left\| D^{(\alpha_t, \alpha_s)} v \right\|_{L^2(\mathcal{E})}^2 . \tag{3.20}$$

Let $\mathcal{K}$ denote any space-time prism that is constructed as $\mathcal{K} = K \times I$, where K is a spatial triangular element and I is an interval. Let h_K and ρ_K denote, respectively, the radii of the 2-dimensional circumcircle and inscribed circle of K. We will assume spatial shape regularity, i.e., we assume there exists a constant $c_r > 0$ such that

$$\frac{h_K}{\rho_K} \leq c_r, \quad \forall \mathcal{K} \in \mathcal{T}^n. \tag{3.21}$$

Additionally, we assume that $\mathcal{T}^n$ does not have any hanging nodes. Throughout the remainder of this chapter we will denote by $C > 0$ a generic constant that is independent of h_K and Δt.

3.3.2 Space-time mappings

Let $\widehat{K}$ denote the reference triangle defined by the vertices $(0, 0)$, $(1, 0)$, $(0, 1)$, and with reference coordinates $\widehat{\boldsymbol{x}} = (\widehat{x}_1, \widehat{x}_2)$. Furthermore, let H_K denote the affine mapping $H_K : \widehat{K} \to K$ defined as $H_K(\widehat{\boldsymbol{x}}) = B_K \widehat{\boldsymbol{x}} + \boldsymbol{c}$, where B_K is a matrix and $\boldsymbol{c}$ is a vector.

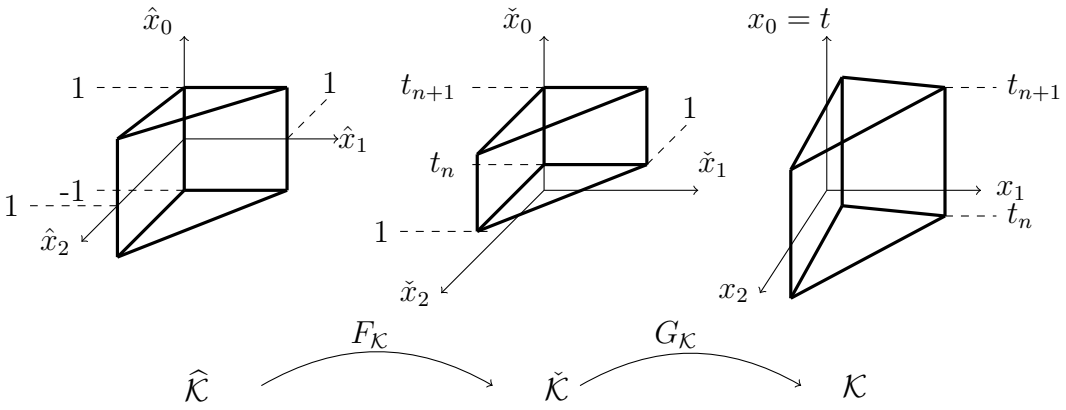

Figure 3.2: An illustration of the different space-time mappings.

To construct each space-time prism we follow a similar approach as [75]. Consider a reference prism $\widehat{\mathcal{K}}$ defined by the vertices $(-1,0,0)$, $(-1,1,0)$, $(-1,0,1)$, $(1,0,0)$, $(1,1,0)$, $(1,0,1)$. The reference coordinates in $\widehat{\mathcal{K}}$ are denoted by $(\widehat{x}_0, \widehat{\boldsymbol{x}})$. The space-time prism $\mathcal{K}$ is obtained as follows. First, we construct an intermediate element $\check{\mathcal{K}}$ from an affine mapping $F_{\mathcal{K}} : \widehat{\mathcal{K}} \mapsto \check{\mathcal{K}}$ defined as $F_{\mathcal{K}}(\widehat{x}_0, \widehat{\boldsymbol{x}}) = A_{\mathcal{K}} [\widehat{x}_0, \widehat{\boldsymbol{x}}]^T + \boldsymbol{b}$, where $A_{\mathcal{K}} = \text{diag}\left(\frac{\Delta t}{2}, 1, 1\right)$ and $\boldsymbol{b}$ is a vector of the form $[b_0, 0, 0]^T$, where $b_0 \in \mathbb{R}$. The coordinates on $\check{\mathcal{K}}$ are $(\check{x}_0, \check{\boldsymbol{x}})$. Then, $\mathcal{K}$ is obtained via the affine mapping, $G_{\mathcal{K}} : \check{\mathcal{K}} \mapsto \mathcal{K}$ defined as:

$$G_{\mathcal{K}}(\check{x}_0, \check{\boldsymbol{x}}) = \begin{bmatrix} 1 & \mathbf{0} \\ \mathbf{0}^T & B_K \end{bmatrix} \begin{bmatrix} \check{x}_0 \\ \check{\boldsymbol{x}} \end{bmatrix} + \begin{bmatrix} 0 \\ \boldsymbol{c} \end{bmatrix}, \tag{3.22}$$

where $\mathbf{0} = [0,0]$ and B_K denotes the matrix associated with the mapping H_K defined above. See fig. 3.2.

We denote by $\partial\widehat{\mathcal{K}}_1$ the boundary face of $\widehat{\mathcal{K}}$ with $\widehat{x}_1 = 0$. Similarly, $\partial\widehat{\mathcal{K}}_2$ and $\partial\widehat{\mathcal{K}}_3$ are the boundary faces of $\widehat{\mathcal{K}}$ with, respectively, $\widehat{x}_2 = 0$ and $\widehat{x}_1 + \widehat{x}_2 = 1$. By $\partial\widehat{\mathcal{K}}_0$ we denote the boundary faces of $\widehat{\mathcal{K}}$ with $\widehat{x}_0 = -1$ and $\widehat{x}_0 = 1$. Furthermore, $\partial\check{\mathcal{K}}_i$, $i = 0, 1, 2, 3$, will denote the boundary faces of $\check{\mathcal{K}}$ which are obtained by applying the transformation $F_{\mathcal{K}}$ to $\widehat{\mathcal{K}}$.

3.3.3 Trace and inverse trace identities

In this section we prove anisotropic trace and inverse trace identities. This is achieved by first considering different scaling identities. Similar identities were shown on hexahedra in [32, 75], but are modified here for prisms.

Lemma 3.1. *Let $\check{u} \in H^{(s_t,s_s)}(\check{\mathcal{K}})$, $\alpha_t = \alpha_0$, $\alpha_s = (\alpha_1, \alpha_2)$, and $\alpha = (\alpha_t, \alpha_s)$. Then, the following identities hold for $\alpha = (\alpha_t, \alpha_s)$, $\alpha_i \geq 0$, $i = 0, 1, 2$,*

$$\|\check{D}^{\alpha}\check{u}\|^2_{\check{\mathcal{K}}} = \left(\frac{2}{\Delta t}\right)^{2\alpha_0 - 1} \|\widehat{D}^{\alpha}\widehat{u}\|^2_{\widehat{\mathcal{K}}}\,, \tag{3.23a}$$

$$\|\check{D}^{\alpha}\check{u}\|^2_{\partial\check{\mathcal{K}}_0} = \left(\frac{2}{\Delta t}\right)^{2\alpha_0} \|\widehat{D}^{\alpha}\widehat{u}\|^2_{\partial\widehat{\mathcal{K}}_0}\,, \tag{3.23b}$$

$$\|\check{D}^{\alpha}\check{u}\|^2_{\partial\check{\mathcal{K}}_j} = \left(\frac{2}{\Delta t}\right)^{2\alpha_0 - 1} \|\widehat{D}^{\alpha}\widehat{u}\|^2_{\partial\widehat{\mathcal{K}}_j}\,, \quad j = 1, 2, 3, \tag{3.23c}$$

where $\widehat{u} = \check{u} \circ F_{\mathcal{K}}$.

Proof. Note that by the chain rule,

$$\check{D}^{\alpha}\check{u} = \left(\frac{2}{\Delta t}\right)^{\alpha_0} \widehat{D}^{\alpha}\left(\check{u} \circ F_{\mathcal{K}}\right) \circ F_{\mathcal{K}}^{-1}. \tag{3.24}$$

We first show eq. (3.23a). By eq. (3.24)

$$\|\check{D}^{\alpha}\check{u}\|^2_{\check{\mathcal{K}}} = \left(\frac{2}{\Delta t}\right)^{2\alpha_0} \int_{\check{\mathcal{K}}} \left(\widehat{D}^{\alpha}\left(\check{u} \circ F_{\mathcal{K}}\right) \circ F_{\mathcal{K}}^{-1}\right)^2 \mathrm{d}\check{x}_0\, \mathrm{d}\check{\boldsymbol{x}}. \tag{3.25}$$

Changing variables, we obtain

$$\begin{aligned}
\|\check{D}^{\alpha}\check{u}\|^2_{\check{\mathcal{K}}} &= \left(\frac{2}{\Delta t}\right)^{2\alpha_0} \int_{\widehat{\mathcal{K}}} \left(\widehat{D}^{\alpha}\left(\check{u} \circ F_{\mathcal{K}}\right) \circ F_{\mathcal{K}}^{-1} \circ F_{\mathcal{K}}\right)^2 |\det A_{\mathcal{K}}|\, \mathrm{d}\widehat{x}_0\, \mathrm{d}\widehat{\boldsymbol{x}} \\
&= \left(\frac{2}{\Delta t}\right)^{2\alpha_0} \int_{\widehat{\mathcal{K}}} \left(\widehat{D}^{\alpha}\left(\check{u} \circ F_{\mathcal{K}}\right)\right)^2 |\det A_{\mathcal{K}}|\, \mathrm{d}\widehat{x}_0\, \mathrm{d}\widehat{\boldsymbol{x}} \\
&= \left(\frac{2}{\Delta t}\right)^{2\alpha_0} \frac{\Delta t}{2} \int_{\widehat{\mathcal{K}}} \left(\widehat{D}^{\alpha}\widehat{u}\right)^2 \mathrm{d}\widehat{x}_0\, \mathrm{d}\widehat{\boldsymbol{x}} \\
&= \left(\frac{2}{\Delta t}\right)^{2\alpha_0 - 1} \|\widehat{D}^{\alpha}\widehat{u}\|^2_{\widehat{\mathcal{K}}}\,.
\end{aligned} \tag{3.26}$$

To show eq. (3.23b) we note that time is fixed on $\partial\check{\mathcal{K}}_0$. Furthermore, since $\check{\boldsymbol{x}} = \widehat{\boldsymbol{x}}$ we note that for any function $\check{v}$ on $\check{\mathcal{K}}$ we have $\check{v}(t_{n+1}, \check{\boldsymbol{x}}) = \widehat{v}(1, \widehat{\boldsymbol{x}})$, i.e., $\check{v}|_{\partial\check{\mathcal{K}}_0} = \widehat{v}|_{\partial\widehat{\mathcal{K}}_0}$. In particular, if $\check{v} = \check{D}^{\alpha}\check{u}$,

$$\left(\check{D}^{\alpha}\check{u}\right)|_{\partial\check{\mathcal{K}}_0} = \left(\frac{2}{\Delta t}\right)^{\alpha_0} \left(\widehat{D}^{\alpha}\left(\check{u} \circ F_{\mathcal{K}}\right)\right)|_{\partial\widehat{\mathcal{K}}_0}. \tag{3.27}$$

Therefore,

$$\begin{aligned}\|\check{D}^{\alpha}\check{u}\|^2_{\partial\check{\mathcal{K}}_0} &= \int_{\partial\check{\mathcal{K}}_0} \left(\check{D}^{\alpha}\check{u}\right)^2 \mathrm{d}\check{\boldsymbol{x}} \\ &= \left(\frac{2}{\Delta t}\right)^{2\alpha_0} \int_{\partial\widehat{\mathcal{K}}_0} \left(\widehat{D}^{\alpha}\widehat{u}\right)^2 \mathrm{d}\widehat{\boldsymbol{x}} \\ &= \left(\frac{2}{\Delta t}\right)^{2\alpha_0} \|\widehat{D}^{\alpha}\widehat{u}\|^2_{\partial\widehat{\mathcal{K}}_0},\end{aligned} \tag{3.28}$$

which concludes the proof for eq. (3.23b).

Finally, we prove eq. (3.23c) for $j = 1$. The proofs for $j = 2, 3$ are analogous. First let us define the mapping $J_{\partial\mathcal{K}}$ that maps $\partial\widehat{\mathcal{K}}_1$ onto $\partial\check{\mathcal{K}}_1$. This mapping is given by

$$J_{\partial\mathcal{K}}(\widehat{x}_0, \widehat{x}_2) = \begin{bmatrix} \frac{\Delta t}{2} & 0 \\ 0 & 1 \end{bmatrix} \begin{bmatrix} \widehat{x}_0 \\ \widehat{x}_2 \end{bmatrix} + \boldsymbol{d}, \tag{3.29}$$

where $\boldsymbol{d}$ is a constant two dimensional vector. Then, by the chain rule,

$$\begin{aligned}\left(\check{D}^{\alpha}\check{u}\right)|_{\partial\check{\mathcal{K}}_1} &= \left(\check{D}^{\alpha}\check{u}\right)(\check{x}_0, 0, \check{x}_2) \\ &= \left(\frac{2}{\Delta t}\right)^{\alpha_0} \left(\widehat{D}^{\alpha}\left(\check{u}\circ F_{\mathcal{K}}\right)\right)|_{\partial\widehat{\mathcal{K}}_1} \circ J^{-1}_{\partial\mathcal{K}} \\ &= \left(\frac{2}{\Delta t}\right)^{\alpha_0} \left[\left(\widehat{D}^{\alpha}\left(\check{u}\circ F_{\mathcal{K}}\right)\right)(\widehat{x}_0, 0, \widehat{x}_2)\right] \circ J^{-1}_{\partial\mathcal{K}}.\end{aligned} \tag{3.30}$$

We now find:

$$\begin{aligned}\|\check{D}^{\alpha}\check{u}\|^2_{\partial\check{\mathcal{K}}_1} &= \int_{\partial\check{\mathcal{K}}_1} \left(\check{D}^{\alpha}\check{u}\right)^2 \mathrm{d}\check{x}_0\,\mathrm{d}\check{x}_2 \\ &= \left(\frac{2}{\Delta t}\right)^{2\alpha_0} \int_{\partial\check{\mathcal{K}}_1} \left(\left[\left(\widehat{D}^{\alpha}\left(\check{u}\circ F_{\mathcal{K}}\right)\right)(\widehat{x}_0, 0, \widehat{x}_2)\right] \circ J^{-1}_{\partial\mathcal{K}}\right)^2 \mathrm{d}\check{x}_0\,\mathrm{d}\check{x}_2.\end{aligned} \tag{3.31}$$

Note that the determinant of the Jacobian of $J_{\partial\mathcal{K}}$ is $\Delta t/2$. Changing variables,

$$\begin{aligned}\|\check{D}^{\alpha}\check{u}\|^2_{\partial\check{\mathcal{K}}_1} &= \left(\frac{2}{\Delta t}\right)^{2\alpha_0} \frac{\Delta t}{2} \int_{\partial\widehat{\mathcal{K}}_1} \left(\left(\widehat{D}^{\alpha}\widehat{u}\right)(\widehat{x}_0, 0, \widehat{x}_2)\right)^2 \mathrm{d}\widehat{x}_0\,\mathrm{d}\widehat{x}_2 \\ &= \left(\frac{2}{\Delta t}\right)^{2\alpha_0-1} \int_{\partial\widehat{\mathcal{K}}_1} \left(\left(\widehat{D}^{\alpha}\widehat{u}\right)(\widehat{x}_0, 0, \widehat{x}_2)\right)^2 \mathrm{d}\widehat{x}_0\,\mathrm{d}\widehat{x}_2 \\ &= \left(\frac{2}{\Delta t}\right)^{2\alpha_0-1} \|\widehat{D}^{\alpha}\widehat{u}\|^2_{\partial\widehat{\mathcal{K}}_1}.\end{aligned} \tag{3.32}$$

The result follows. □

In what follows we use the following inequalities that can be shown by standard scaling arguments:

$$|\det B_K| \le C h_K^2, \tag{3.33a}$$
$$\|\tilde{u}\|_{\tilde{F}}^2 \le C h_K^{-1} \|u\|_{F_K}^2 , \tag{3.33b}$$
$$\|u\|_{F_K}^2 \le C h_K \|\tilde{u}\|_{\tilde{F}}^2 , \tag{3.33c}$$

where $F_K \in \partial K$, and where $\tilde{u} = \widehat{u}$ and $\tilde{F} = F_{\widehat{K}} \in \partial \widehat{K}$, or $\tilde{u} = \check{u}$ and $\tilde{F} = F_{\check{K}} \in \partial \check{K}$.

Lemma 3.2. *Let $u \in H^{(s_t,s_s)}(\mathcal{K})$. The following inequalities hold*

$$\|u\|_{\mathcal{K}}^2 \le C h_K^2 \, \|\check{u}\|_{\check{\mathcal{K}}}^2 , \tag{3.34a}$$
$$\|\check{u}\|_{\check{\mathcal{K}}}^2 \le C h_K^{-2} \, \|u\|_{\mathcal{K}}^2 , \tag{3.34b}$$
$$\|\check{u}\|_{\mathcal{F}_{\check{\mathcal{K}}}}^2 \le C h_K^{-1} \, \|u\|_{\mathcal{F}_{\mathcal{K}}}^2 , \tag{3.34c}$$

where $\check{u} = u \circ G_{\mathcal{K}}$, $\mathcal{F}_{\check{\mathcal{K}}} \in \mathcal{Q}_{\check{\mathcal{K}}}$, and $\mathcal{F}_{\mathcal{K}} \in \mathcal{Q}_{\mathcal{K}}$.

Proof. We begin by proving eq. (3.34a).

$$\begin{aligned}
\|u\|_{\mathcal{K}}^2 &= \int_{\mathcal{K}} \left(\left(u \circ G_{\mathcal{K}} \right) \circ G_{\mathcal{K}}^{-1} \right)^2 \mathrm{d}x_0 \, \mathrm{d}\boldsymbol{x} \\
&= \int_{\check{\mathcal{K}}} \left(u \circ G_{\mathcal{K}} \right)^2 |\det B_K| \, \mathrm{d}x_0 \, \mathrm{d}\check{\boldsymbol{x}} \\
&\le C h_K^2 \int_{\check{\mathcal{K}}} \check{u}^2 \, \mathrm{d}x_0 \, \mathrm{d}\check{\boldsymbol{x}} \qquad \text{(by eq. (3.33a))} \\
&= C h_K^2 \|\check{u}\|_{\check{\mathcal{K}}}^2 .
\end{aligned} \tag{3.35}$$

The proof of eq. (3.34b) is completely analogous.

Finally, we prove eq. (3.34c). Notice that

$$\|\check{u}\|_{\mathcal{F}_{\check{\mathcal{K}}}}^2 = \int_{t_n}^{t_{n+1}} \|\check{u}\|_{F_{\check{K}}}^2 \, \mathrm{d}\check{x}_0, \tag{3.36}$$

where $F_{\check{K}}$ denotes the face of $\check{K}$ corresponding to $\mathcal{F}_{\check{\mathcal{K}}}$. Then, by eq. (3.33b),

$$\|\check{u}\|_{\mathcal{F}_{\check{\mathcal{K}}}}^2 \le \int_{t_n}^{t_{n+1}} C h_K^{-1} \, \|u\|_{F_K}^2 \, \mathrm{d}\check{x}_0, \tag{3.37}$$

Note that time is left invariant under the mapping from $\check{\mathcal{K}}$ to $\mathcal{K}$. Therefore,

$$\|\check{u}\|^2_{\mathcal{F}_{\check{\mathcal{K}}}} \leq Ch_K^{-1} \int_{t_n}^{t_{n+1}} \|u\|^2_{F_K} \,\mathrm{d}x_0 = Ch_K^{-1} \|u\|^2_{\mathcal{F}_{\mathcal{K}}}\,, \tag{3.38}$$

and the result follows. □

We end this section by stating a continuous and a discrete trace inequalities, and two inverse trace inequalities.

Lemma 3.3 (Continuous trace inequality)**.** *Let $\mathcal{K} = K \times I_n$. For $\phi \in H^{(0,1)}(\mathcal{K})$, the following holds:*

$$\left\|\phi\right\|^2_{\mathcal{Q}_{\mathcal{K}}} \leq C \left(\|\nabla\phi\|_{\mathcal{K}} + h_K^{-1} \|\phi\|_{\mathcal{K}}\right) \|\phi\|_{\mathcal{K}}\,. \tag{3.39}$$

Proof. The proof is analogous to the proof of [24, Lemma 1.49]. □

Lemma 3.4. *Let $X_h(\mathcal{K}) \subset W_h(\mathcal{K})$ be a finite dimensional subspace such that the trace map $\gamma_{\mathcal{F}_{\mathcal{K}}} : X_h(\mathcal{K}) \mapsto M_h(\mathcal{F})$ defined by $\gamma_{\mathcal{F}_{\mathcal{K}}}(v_h) = v_h|_{\mathcal{F}_{\mathcal{K}}}$, for a face $\mathcal{F}_{\mathcal{K}} \subset \mathcal{Q}_{\mathcal{K}}$ is injective, then*

$$\|v_h\|^2_{\mathcal{K}} \leq Ch_K \|v_h\|^2_{\mathcal{F}_{\mathcal{K}}}\,, \quad \forall v_h \in X_h(\mathcal{K}). \tag{3.40}$$

Proof. By eq. (3.34a), we obtain

$$\|v_h\|^2_{\mathcal{K}} \leq Ch_K^2 \|\check{v}_h\|^2_{\check{\mathcal{K}}}\,. \tag{3.41}$$

Since v_h is a polynomial and $\gamma_{\mathcal{F}_{\mathcal{K}}}$ is injective, we have $\|\check{v}_h\|^2_{\check{\mathcal{K}}} \leq C \|\check{v}_h\|^2_{\mathcal{F}_{\check{\mathcal{K}}}}$. Combining this with eq. (3.41), the result follows after using eq. (3.34c). □

Lemma 3.5. *Let $\mathcal{K} = K \times I_n$ be a space-time element in $\mathcal{T}^n$, $\mathcal{F} \subset \partial\mathcal{E}^n_{\mathcal{S}}$ a face on the free-surface boundary and $\partial\mathcal{F}_0$ the two edges of the face $\mathcal{F}$ that are on the time levels. For $v_h \in W_h(\mathcal{K})$ and $\lambda_h \in M_h(\mathcal{F})$, the following inverse trace inequalities hold*

$$\|\lambda_h\|^2_{\partial\mathcal{F}_0} \leq C\Delta t^{-1} \|\lambda_h\|^2_{\mathcal{F}}\,, \tag{3.42a}$$

$$\|v_h\|^2_{\partial\mathcal{K}_0} \leq C\Delta t^{-1} \|v_h\|^2_{\mathcal{K}}\,, \tag{3.42b}$$

$$\|v_h\|^2_{\mathcal{Q}_{\mathcal{K}}} \leq Ch_K^{-1} \|v_h\|^2_{\mathcal{K}}\,. \tag{3.42c}$$

Proof. Since the face $\mathcal{F}$ is a quadrilateral, the proof for eq. (3.42a) can be found, e.g., in [32, Corollary 3.49]. We first show eq. (3.42b). Notice that

$$\begin{aligned}
\|v_h\|^2_{\partial\mathcal{K}_0} &= \|v_h\|^2_{K_j^n} + \|v_h\|^2_{K_j^{n+1}} \\
&= \int_K (v_h(t_n, \boldsymbol{x}))^2 \,\mathrm{d}\boldsymbol{x} + \int_K (v_h(t_{n+1}, \boldsymbol{x}))^2 \,\mathrm{d}\boldsymbol{x} && \text{(by definition)} \\
&\leq Ch_K^2 \int_{\widehat{K}} (\check{v}_h(t_n, \widehat{\boldsymbol{x}}))^2 \,\mathrm{d}\widehat{\boldsymbol{x}} \\
&\qquad + Ch_K^2 \int_{\widehat{K}} (\check{v}_h(t_{n+1}, \widehat{\boldsymbol{x}}))^2 \,\mathrm{d}\widehat{\boldsymbol{x}} && \text{(by eq. (3.33a))} \\
&= Ch_K^2 \,\|\check{v}_h\|^2_{\partial\check{\mathcal{K}}_0} && \text{(by definition)} \\
&= Ch_K^2 \,\|\widehat{v}_h\|^2_{\partial\widehat{\mathcal{K}}_0} && \text{(by eq. (3.23b))} \\
&\leq Ch_K^2 \,\|\widehat{v}_h\|^2_{\widehat{\mathcal{K}}} && (v_h \in W_h(\mathcal{K})) \\
&= Ch_K^2 2\Delta t^{-1} \,\|\check{v}_h\|^2_{\check{\mathcal{K}}} && \text{(by eq. (3.23a))} \\
&\leq C\Delta t^{-1} \,\|v_h\|^2_{\mathcal{K}} && \text{(by eq. (3.33a)).}
\end{aligned} \tag{3.43}$$

In order to show eq. (3.42c), note that

$$\begin{aligned}
\|v_h\|^2_{\mathcal{Q}_\mathcal{K}} &= \int_{t_n}^{t_{n+1}} \|v_h\|^2_{\partial K} \,\mathrm{d}t && \text{(by definition)} \\
&\leq Ch_K \int_{t_n}^{t_{n+1}} \|\check{v}_h\|^2_{\partial\widehat{K}} \,\mathrm{d}t && \text{(by eq. (3.33c))} \\
&= Ch_K \|\check{v}_h\|^2_{\mathcal{Q}_{\check{\mathcal{K}}}} && \text{(by definition)} \\
&= Ch_K \frac{\Delta t}{2} \|\widehat{v}_h\|^2_{\mathcal{Q}_{\widehat{\mathcal{K}}}} && \text{(by eq. (3.23c))} \\
&\leq Ch_K \frac{\Delta t}{2} \|\widehat{v}_h\|^2_{\widehat{\mathcal{K}}} && (v_h \in W_h(\mathcal{K})) \\
&= Ch_K \|\check{v}_h\|^2_{\check{\mathcal{K}}} && \text{(by eq. (3.23a))} \\
&\leq Ch_K^{-1} \|v_h\|^2_{\mathcal{K}} && \text{(by eq. (3.34b)).}
\end{aligned} \tag{3.44}$$

□

3.4 Error analysis

In this section we present an *a priori* error analysis for the space-time HDG method eq. (3.11). For this we require the following subspaces of $W_h(\mathcal{K})$ and $\boldsymbol{V}_h(\mathcal{K})$:

$$\widetilde{W}_h(\mathcal{K}) := P_{p-1}(K) \otimes P_p(I_n), \qquad \widetilde{\boldsymbol{V}}_h(\mathcal{K}) := \left[P_{p-1}(K) \otimes P_p(I_n)\right]^2. \tag{3.45}$$

We require also the f_n-weighted L^2-norm defined on a domain D. For any $v \in L^2(D)$ this norm is defined as $\|v\|^2_{f_n,D} := (f_n v, v)_D$ while for $\boldsymbol{q} \in [L^2(D)]^2$ it is defined as $\|\boldsymbol{q}\|^2_{f_n,D} := (f_n \boldsymbol{q}, \boldsymbol{q})_D$.

3.4.1 The projection

The projection Π_h onto $\boldsymbol{V}_h \times W_h$ used here is based on the projection defined in [19], but tailored to the space-time finite element spaces used in this work. The projected function is denoted by $\Pi_h(\boldsymbol{q}, v)$ or $(\boldsymbol{\Pi_V q}, \Pi_W v)$, and is defined by requiring that the following equations are satisfied on each space-time element $\mathcal{K} \in \mathcal{T}^n$:

$$(\boldsymbol{\Pi_V q}, \boldsymbol{s}_h f_n)_{\mathcal{K}} = (\boldsymbol{q}, \boldsymbol{s}_h f_n)_{\mathcal{K}} \qquad \forall \boldsymbol{s}_h \in \widetilde{\boldsymbol{V}}_h(\mathcal{K}), \tag{3.46a}$$

$$(\Pi_W v, z_h f_n)_{\mathcal{K}} = (v, z_h f_n)_{\mathcal{K}} \qquad \forall z_h \in \widetilde{W}_h(\mathcal{K}), \tag{3.46b}$$

$$\langle \boldsymbol{\Pi_V q} \cdot \boldsymbol{n} - \tau \Pi_W v, \sigma_h f_n \rangle_{\mathcal{F}} = \langle \boldsymbol{q} \cdot \boldsymbol{n} - \tau v, \sigma_h f_n \rangle_{\mathcal{F}} \qquad \forall \sigma_h \in M_h(\mathcal{F}),\ \mathcal{F} \in \mathcal{Q}_{\mathcal{K}}. \tag{3.46c}$$

Notice that Π_h is well defined for functions $\boldsymbol{q}$ and v such that their traces are in $L^2(\mathcal{Q}_{\mathcal{K}})$. Therefore, the domain of Π_h is in $\left[H^1(\mathcal{T}^n)\right]^2 \times H^1(\mathcal{T}^n)$, where $H^1(\mathcal{T}^n) := \prod_{\mathcal{K} \in \mathcal{T}^n} H^1(\mathcal{K})$.

In order to show existence and uniqueness of the projection and its approximation properties, it will be useful to define the following spaces:

$$W_h^{\perp}(\mathcal{K}) := \left\{ w \in W_h(\mathcal{K}) : \left(w, \widetilde{w} f_n\right)_{\mathcal{K}} = 0, \forall\, \widetilde{w} \in \widetilde{W}_h(\mathcal{K}) \right\}, \tag{3.47a}$$

$$\boldsymbol{V}_h^{\perp}(\mathcal{K}) := \left\{ \boldsymbol{v} \in \boldsymbol{V}_h(\mathcal{K}) : \left(\boldsymbol{v}, \widetilde{\boldsymbol{v}} f_n\right)_{\mathcal{K}} = 0, \forall\, \widetilde{\boldsymbol{v}} \in \widetilde{\boldsymbol{V}}_h(\mathcal{K}) \right\}. \tag{3.47b}$$

The following lemma will be useful when showing the existence and uniqueness of the projection and its approximation properties.

Lemma 3.6. *For any space-time element $\mathcal{K}$, the following is satisfied for any face $\mathcal{F}_{\mathcal{K}} \in \mathcal{Q}_{\mathcal{K}}$:*

$$w_h \in W_h^{\perp}(\mathcal{K}) \text{ and } w_h|_{\mathcal{F}_{\mathcal{K}}} = 0, \quad \text{implies } w_h = 0 \text{ on } \mathcal{K}, \tag{3.48a}$$

$$\boldsymbol{v}_h \in \boldsymbol{V}_h^{\perp}(\mathcal{K}) \text{ and } \boldsymbol{v}_h \cdot \boldsymbol{n}|_{\mathcal{Q}_{\mathcal{K}} \setminus \mathcal{F}_{\mathcal{K}}} = 0 \quad \text{implies } \boldsymbol{v}_h = 0 \text{ on } \mathcal{K}. \tag{3.48b}$$

Moreover, the following estimates are satisfied

$$\|w_h\|_{f_n,\mathcal{K}} \leq Ch_K^{1/2} \|w_h\|_{f_n,\mathcal{F}_\mathcal{K}} \quad \forall w_h \in W_h^\perp(\mathcal{K}), \tag{3.49a}$$

$$\|\boldsymbol{v}_h\|_{f_n,\mathcal{K}} \leq Ch_K^{1/2} \|\boldsymbol{v}_h \cdot \boldsymbol{n}\|_{f_n,\mathcal{Q}_\mathcal{K}} \quad \forall \boldsymbol{v}_h \in \boldsymbol{V}_h^\perp(\mathcal{K}). \tag{3.49b}$$

Proof. We first show eq. (3.48a). Take $w_h \in W_h^\perp(\mathcal{K})$ such that $w_h|_{\mathcal{F}_\mathcal{K}} = 0$ and let L be a nonzero linear function that is constant in time and that vanishes on $\mathcal{F}_\mathcal{K}$. Then, w_h can be written as $w_h = L\widetilde{p}$, where $\widetilde{p} \in \widetilde{W}_h(\mathcal{K})$ [11, Lemma 3.1.10]. Since $w_h \in W_h^\perp(\mathcal{K})$, we have that $\left(L\widetilde{p}, f_n\widetilde{p}\right)_\mathcal{K} = 0$. Since L cannot be zero on $\mathcal{K}$, we conclude that $\widetilde{p}$ must be zero and therefore, w_h is zero on $\mathcal{K}$.

We next show eq. (3.48b). Let $p_h = \boldsymbol{v}_h \cdot \boldsymbol{n}_\mathcal{F}$, for any face $\mathcal{F}$ different than $\mathcal{F}_\mathcal{K}$. Notice that $p_h \in W_h^\perp(\mathcal{K})$ and $p_h|_\mathcal{F} = 0$. Using a similar argument as above, we can conclude that $p_h = 0$ on $\mathcal{K}$. Therefore, $\boldsymbol{v}_h \cdot \boldsymbol{n}_\mathcal{F} = 0$ on $\mathcal{K}$. Since the set $\left\{\boldsymbol{n}_\mathcal{F} : \mathcal{F} \in \mathcal{Q}_\mathcal{K} \backslash \mathcal{F}_\mathcal{K}\right\}$ is a basis of $\mathbb{R}^2$, we conclude that $\boldsymbol{v}_h$ must be zero on $\mathcal{K}$.

To show eq. (3.49a), we use the identities from section 3.3.3. Since $\|\cdot\|_{f_n,\mathcal{K}}$ is a weighted norm and $w_h f_n$, for $w_h \in W_h^\perp(\mathcal{K})$, is not a broken polynomial, as required in the proof of Lemma 3.4, we cannot use Lemma 3.4 directly. However, since f_n is uniformly bounded, there exists a constant $C_{f_n} > 0$ such that $\sup_t f_n(t) \leq C_{f_n}$ for all n. Therefore,

$$\|w_h\|_{f_n,\mathcal{K}}^2 \leq C_{f_n} \|w_h\|_\mathcal{K}^2 . \tag{3.50}$$

Notice that eq. (3.48a) implies that the trace map $\gamma_{\mathcal{F}_\mathcal{K}} : W_h^\perp(\mathcal{K}) \mapsto M_h(\mathcal{F}_\mathcal{K})$ defined by $\gamma_{\mathcal{F}_\mathcal{K}}(w_h) = w_h|_{\mathcal{F}_\mathcal{K}}$ is injective. By Lemma 3.4 we then obtain

$$\|w_h\|_{f_n,\mathcal{K}}^2 \leq Ch_K \|w_h\|_{\mathcal{F}_\mathcal{K}}^2 . \tag{3.51}$$

Equation (3.49a) now follows by equivalence of norms on finite-dimensional spaces.

Finally, we show eq. (3.49b). Let $\mathcal{F}_1, \mathcal{F}_2 \in \mathcal{Q}_\mathcal{K}$ with $\mathcal{F}_1 \neq \mathcal{F}_\mathcal{K}$ and $\mathcal{F}_2 \neq \mathcal{F}_\mathcal{K}$. Notice that $\{\boldsymbol{n}_{\mathcal{F}_1}, \boldsymbol{n}_{\mathcal{F}_2}\}$ is a basis of $\mathbb{R}^2$, therefore, we can write $\boldsymbol{v}_h$ as $\boldsymbol{v}_h = \boldsymbol{v}_1 \boldsymbol{v}_h \cdot \boldsymbol{n}_{\mathcal{F}_1} + \boldsymbol{v}_2 \boldsymbol{v}_h \cdot \boldsymbol{n}_{\mathcal{F}_2}$, where $\boldsymbol{v}_1, \boldsymbol{v}_2 \in \mathbb{R}^2$ are constant vectors. Thus,

$$\begin{aligned} \left\|\boldsymbol{v}_h\right\|_{f_n,\mathcal{K}} &= \left\|\boldsymbol{v}_1 \boldsymbol{v}_h \cdot \boldsymbol{n}_{\mathcal{F}_1} + \boldsymbol{v}_2 \boldsymbol{v}_h \cdot \boldsymbol{n}_{\mathcal{F}_2}\right\|_{f_n,\mathcal{K}} \\ &\leq \left\|\boldsymbol{v}_1\right\|_{f_n,\mathcal{K}} \left\|\boldsymbol{v}_h \cdot \boldsymbol{n}_{\mathcal{F}_1}\right\|_{f_n,\mathcal{K}} + \left\|\boldsymbol{v}_2\right\|_{f_n,\mathcal{K}} \left\|\boldsymbol{v}_h \cdot \boldsymbol{n}_{\mathcal{F}_2}\right\|_{f_n,\mathcal{K}} \\ &\leq C \left(\left\|\boldsymbol{v}_h \cdot \boldsymbol{n}_{\mathcal{F}_1}\right\|_{f_n,\mathcal{K}} + \left\|\boldsymbol{v}_h \cdot \boldsymbol{n}_{\mathcal{F}_2}\right\|_{f_n,\mathcal{K}}\right) . \end{aligned} \tag{3.52}$$

Applying eq. (3.49a) to the scalar functions $\boldsymbol{v}_h \cdot \boldsymbol{n}_{\mathcal{F}_1}$ and $\boldsymbol{v}_h \cdot \boldsymbol{n}_{\mathcal{F}_2}$, we have

$$\begin{aligned} \left\|\boldsymbol{v}_h\right\|_{f_n,\mathcal{K}} &\leq C h_K^{1/2} \left(\left\|\boldsymbol{v}_h \cdot \boldsymbol{n}_{\mathcal{F}_1}\right\|_{f_n,\mathcal{F}_1} + \left\|\boldsymbol{v}_h \cdot \boldsymbol{n}_{\mathcal{F}_2}\right\|_{f_n,\mathcal{F}_2} \right) \\ &\leq C h_K^{1/2} \left\|\boldsymbol{v}_h \cdot \boldsymbol{n}\right\|_{f_n,\mathcal{Q}_\mathcal{K}}, \end{aligned} \tag{3.53}$$

proving the result. □

We next prove existence and uniqueness of Π_h.

Lemma 3.7. *The projection Π_h defined by eq. (3.46) exists and is unique.*

Proof. To see that Π_h exists and is unique, we first verify that eq. (3.46) is a square system. First, recall that in two dimensions,

$$\dim P_p(K_j^n) = \tfrac{1}{2}(p+1)(p+2), \quad \dim Q_p(\mathcal{F}) = (p+1)^2. \tag{3.54}$$

Thus,

$$\begin{aligned} \dim W_h(\mathcal{K}) &= \tfrac{1}{2}(p+1)^2(p+2), \\ \dim \boldsymbol{V}_h(\mathcal{K}) &= (p+1)^2(p+2), \\ \dim M_h(\mathcal{F}) &= (p+1)^2. \end{aligned} \tag{3.55}$$

Moreover,

$$\begin{aligned} \dim \widetilde{W}_h(\mathcal{K}) &= \tfrac{1}{2}p(p+1)^2, \\ \dim \widetilde{\boldsymbol{V}}_h(\mathcal{K}) &= p(p+1)^2. \end{aligned} \tag{3.56}$$

It follows that the number of unknowns in eq. (3.46) is

$$\dim W_h(\mathcal{K}) + \dim \boldsymbol{V}_h(\mathcal{K}) = \tfrac{3}{2}(p+1)^2(p+2). \tag{3.57}$$

Since any space-time prism element $\mathcal{K}$ has only three faces in $\mathcal{Q}_\mathcal{K}$, the number of equations in eq. (3.46) is

$$\begin{aligned} &\dim \widetilde{W}_h(\mathcal{K}) + \dim \widetilde{\boldsymbol{V}}_h(\mathcal{K}) + 3 \dim M_h(\mathcal{F}) \\ &\qquad = \tfrac{1}{2}p(p+1)^2 + p(p+1)^2 + 3(p+1)^2 = \tfrac{3}{2}(p+1)^2(p+2). \end{aligned} \tag{3.58}$$

Since the number of equations and unknowns in eq. (3.46) coincide, eq. (3.46) is a square system.

Now, taking $\boldsymbol{q} = 0$ and $v = 0$ in eq. (3.46), we see that

$$(\boldsymbol{\Pi}_{\boldsymbol{V}}\boldsymbol{q}, \boldsymbol{s}_h f_n)_{\mathcal{K}} = 0 \qquad \forall \boldsymbol{s}_h \in \widetilde{\boldsymbol{V}}_h(\mathcal{K}), \tag{3.59a}$$

$$(\Pi_W v, z_h f_n)_{\mathcal{K}} = 0 \qquad \forall z_h \in \widetilde{W}_h(\mathcal{K}), \tag{3.59b}$$

$$\langle \boldsymbol{\Pi}_{\boldsymbol{V}}\boldsymbol{q} \cdot \boldsymbol{n} - \tau \Pi_W v, \sigma_h f_n \rangle_{\mathcal{F}} = 0 \qquad \forall \sigma_h \in M_h(\mathcal{F}),\ \mathcal{F} \subset \mathcal{Q}_{\mathcal{K}}. \tag{3.59c}$$

Let $w_h \in W_h^{\perp}(\mathcal{K})$. By eq. (3.59a), since $\nabla w_h \in \widetilde{\boldsymbol{V}}_h(\mathcal{K})$, we have

$$(\boldsymbol{\Pi}_{\boldsymbol{V}}\boldsymbol{q}, \nabla w_h f_n)_{\mathcal{K}} = 0. \tag{3.60}$$

Applying integration by parts in space,

$$-(\nabla \cdot \boldsymbol{\Pi}_{\boldsymbol{V}}\boldsymbol{q}, w_h f_n)_{\mathcal{K}} + \langle \boldsymbol{\Pi}_{\boldsymbol{V}}\boldsymbol{q} \cdot \boldsymbol{n}, w_h f_n \rangle_{\mathcal{Q}_{\mathcal{K}}} = 0. \tag{3.61}$$

Since $\nabla \cdot \boldsymbol{\Pi}_{\boldsymbol{V}}\boldsymbol{q} \in \widetilde{W}_h(\mathcal{K})$, then $\left(\nabla \cdot \boldsymbol{\Pi}_{\boldsymbol{V}}\boldsymbol{q}, w_h f_n\right)_{\mathcal{K}} = 0$, thus

$$\langle \boldsymbol{\Pi}_{\boldsymbol{V}}\boldsymbol{q} \cdot \boldsymbol{n}, w_h f_n \rangle_{\mathcal{Q}_{\mathcal{K}}} = 0 \quad \forall w_h \in W_h^{\perp}(\mathcal{K}). \tag{3.62}$$

By eq. (3.59c) and recalling that $\tau > 0$, we have

$$\langle \Pi_W v, w_h f_n \rangle_{\mathcal{Q}_{\mathcal{K}}} = 0 \quad \forall w_h \in W_h^{\perp}(\mathcal{K}). \tag{3.63}$$

Note that by eq. (3.59b), $\Pi_W v \in W_h^{\perp}(\mathcal{K})$. Thus, taking $w_h = \Pi_W v$ in eq. (3.63), we see that $\Pi_W v = 0$ on $\mathcal{Q}_{\mathcal{K}}$. Then, using eq. (3.48a) we conclude that $\Pi_W v = 0$ in $\mathcal{K}$. Taking $\sigma_h = \boldsymbol{\Pi}_{\boldsymbol{V}}\boldsymbol{q} \cdot \boldsymbol{n}$ in eq. (3.59c), since $\Pi_W v = 0$, we see that $\boldsymbol{\Pi}_{\boldsymbol{V}}\boldsymbol{q} \cdot \boldsymbol{n} = 0$ on $\mathcal{Q}_{\mathcal{K}}$. Using eq. (3.48b), we conclude that $\boldsymbol{\Pi}_{\boldsymbol{V}}\boldsymbol{q} = 0$ in $\mathcal{K}$. The result follows. □

In addition to the projection Π_h, we define also $P_M^{f_n}$ as the f_n-weighted L^2-projection onto M_h, so that

$$\langle P_M^{f_n} v, \sigma_h f_n \rangle_{\mathcal{F}} = \langle v, \sigma_h f_n \rangle_{\mathcal{F}} \qquad \forall \sigma_h \in M_h(\mathcal{F}), \mathcal{F} \subset \mathcal{Q}_{\mathcal{K}}. \tag{3.64}$$

Note that the domain of $P_M^{f_n}$ is $L^2(\Gamma_{\mathcal{Q}}^n)$.

We next show approximation properties of Π_h. For this, let $P_W^{f_n}$, $P_{\widetilde{W}}^{f_n}$, and $\boldsymbol{P}_{\boldsymbol{V}}{}^{f_n}$ denote, respectively, the f_n-weighted L^2-projections onto W_h, $\widetilde{W}_h$, and $\boldsymbol{V}_h$.

Theorem 3.2 (Approximation properties of the projection)**.** *Assume that τ is uniformly bounded above and below by constants $C_\tau^{\max}$ and $C_\tau^{\min}$, respectively. The projection Π_h satisfies the following bounds*

$$\begin{aligned} \|v - \Pi_W v\|_{f_n,\mathcal{K}} \leq \|v - P_W^{f_n} v\|_{f_n,\mathcal{K}} + CC_\tau h_K^{1/2} \|v - P_W^{f_n} v\|_{f_n,\mathcal{Q}_{\mathcal{K}}} \\ + \frac{C}{C_\tau^{\min}} h_K \|\nabla \cdot \boldsymbol{q} - P_{\widetilde{W}}^{f_n} \nabla \cdot \boldsymbol{q}\|_{f_n,\mathcal{K}}, \end{aligned} \tag{3.65a}$$

$$\begin{aligned}\|\boldsymbol{q}-\boldsymbol{\Pi}_{\boldsymbol{V}}\boldsymbol{q}\|_{f_n,\mathcal{K}} \le \|\boldsymbol{q}-\boldsymbol{P_V}^{f_n}\boldsymbol{q}\|_{f_n,\mathcal{K}} + Ch_K^{1/2}\|(\boldsymbol{q}-\boldsymbol{P_V}^{f_n}\boldsymbol{q})\cdot\boldsymbol{n}\|_{f_n,\mathcal{Q}_\mathcal{K}} \\ + CC_\tau^{\max}h_K^{1/2}\|v-P_W^{f_n}v\|_{f_n,\mathcal{Q}_\mathcal{K}},\end{aligned} \tag{3.65b}$$

$$\begin{aligned}\|\boldsymbol{q}-\boldsymbol{\Pi}_{\boldsymbol{V}}\boldsymbol{q}\|_{f_n,\partial\mathcal{K}_0} \le \|\boldsymbol{q}-\boldsymbol{P_V}^{f_n}\boldsymbol{q}\|_{f_n,\partial\mathcal{K}_0} + C\Delta t^{-1/2}\|\boldsymbol{q}-\boldsymbol{P_V}^{f_n}\boldsymbol{q}\|_{f_n,\mathcal{K}} \\ + C\Delta t^{-1/2}\|\boldsymbol{q}-\boldsymbol{\Pi}_{\boldsymbol{V}}\boldsymbol{q}\|_{f_n,\mathcal{K}},\end{aligned} \tag{3.65c}$$

where $C_\tau = C_\tau^{\max}/C_\tau^{\min}$.

Proof. Let $\boldsymbol{\delta_q} := \boldsymbol{\Pi}_{\boldsymbol{V}}\boldsymbol{q} - \boldsymbol{P_V}^{f_n}\boldsymbol{q}$ and $\delta_v := \Pi_W v - P_W^{f_n}v$. Note that $\boldsymbol{\delta_q}$ and δ_v satisfy the following equations

$$(\boldsymbol{\delta_q}, \boldsymbol{s}_h f_n)_\mathcal{K} = 0 \qquad \forall \boldsymbol{s}_h \in \widetilde{\boldsymbol{V}}_h(\mathcal{K}), \tag{3.66a}$$

$$(\delta_v, z_h f_n)_\mathcal{K} = 0 \qquad \forall z_h \in \widetilde{W}_h(\mathcal{K}), \tag{3.66b}$$

$$\langle(\boldsymbol{\delta_q}\cdot\boldsymbol{n} - \tau\delta_v), \sigma_h f_n\rangle_\mathcal{F} = \langle(\boldsymbol{I_q}\cdot\boldsymbol{n} - \tau I_v), \sigma_h f_n\rangle_\mathcal{F} \qquad \forall \sigma_h \in M_h(\mathcal{F}),\ \mathcal{F}\subset\mathcal{Q}_\mathcal{K}, \tag{3.66c}$$

where $\boldsymbol{I_q} = \boldsymbol{q} - \boldsymbol{P_V}^{f_n}\boldsymbol{q}$ and $I_v = v - P_W^{f_n}v$.

We first prove eq. (3.65a). Notice that for any $w_h \in W_h^\perp(\mathcal{K})$, $w_h|_\mathcal{F} \in M_h(\mathcal{F})$, for any $\mathcal{F}\subset\mathcal{Q}_\mathcal{K}$. Therefore, by eq. (3.66c),

$$\langle(\boldsymbol{\delta_q}\cdot\boldsymbol{n} - \tau\delta_v), w_h f_n\rangle_{\mathcal{Q}_\mathcal{K}} = \langle(\boldsymbol{I_q}\cdot\boldsymbol{n} - \tau I_v), w_h f_n\rangle_{\mathcal{Q}_\mathcal{K}} \quad \forall w_h \in W_h^\perp(\mathcal{K}). \tag{3.67}$$

Using integration by parts in space, note that

$$\langle\boldsymbol{\delta_q}\cdot\boldsymbol{n}, w_h f_n\rangle_{\mathcal{Q}_\mathcal{K}} = \left(\nabla\cdot\boldsymbol{\delta_q}, w_h f_n\right)_\mathcal{K} + \left(\boldsymbol{\delta_q}, f_n\nabla w_h\right)_\mathcal{K}. \tag{3.68}$$

Since $\nabla\cdot\boldsymbol{\delta_q} \in \widetilde{W}_h(\mathcal{K})$ and $w_h \in W_h^\perp(\mathcal{K})$, then $\left(\nabla\cdot\boldsymbol{\delta_q}, w_h f_n\right)_\mathcal{K} = 0$. Also, since $\nabla w_h \in \widetilde{\boldsymbol{V}}_h(\mathcal{K})$, by eq. (3.66a), $\left(\boldsymbol{\delta_q}, f_n\nabla w_h\right)_\mathcal{K} = 0$. Thus,

$$\langle\boldsymbol{\delta_q}\cdot\boldsymbol{n}, w_h f_n\rangle_{\mathcal{Q}_\mathcal{K}} = \quad \forall w_h \in W_h^\perp(\mathcal{K}). \tag{3.69}$$

Similarly,

$$\langle\boldsymbol{I_q}\cdot\boldsymbol{n}, w_h f_n\rangle_{\mathcal{Q}_\mathcal{K}} = \left(\nabla\cdot\boldsymbol{I_q}, w_h f_n\right)_\mathcal{K} + \left(\boldsymbol{I_q}, f_n\nabla w_h\right)_\mathcal{K} \quad \forall w_h \in W_h^\perp(\mathcal{K}). \tag{3.70}$$

By definition of $\boldsymbol{I_q}$, the second term on the right hand side is zero. Furthermore, note that

$$\left(\nabla\cdot\boldsymbol{I_q}, w_h f_n\right)_\mathcal{K} = \left(\nabla\cdot\boldsymbol{q}, w_h f_n\right)_\mathcal{K} - \left(\nabla\cdot\boldsymbol{P_V}^{f_n}\boldsymbol{q}, w_h f_n\right)_\mathcal{K}, \tag{3.71}$$

and $\left(\nabla \cdot \boldsymbol{P_V}^{f_n}\boldsymbol{q}, w_h f_n\right)_{\mathcal{K}} = 0$ since $\nabla \cdot \boldsymbol{P_V}^{f_n}\boldsymbol{q} \in \widetilde{W}_h(\mathcal{K})$ and $w_h \in W_h^{\perp}(\mathcal{K})$. Therefore,

$$\left(\nabla \cdot \boldsymbol{I_q}, w_h f_n\right)_{\mathcal{K}} = \left(\nabla \cdot \boldsymbol{q}, w_h f_n\right)_{\mathcal{K}}. \tag{3.72}$$

Also, since $P_{\widetilde{W}}^{f_n}(\nabla \cdot \boldsymbol{q}) \in \widetilde{W}_h(\mathcal{K})$ and $(\widetilde{w}_h, w_h f_n)_{\mathcal{K}} = 0$ for all $\widetilde{w}_h \in \widetilde{W}_h(\mathcal{K})$, we can write

$$\left(\nabla \cdot \boldsymbol{I_q}, w_h f_n\right)_{\mathcal{K}} = \left(\left(Id - P_{\widetilde{W}}^{f_n}\right)\nabla \cdot \boldsymbol{q}, w_h f_n\right)_{\mathcal{K}}, \tag{3.73}$$

where Id denotes the identity operator. Thus,

$$\langle \boldsymbol{I_q} \cdot \boldsymbol{n}, w_h f_n\rangle_{\mathcal{Q}_{\mathcal{K}}} = \left(\left(Id - P_{\widetilde{W}}^{f_n}\right)\nabla \cdot \boldsymbol{q}, w_h f_n\right)_{\mathcal{K}} \quad \forall w_h \in W_h^{\perp}(\mathcal{K}). \tag{3.74}$$

Using eq. (3.69) and eq. (3.74) in eq. (3.67) and rearranging terms, we obtain

$$\langle \tau\delta_v, w_h f_n\rangle_{\mathcal{Q}_{\mathcal{K}}} = \langle \tau I_v, w_h f_n\rangle_{\mathcal{Q}_{\mathcal{K}}} + \left(\left(P_{\widetilde{W}}^{f_n} - Id\right)\nabla \cdot \boldsymbol{q}, w_h f_n\right)_{\mathcal{K}} \quad \forall w_h \in W_h^{\perp}(\mathcal{K}). \tag{3.75}$$

By eq. (3.66b), $\delta_v \in W_h^{\perp}(\mathcal{K})$. Taking $w_h = \delta_v$ in eq. (3.75) we obtain

$$\langle \tau\delta_v, \delta_v f_n\rangle_{\mathcal{Q}_{\mathcal{K}}} = \langle \tau I_v, \delta_v f_n\rangle_{\mathcal{Q}_{\mathcal{K}}} + \left(\left(P_{\widetilde{W}}^{f_n} - Id\right)\nabla \cdot \boldsymbol{q}, \delta_v f_n\right)_{\mathcal{K}}. \tag{3.76}$$

Apply the Cauchy–Schwarz inequality to the right hand side of eq. (3.76):

$$\langle \tau\delta_v, \delta_v f_n\rangle_{\mathcal{Q}_{\mathcal{K}}} \leq \|\tau I_v\|_{f_n,\mathcal{Q}_{\mathcal{K}}} \|\delta_v\|_{f_n,\mathcal{Q}_{\mathcal{K}}} + \|(Id - P_{\widetilde{W}}^{f_n})\nabla \cdot \boldsymbol{q}\|_{f_n,\mathcal{K}} \|\delta_v\|_{f_n,\mathcal{K}}. \tag{3.77}$$

Using eq. (3.49a) on the right hand side,

$$\langle \tau\delta_v, \delta_v f_n\rangle_{\mathcal{Q}_{\mathcal{K}}} \leq \|\tau I_v\|_{f_n,\mathcal{Q}_{\mathcal{K}}} \|\delta_v\|_{f_n,\mathcal{Q}_{\mathcal{K}}} + Ch_K^{1/2} \|\left(Id - P_{\widetilde{W}}^{f_n}\right)\nabla \cdot \boldsymbol{q}\|_{f_n,\mathcal{K}} \|\delta_v\|_{f_n,\mathcal{Q}_{\mathcal{K}}}. \tag{3.78}$$

Since τ is uniformly bounded above and below by constants $C_\tau^{\max}$ and $C_\tau^{\min}$, respectively,

$$C_\tau^{\min} \|\delta_v\|_{f_n,\mathcal{Q}_{\mathcal{K}}}^2 \leq C_\tau^{\max} \|I_v\|_{f_n,\mathcal{Q}_{\mathcal{K}}} \|\delta_v\|_{f_n,\mathcal{Q}_{\mathcal{K}}} + Ch_K^{1/2} \|\left(Id - P_{\widetilde{W}}^{f_n}\right)\nabla \cdot \boldsymbol{q}\|_{f_n,\mathcal{K}} \|\delta_v\|_{f_n,\mathcal{Q}_{\mathcal{K}}}. \tag{3.79}$$

Canceling terms and using eq. (3.49a) on the left hand side, we obtain the following bound

$$\frac{h_K^{-1/2}}{C} C_\tau^{\min} \|\delta_v\|_{f_n,\mathcal{K}} \leq C_\tau^{\max} \|I_v\|_{f_n,\mathcal{Q}_{\mathcal{K}}} + Ch_K^{1/2} \|\left(Id - P_{\widetilde{W}}^{f_n}\right)\nabla \cdot \boldsymbol{q}\|_{f_n,\mathcal{K}}. \tag{3.80}$$

Rearranging,

$$\|\delta_v\|_{f_n,\mathcal{K}} \leq CC_\tau h_K^{1/2} \|I_v\|_{f_n,\mathcal{Q}_{\mathcal{K}}} + \frac{C}{C_\tau^{\min}} h_K \|\left(Id - P_{\widetilde{W}}^{f_n}\right)\nabla \cdot \boldsymbol{q}\|_{f_n,\mathcal{K}}. \tag{3.81}$$

The estimate eq. (3.65a) follows by applying the triangle inequality.

We next prove eq. (3.65b). We first find an estimate for $\boldsymbol{\delta_q}$. Note that by eq. (3.66a), $\boldsymbol{\delta_q}$ belongs to $\boldsymbol{V}_h^{\perp}(\mathcal{K})$. Therefore, by eq. (3.49b), we have

$$\|\boldsymbol{\delta_q}\|_{f_n,\mathcal{K}} \leq C h_K^{1/2} \|\boldsymbol{\delta_q} \cdot \boldsymbol{n}\|_{f_n,\mathcal{Q}_\mathcal{K}}. \tag{3.82}$$

Taking $\sigma_h = \boldsymbol{\delta_q} \cdot \boldsymbol{n}$ in eq. (3.66c), we obtain

$$\|\boldsymbol{\delta_q} \cdot \boldsymbol{n}\|^2_{f_n,\mathcal{Q}_\mathcal{K}} = \langle \boldsymbol{I_q} \cdot \boldsymbol{n}, \boldsymbol{\delta_q} \cdot \boldsymbol{n} f_n \rangle_{\mathcal{Q}_\mathcal{K}} - \tau \langle I_v, \boldsymbol{\delta_q} \cdot \boldsymbol{n} f_n \rangle_{\mathcal{Q}_\mathcal{K}} + \tau \langle \delta_v, \boldsymbol{\delta_q} \cdot \boldsymbol{n} f_n \rangle_{\mathcal{Q}_\mathcal{K}}. \tag{3.83}$$

Since $\delta_v \in W_h^{\perp}(\mathcal{K})$, by eq. (3.69), $\langle \delta_v, \boldsymbol{\delta_q} \cdot \boldsymbol{n} f_n \rangle_{\mathcal{Q}_\mathcal{K}} = 0$. Thus,

$$\|\boldsymbol{\delta_q} \cdot \boldsymbol{n}\|^2_{f_n,\mathcal{Q}_\mathcal{K}} = \langle \boldsymbol{I_q} \cdot \boldsymbol{n}, \boldsymbol{\delta_q} \cdot \boldsymbol{n} f_n \rangle_{\mathcal{Q}_\mathcal{K}} - \tau \langle I_v, \boldsymbol{\delta_q} \cdot \boldsymbol{n} f_n \rangle_{\mathcal{Q}_\mathcal{K}}. \tag{3.84}$$

Applying the Cauchy–Schwarz inequality and substituting into eq. (3.82), we obtain

$$\|\boldsymbol{\delta_q}\|_{f_n,\mathcal{K}} \leq C h_K^{1/2} \left(\|\boldsymbol{I_q} \cdot \boldsymbol{n}\|_{f_n,\mathcal{Q}_\mathcal{K}} + C_\tau^{\max} \|I_v\|_{f_n,\mathcal{Q}_\mathcal{K}} \right). \tag{3.85}$$

The estimate eq. (3.65b) follows by applying the triangle inequality.

Finally, we show eq. (3.65c). Note that, by the triangle inequality,

$$\|\boldsymbol{q} - \boldsymbol{\Pi_V q}\|_{f_n,\partial\mathcal{K}_0} \leq \|\boldsymbol{q} - \boldsymbol{P_V}^{f_n} \boldsymbol{q}\|_{f_n,\partial\mathcal{K}_0} + \|\boldsymbol{P_V}^{f_n} \boldsymbol{q} - \boldsymbol{\Pi_V q}\|_{f_n,\partial\mathcal{K}_0}. \tag{3.86}$$

Next, we apply the inverse trace inequality in eq. (3.42b) to the second term on the right hand side to obtain:

$$\|\boldsymbol{q} - \boldsymbol{\Pi_V q}\|_{f_n,\partial\mathcal{K}_0} \leq \|\boldsymbol{q} - \boldsymbol{P_V}^{f_n} \boldsymbol{q}\|_{f_n,\partial\mathcal{K}_0} + C\Delta t^{-1/2} \|\boldsymbol{P_V}^{f_n} \boldsymbol{q} - \boldsymbol{\Pi_V q}\|_{f_n,\mathcal{K}}. \tag{3.87}$$

The result follows after adding and subtracting $\boldsymbol{q}$ to the second term on the right hand side and applying the triangle inequality. □

We next prove the equivalence between the standard and the weighted L^2-projections.

Lemma 3.8. *Let $\mathcal{K} \in \mathcal{T}^n$ and $\mathcal{F} \in \mathcal{F}^n_\mathcal{Q}$. Let $P_W, \boldsymbol{P_V}$ and P_M denote the L^2-orthogonal projections onto W_h, $\boldsymbol{V}_h$ and M_h, respectively. If f_n is uniformly bounded, then the following relations are satisfied*

$$\|v - P_W^{f_n} v\|_{f_n,\mathcal{K}} \leq C \|v - P_W v\|_\mathcal{K}, \tag{3.88a}$$

$$\|\boldsymbol{q} - \boldsymbol{P_V}^{f_n} \boldsymbol{q}\|_{f_n,\mathcal{K}} \leq C \|\boldsymbol{q} - \boldsymbol{P_V q}\|_\mathcal{K}, \tag{3.88b}$$

$$\|v - P_M^{f_n} v\|_{f_n,\mathcal{F}} \leq C \|v - P_M v\|_\mathcal{F}. \tag{3.88c}$$

Proof. We will only show eq. (3.88a). The proofs for eq. (3.88b) and eq. (3.88c) are analogous. Note that by definition of $P_W^{f_n}$, for all $w_h \in W_h$

$$\left(P_W^{f_n} v - P_W v, f_n w_h\right)_{\mathcal{K}} = \left(v - P_W v, f_n w_h\right)_{\mathcal{K}}. \tag{3.89}$$

Let $w_h = P_W^{f_n} v - P_W v$, then,

$$\begin{aligned} \left\|P_W^{f_n} v - P_W v\right\|_{f_n,\mathcal{K}}^2 &= \left(v - P_W v, f_n \left(P_W^{f_n} v - P_W v\right)\right)_{\mathcal{K}} \\ &\leq \left\|v - P_W v\right\|_{f_n,\mathcal{K}} \left\|P_W^{f_n} v - P_W v\right\|_{f_n,\mathcal{K}}. \end{aligned} \tag{3.90}$$

Thus,

$$\left\|P_W^{f_n} v - P_W v\right\|_{f_n,\mathcal{K}} \leq \left\|v - P_W v\right\|_{f_n,\mathcal{K}} \leq C \left\|v - P_W v\right\|_{\mathcal{K}}, \tag{3.91}$$

since f_n is uniformly bounded. The result follows by the triangle inequality. □

We next find L^2 projection esimates of the different projection operators.

Theorem 3.3 (L^2 orthogonal projection estimates)**.** *Let $\mathcal{K} = K \times I_n$ and $\mathcal{F}$ be a face on the free-surface boundary, i.e., $\mathcal{F} \in \mathcal{F}_{\mathcal{S}}^n$. Let $\partial\mathcal{F}_0$ denote the two edges of the face $\mathcal{F}$ that are on the time levels. Assume that the spatial shape-regularity condition eq. (3.21) holds and that the triangulation $\mathcal{T}^n$ does not have any hanging nodes. Suppose that $(\boldsymbol{q}, v)$ are such that $\boldsymbol{q}|_{\mathcal{K}} \in \left[H^{(s_t,s_s)}(\mathcal{K})\right]^2$, $v|_{\mathcal{K}} \in H^{(s_t,s_s)}(\mathcal{K})$, where $1/2 < s_t \leq p+1$ and $1 \leq s_s \leq p+1$. Then we have the following estimates:*

$$\left\|v - P_W v\right\|_{\mathcal{K}} \leq C \left(h_K^{s_s} + \Delta t^{s_t}\right) \left\|v\right\|_{H^{(s_t,s_s)}(\mathcal{K})}, \tag{3.92a}$$

$$\left\|v - P_W v\right\|_{\mathcal{Q}_{\mathcal{K}}} \leq C \left(h_K^{s_s - 1/2} + h_K^{-1/2} \Delta t^{s_t}\right) \left\|v\right\|_{H^{(s_t,s_s)}(\mathcal{K})}, \tag{3.92b}$$

$$\left\|\boldsymbol{q} - \boldsymbol{P_V q}\right\|_{\mathcal{K}} \leq C \left(h_K^{s_s} + \Delta t^{s_t}\right) \left\|\boldsymbol{q}\right\|_{H^{(s_t,s_s)}(\mathcal{K})}, \tag{3.92c}$$

$$\left\|(\boldsymbol{q} - \boldsymbol{P_V q}) \cdot \boldsymbol{n}\right\|_{\mathcal{Q}_{\mathcal{K}}} \leq C \left(h_K^{s_s - 1/2} + h_K^{-1/2} \Delta t^{s_t}\right) \left\|\boldsymbol{q}\right\|_{H^{(s_t,s_s)}(\mathcal{K})}, \tag{3.92d}$$

$$\left\|v - P_W v\right\|_{\partial\mathcal{K}_0} \leq C \left(\Delta t^{-1/2} h_K^{s_s} + \Delta t^{s_t - 1/2}\right) \left\|v\right\|_{H^{(s_t,s_s)}(\mathcal{K})}, \tag{3.92e}$$

$$\left\|\boldsymbol{q} - \boldsymbol{P_V q}\right\|_{\partial\mathcal{K}_0} \leq C \left(\Delta t^{-1/2} h_K^{s_s} + \Delta t^{s_t - 1/2}\right) \left\|\boldsymbol{q}\right\|_{H^{(s_t,s_s)}(\mathcal{K})}, \tag{3.92f}$$

$$\left\|v - P_M v\right\|_{\mathcal{F}} \leq C \left(h_K^{s_s} + \Delta t^{s_t}\right) \left\|v\right\|_{H^{(s_t,s_s)}(\mathcal{F})}, \tag{3.92g}$$

$$\left\|v - P_M v\right\|_{\partial\mathcal{F}_0} \leq C \left(\Delta t^{-1/2} h_K^{s_s} + \Delta t^{s_t - 1/2}\right) \left\|v\right\|_{H^{(s_t,s_s)}(\mathcal{F})}. \tag{3.92h}$$

Proof. First note that eq. (3.92c) and eq. (3.92f) result from applying eq. (3.92a) and eq. (3.92e), respectively, on each component of $\boldsymbol{q}$, so the proof for those estimates is not

shown. Since the face $\mathcal{F}$ is a quadrilateral, the proof for eq. (3.92g) and eq. (3.92h) can be found in [74, Lemma B.14].

Let π^t and π^s denote the orthogonal L^2-projections onto $L^2(K) \otimes P_p(I_n)$ and onto $P_p(K) \otimes L^2(I_n)$, respectively. We can define P_W as $P_W := \pi^t \circ \pi^s$.

We first show eq. (3.92a). Notice that

$$\begin{aligned}\|v - P_W v\|_{\mathcal{K}}^2 = \left\|v - \pi^t \circ \pi^s v\right\|_{\mathcal{K}}^2 = \left\|v - \pi^t v + \pi^t(v - \pi^s v)\right\|_{\mathcal{K}}^2 \\ \leq C\left(\left\|v - \pi^t v\right\|_{\mathcal{K}}^2 + \left\|\pi^t(v - \pi^s v)\right\|_{\mathcal{K}}^2\right). \quad (3.93)\end{aligned}$$

Since π^t is bounded and $\left\|\pi^t\right\| = 1$, then

$$\|v - P_W v\|_{\mathcal{K}}^2 \leq C\left(\left\|v - \pi^t v\right\|_{\mathcal{K}}^2 + \|v - \pi^s v\|_{\mathcal{K}}^2\right). \quad (3.94)$$

Let us treat each term separately. For the second term on the right hand side of eq. (3.94), by [24, Lemma 1.58], since we assume eq. (3.21) and no hanging nodes,

$$\begin{aligned}\|v - \pi^s v\|_{\mathcal{K}}^2 = \int_{t_n}^{t_{n+1}} \int_K (v - \pi^s v)^2 \,\mathrm{d}\boldsymbol{x}\,\mathrm{d}x_0 \leq C h_K^{2s_s} \int_{t_n}^{t_{n+1}} |v|_{H^{s_s}(K)}^2 \,\mathrm{d}x_0 \\ \leq C h_K^{2s_s} \|v\|_{H^{(0,s_s)}(\mathcal{K})}^2, \quad (3.95)\end{aligned}$$

where $0 \leq s_s \leq p+1$. Similarly, for the temporal projection we have

$$\left\|v - \pi^t v\right\|_{\mathcal{K}}^2 = \int_K \int_{t_n}^{t_{n+1}} (v - \pi^t v)^2 \,\mathrm{d}x_0\,\mathrm{d}\boldsymbol{x} \leq C\Delta t^{2s_t} \|v\|_{H^{(s_t,0)}(\mathcal{K})}^2, \quad (3.96)$$

where $0 \leq s_t \leq p+1$. Equation (3.92a) follows by combining eq. (3.95) and eq. (3.96).

Next, we show eq. (3.92b). Similarly as above, we have

$$\|v - P_W v\|_{\mathcal{Q}_{\mathcal{K}}}^2 \leq C\left(\left\|v - \pi^t v\right\|_{\mathcal{Q}_{\mathcal{K}}}^2 + \|v - \pi^s v\|_{\mathcal{Q}_{\mathcal{K}}}^2\right). \quad (3.97)$$

For the spatial projection, using [24, Lemma 1.59], we have

$$\begin{aligned}\|v - \pi^s v\|_{\mathcal{Q}_{\mathcal{K}}}^2 = \int_{t_n}^{t_{n+1}} \int_{\partial K} (v - \pi^s v)^2 \,\mathrm{d}\boldsymbol{x}\,\mathrm{d}x_0 \\ \leq C h_K^{2s_s - 1} \int_{t_n}^{t_{n+1}} |v|_{H^{s_s}(K)}^2 \,\mathrm{d}x_0 \leq C h_K^{2s_s - 1} \|v\|_{H^{(0,s_s)}(\mathcal{K})}^2. \quad (3.98)\end{aligned}$$

For the temporal projection, similarly as above,

$$\left\|v - \pi^t v\right\|_{\mathcal{Q}_\mathcal{K}}^2 = \int_{\partial K} \int_{t_n}^{t_{n+1}} (v - \pi^t v)^2 \,\mathrm{d}x_0 \,\mathrm{d}\boldsymbol{x} \leq C\Delta t^{2s_t} \|v\|_{H^{(s_t,0)}(\mathcal{Q}_\mathcal{K})}^2 . \tag{3.99}$$

Combining eq. (3.98) and eq. (3.99), we obtain

$$\|v - P_W v\|_{\mathcal{Q}_\mathcal{K}}^2 \leq C h_K^{2s_s - 1} \|v\|_{H^{(0,s_s)}(\mathcal{K})}^2 + C\Delta t^{2s_t} \|v\|_{H^{(s_t,0)}(\mathcal{Q}_\mathcal{K})}^2 . \tag{3.100}$$

Note that, by Lemma 3.3, since $v \in H^{(s_t,s_s)}(\mathcal{K})$ with $s_s \geq 1$, we have

$$\left\|\partial_{x_0}^{\alpha_t} v\right\|_{\mathcal{Q}_\mathcal{K}}^2 \leq C \left\|\nabla \partial_{x_0}^{\alpha_t} v\right\|_{\mathcal{K}} \left\|\partial_{x_0}^{\alpha_t} v\right\|_{\mathcal{K}} + C h_K^{-1} \left\|\partial_{x_0}^{\alpha_t} v\right\|_{\mathcal{K}}^2 , \tag{3.101}$$

for all $0 \leq \alpha_t \leq s_t$. Thus,

$$\|v\|_{H^{(s_t,0)}(\mathcal{Q}_\mathcal{K})}^2 \leq C \|v\|_{H^{(s_t,s_s)}(\mathcal{K})}^2 + C h_K^{-1} \|v\|_{H^{(s_t,s_s)}(\mathcal{K})}^2 , \tag{3.102}$$

and the result follows.

To show eq. (3.92d), we note the following

$$\|(\boldsymbol{q} - \boldsymbol{P_V q}) \cdot \boldsymbol{n}\|_{\mathcal{Q}_\mathcal{K}} \leq \|\boldsymbol{q} - \boldsymbol{P_V q}\|_{\mathcal{Q}_\mathcal{K}} . \tag{3.103}$$

The result follows by applying eq. (3.92b) component wise.

Finally, we show eq. (3.92e). For the spatial component of the projection, notice that

$$\begin{aligned} \|v - \pi^s v\|_{\partial\mathcal{K}_0}^2 &= \|v - \pi^s v\|_{K_j^{n+1}}^2 + \|v - \pi^s v\|_{K_j^n}^2 \\ &\leq C h_K^{2s_s} \left(|v|_{H^{s_s}(K_j^{n+1})}^2 + |v|_{H^{s_s}(K_j^n)}^2 \right) \\ &\leq C h_K^{2s_s} \|v\|_{H^{s_s}(\partial\mathcal{K}_0)}^2 . \end{aligned} \tag{3.104}$$

By the Sobolev embedding theorem, the definition of fractional Sobolev norms [11, Chapter 14], and a standard scaling argument, we have for $s_t > 1/2$,

$$\|v\|_{H^{s_s}(\partial\mathcal{K}_0)} \leq C\Delta t^{-1/2} \|v\|_{H^{(s_t,s_s)}(\mathcal{K})} . \tag{3.105}$$

Thus,

$$\|v - \pi^s v\|_{\partial\mathcal{K}_0}^2 \leq C\Delta t^{-1} h_K^{2s_s} \|v\|_{H^{(s_t,s_s)}(\mathcal{K})}^2 . \tag{3.106}$$

For the temporal projection, we have

$$
\begin{aligned}
\left\|v-\pi^t v\right\|_{\partial\mathcal{K}_0}^2 &= \left\|v-\pi^t v\right\|_{K_j^{n+1}}^2 + \left\|v-\pi^t v\right\|_{K_j^n}^2 \\
&= \int_K \left((v-\pi^t v)(t_{n+1},\boldsymbol{x})\right)^2 \mathrm{d}\boldsymbol{x} + \int_K \left((v-\pi^t v)(t_n,\boldsymbol{x})\right)^2 \mathrm{d}\boldsymbol{x} && \text{(by def.)} \\
&\leq h_K^2 \int_{\widehat{K}} \left((v-\pi^t v)(t_{n+1},\widehat{\boldsymbol{x}})\right)^2 \mathrm{d}\widehat{\boldsymbol{x}} + h_K^2 \int_{\widehat{K}} \left((v-\pi^t v)(t_n,\widehat{\boldsymbol{x}})\right)^2 \mathrm{d}\widehat{\boldsymbol{x}} && \text{(by eq. (3.33a))} \\
&= h_K^2 \left\|\check{v}-\pi^t\check{v}\right\|_{\partial\check{\mathcal{K}}_0}^2 && \text{(by def.)} \\
&= h_K^2 \left\|\widehat{v}-\widehat{\pi}^t\widehat{v}\right\|_{\partial\widehat{\mathcal{K}}_0}^2 && \text{(by eq. (3.23b))} \\
&= h_K^2 \int_{\widehat{K}} \left((\widehat{v}-\widehat{\pi}^t\widehat{v})(1,\widehat{\boldsymbol{x}})\right)^2 \mathrm{d}\widehat{\boldsymbol{x}} + h_K^2 \int_{\widehat{K}} \left((\widehat{v}-\widehat{\pi}^t\widehat{v})(-1,\widehat{\boldsymbol{x}})\right)^2 \mathrm{d}\widehat{\boldsymbol{x}} && \text{(by def.)} \\
&\leq C h_K^2 \left\|\partial_{\widehat{x}_0}^{s_t}\widehat{v}\right\|_{\widehat{\mathcal{K}}}^2 && \text{(by [39])} \\
&= C h_K^2 \left(\frac{\Delta t}{2}\right)^{2s_t-1} \left\|\partial_{\check{x}_0}^{s_t}\check{v}\right\|_{\check{\mathcal{K}}}^2 && \text{(by eq. (3.23a))} \\
&\leq C h_K^2 \left(\frac{\Delta t}{2}\right)^{2s_t-1} h_K^{-2} \left\|\partial_{x_0}^{s_t} v\right\|_{\mathcal{K}}^2 && \text{(by eq. (3.33a))} \\
&\leq C \Delta t^{2s_t-1} \|v\|_{H^{(s_t,0)}(\mathcal{K})}^2 .
\end{aligned}
\tag{3.107}
$$

Note that here we have used that $\left|\widehat{v}-\widehat{\pi}^t\widehat{v}(\pm 1)\right| \leq C \left\|\partial_{\widehat{x}_0}^{s_t}\widehat{v}\right\|_{\widehat{I}}$ which was shown in [39, Lemma 3.5]. This concludes the proof. □

Corollary 3.1. *Under the same assumptions as in Theorem 3.3, the following estimates are satisfied:*

$$
\left\|v-P_W^{f_n} v\right\|_{f_n,\mathcal{K}} \leq C\left(h_K^{s_s}+\Delta t^{s_t}\right)\|v\|_{H^{(s_t,s_s)}(\mathcal{K})}, \tag{3.108a}
$$

$$
\left\|v-P_W^{f_n} v\right\|_{f_n,\mathcal{Q}_\mathcal{K}} \leq C\left(h_K^{s_s-1/2}+h_K^{-1/2}\Delta t^{s_t}\right)\|v\|_{H^{(s_t,s_s)}(\mathcal{K})}, \tag{3.108b}
$$

$$
\left\|\boldsymbol{q}-\boldsymbol{P_V}^{f_n}\boldsymbol{q}\right\|_{f_n,\mathcal{K}} \leq C\left(h_K^{s_s}+\Delta t^{s_t}\right)\|\boldsymbol{q}\|_{H^{(s_t,s_s)}(\mathcal{K})}, \tag{3.108c}
$$

$$
\left\|(\boldsymbol{q}-\boldsymbol{P_V}^{f_n}\boldsymbol{q})\cdot\boldsymbol{n}\right\|_{f_n,\mathcal{Q}_\mathcal{K}} \leq C\left(h_K^{s_s-1/2}+h_K^{-1/2}\Delta t^{s_t}\right)\|\boldsymbol{q}\|_{H^{(s_t,s_s)}(\mathcal{K})}, \tag{3.108d}
$$

$$
\left\|v-P_W^{f_n} v\right\|_{f_n,\partial\mathcal{K}_0} \leq C\left(\Delta t^{-1/2}h_K^{s_s}+\Delta t^{s_t-1/2}\right)\|v\|_{H^{(s_t,s_s)}(\mathcal{K})}, \tag{3.108e}
$$

$$
\left\|\boldsymbol{q}-\boldsymbol{P_V}^{f_n}\boldsymbol{q}\right\|_{f_n,\partial\mathcal{K}_0} \leq C\left(\Delta t^{-1/2}h_K^{s_s}+\Delta t^{s_t-1/2}\right)\|\boldsymbol{q}\|_{H^{(s_t,s_s)}(\mathcal{K})}, \tag{3.108f}
$$

$$
\left\|v-P_M^{f_n} v\right\|_{f_n,\mathcal{F}} \leq C\left(h_K^{s_s}+\Delta t^{s_t}\right)\|v\|_{H^{(s_t,s_s)}(\mathcal{F})}, \tag{3.108g}
$$

$$
\left\|v-P_M^{f_n} v\right\|_{f_n,\partial\mathcal{F}_0} \leq C\left(\Delta t^{-1/2}h_K^{s_s}+\Delta t^{s_t-1/2}\right)\|v\|_{H^{(s_t,s_s)}(\mathcal{F})}. \tag{3.108h}
$$

Proof. Equation (3.108a), eq. (3.108c) and eq. (3.108g) follow directly from Lemma 3.8 and Theorem 3.3. Moreover, eq. (3.108d) and eq. (3.108f) follow from eq. (3.108b) and eq. (3.108e), respectively. Therefore, we only show eq. (3.108b), eq. (3.108e) and eq. (3.108h).

In order to prove eq. (3.108b), notice that since f_n has a uniform upper bound, and using the triangle inequality, we obtain

$$\|v - P_W^{f_n} v\|_{f_n,\mathcal{Q}_\mathcal{K}} \leq C \|v - P_W v\|_{\mathcal{Q}_\mathcal{K}} + C \|P_W v - P_W^{f_n} v\|_{\mathcal{Q}_\mathcal{K}} . \tag{3.109}$$

By eq. (3.42c), we obtain

$$\|v - P_W^{f_n} v\|_{f_n,\mathcal{Q}_\mathcal{K}} \leq C \|v - P_W v\|_{\mathcal{Q}_\mathcal{K}} + C h_K^{-1/2} \|P_W v - P_W^{f_n} v\|_{\mathcal{K}} . \tag{3.110}$$

Since $f_n(t)$ is positive for all t, with a uniformly positive lower bound independent of t and n for all t, we have that

$$\|v_h\|_\mathcal{K} \leq C \|v_h\|_{f_n,\mathcal{K}} , \quad \forall v_h \in W_h. \tag{3.111}$$

Using the triangle inequality, we arrive at

$$\begin{aligned}\|v - P_W^{f_n} v\|_{f_n,\mathcal{Q}_\mathcal{K}} \leq C \|v - P_W v\|_{\mathcal{Q}_\mathcal{K}} + C h_K^{-1/2} \|P_W v - v\|_{f_n,\mathcal{K}} \\ + C h_K^{-1/2} \|v - P_W^{f_n} v\|_{f_n,\mathcal{K}} .\end{aligned} \tag{3.112}$$

Equation (3.108b) follows by recalling that f_n is uniformly bounded and using the estimates eq. (3.92b), eq. (3.92a) and eq. (3.108a).

In order to show eq. (3.108e), since f_n has a uniform upper bound, we obtain by the triangle inequality

$$\|v - P_W^{f_n} v\|_{f_n,\partial\mathcal{K}_0} \leq C \|v - P_W v\|_{\partial\mathcal{K}_0} + C \|P_W v - P_W^{f_n} v\|_{\partial\mathcal{K}_0} . \tag{3.113}$$

Using eq. (3.42b) on the second term of the right hand side of eq. (3.113),

$$\|v - P_W^{f_n} v\|_{f_n,\partial\mathcal{K}_0} \leq C \|v - P_W v\|_{\partial\mathcal{K}_0} + C \Delta t^{-1/2} \|P_W v - P_W^{f_n} v\|_{\mathcal{K}} . \tag{3.114}$$

By the triangle inequality,

$$\begin{aligned}\|v - P_W^{f_n} v\|_{f_n,\partial\mathcal{K}_0} \leq C \|v - P_W v\|_{\partial\mathcal{K}_0} + C \Delta t^{-1/2} \|P_W v - v\|_{f_n,\mathcal{K}} \\ + C \Delta t^{-1/2} \|v - P_W^{f_n} v\|_{f_n,\mathcal{K}} .\end{aligned} \tag{3.115}$$

Then, eq. (3.108e) is obtained by eq. (3.92e), eq. (3.108a) and eq. (3.92a).

Finally, we show eq. (3.108h). Using that f_n is uniformly bounded and by the triangle inequality,

$$\|v - P_M^{f_n} v\|_{f_n,\partial\mathcal{F}_0} \leq C \|v - P_M v\|_{\partial\mathcal{F}_0} + C \|P_M v - P_M^{f_n} v\|_{\partial\mathcal{F}_0}. \tag{3.116}$$

By eq. (3.42a),

$$\|v - P_M^{f_n} v\|_{f_n,\partial\mathcal{F}_0} \leq C \|v - P_M v\|_{\partial\mathcal{F}_0} + C\Delta t^{-1/2} \|P_M v - P_M^{f_n} v\|_{\mathcal{F}}. \tag{3.117}$$

By the triangle inequality, we then obtain:

$$\begin{aligned}\|v - P_M^{f_n} v\|_{f_n,\partial\mathcal{F}_0} \leq C \|v - P_M v\|_{\partial\mathcal{F}_0} + C\Delta t^{-1/2} \|P_M v - v\|_{f_n,\mathcal{F}} \\ + C\Delta t^{-1/2} \|v - P_M^{f_n} v\|_{f_n,\mathcal{F}}.\end{aligned} \tag{3.118}$$

Equation (3.108h) follows by the uniform boundedness of f_n and the estimates eq. (3.92h), eq. (3.92g), and eq. (3.108g). □

To conclude this subsection, we show the error estimates of our projection Π_h.

Lemma 3.9. *Under the same conditions as in Theorem 3.3, the following estimates hold:*

$$\begin{aligned}\|\boldsymbol{q} - \boldsymbol{\Pi}_{\boldsymbol{V}}\boldsymbol{q}\|_{f_n,\mathcal{K}} \leq C\,(h_K^{s_s} + \Delta t^{s_t})\|\boldsymbol{q}\|_{H^{(s_t,s_s)}(\mathcal{K})} \\ + C\,(h_K^{s_s} + \Delta t^{s_t})\|v\|_{H^{(s_t,s_s)}(\mathcal{K})},\end{aligned} \tag{3.119a}$$

$$\begin{aligned}\|\boldsymbol{q} - \boldsymbol{\Pi}_{\boldsymbol{V}}\boldsymbol{q}\|_{f_n,\partial\mathcal{K}_0} \leq C\,(\Delta t^{-1/2} h_K^{s_s} + \Delta t^{s_t - 1/2})\|\boldsymbol{q}\|_{H^{(s_t,s_s)}(\mathcal{K})} \\ + C\,(h_K^{s_s}\Delta t^{-1/2} + \Delta t^{s_t - 1/2})\|v\|_{H^{(s_t,s_s)}(\mathcal{K})}.\end{aligned} \tag{3.119b}$$

Proof. These estimates follow from substituting eq. (3.108b), eq. (3.108c), eq. (3.108d), and eq. (3.108f) in Theorem 3.2. □

3.4.2 The *a priori* error estimates

In this section we present the main result of this chapter, namely *a priori* error estimates for the space-time HDG method eq. (3.11).

In order to obtain *a priori* error estimates, we first require to obtain the error equations and a bound for the projection errors. Define these projection errors as

$$\begin{aligned}&\boldsymbol{\varepsilon}_h^{\boldsymbol{q}} = \boldsymbol{\Pi}_{\boldsymbol{V}}\boldsymbol{q} - \boldsymbol{q}_h, \quad \boldsymbol{\varepsilon}_h^{\boldsymbol{q}^-} = \boldsymbol{\Pi}_{\boldsymbol{V}^-}\boldsymbol{q} - \boldsymbol{q}_h^-, \quad \varepsilon_h^v = \Pi_W v - v_h, \\ &\varepsilon_h^\lambda = P_M^{f_n} v - \lambda_h, \quad \varepsilon_h^{\lambda^-} = P_{M^-}^{f_{n-1}} v - \lambda_h^-,\end{aligned} \tag{3.120}$$

where $\boldsymbol{\Pi}_{\boldsymbol{V}^-}$ and $P_{M^-}^{f_{n-1}}$ denote the projection onto the spaces $\boldsymbol{V}_h$ and M_h, respectively, defined on the time slab $n-1$ for $n>0$. We furthermore remark that $\boldsymbol{\varepsilon}_{\boldsymbol{h}}^{\boldsymbol{q}-}=0$ and $\varepsilon_h^{\lambda-}=0$ when $n=0$.

The following lemma describes the error equations.

Lemma 3.10. *The error equations are given by*

$$\begin{aligned}
&\left(\varepsilon_h^v, f_n\nabla\cdot\boldsymbol{r}_h\right)_{\mathcal{T}^n}-\left(\boldsymbol{\varepsilon}_h^{\boldsymbol{q}}, \boldsymbol{r}_h f_n'\right)_{\mathcal{T}^n}+\langle\boldsymbol{\varepsilon}_h^{\boldsymbol{q}}, \boldsymbol{r}_h f_n\rangle_{\mathcal{F}_\Omega^n(t_{n+1})}\\
&-\left(\boldsymbol{\varepsilon}_h^{\boldsymbol{q}}, f_n\partial_t\boldsymbol{r}_h\right)_{\mathcal{T}^n}-\langle\varepsilon_h^\lambda, \boldsymbol{r}_h\cdot\boldsymbol{n} f_n\rangle_{\mathcal{F}_\mathcal{Q}^n}\\
=&\langle\boldsymbol{\varepsilon}_h^{\boldsymbol{q}-}, \boldsymbol{r}_h f_n\rangle_{\mathcal{F}_\Omega^n(t_n)}-\left(\boldsymbol{\Pi}_{\boldsymbol{V}}\boldsymbol{q}-\boldsymbol{q}, f_n\partial_t\boldsymbol{r}_h\right)_{\mathcal{T}^n}-\left(\boldsymbol{\Pi}_{\boldsymbol{V}}\boldsymbol{q}-\boldsymbol{q}, \boldsymbol{r}_h f_n'\right)_{\mathcal{T}^n}\\
&+\langle\boldsymbol{\Pi}_{\boldsymbol{V}}\boldsymbol{q}-\boldsymbol{q}, \boldsymbol{r}_h f_n\rangle_{\mathcal{F}_\Omega^n(t_{n+1})}-\langle\boldsymbol{\Pi}_{\boldsymbol{V}^-}\boldsymbol{q}-\boldsymbol{q}, \boldsymbol{r}_h f_n\rangle_{\mathcal{F}_\Omega^n(t_n)},
\end{aligned}\tag{3.121a}$$

$$\left(\boldsymbol{\varepsilon}_h^{\boldsymbol{q}}, f_n\nabla w_h\right)_{\mathcal{T}^n}-\langle\widehat{\boldsymbol{\varepsilon}}_h\cdot\boldsymbol{n}, w_h f_n\rangle_{\mathcal{F}_\mathcal{Q}^n}=0,\tag{3.121b}$$

$$\begin{aligned}
&\langle\widehat{\boldsymbol{\varepsilon}}_h\cdot\boldsymbol{n}, \mu_h f_n\rangle_{\mathcal{F}_\mathcal{Q}^n}-\langle\varepsilon_h^\lambda, f_n\partial_t\mu_h\rangle_{\mathcal{F}_\mathcal{S}^n}-\langle\varepsilon_h^\lambda, \mu_h f_n'\rangle_{\mathcal{F}_\mathcal{S}^n}+\langle\!\langle\varepsilon_h^\lambda, \mu_h f_n\rangle\!\rangle_{\partial\mathcal{E}_\mathcal{S}^n(t_{n+1})}\\
&=\langle\!\langle\varepsilon_h^{\lambda-}, \mu_h f_n\rangle\!\rangle_{\partial\mathcal{E}_\mathcal{S}^n(t_n)}+\langle\!\langle P_M^{f_n}v-v, \mu_h f_n\rangle\!\rangle_{\partial\mathcal{E}_\mathcal{S}^n(t_{n+1})}\\
&\quad-\langle\!\langle P_{M^-}^{f_{n-1}}v-v, \mu_h f_n\rangle\!\rangle_{\partial\mathcal{E}_\mathcal{S}^n(t_n)},
\end{aligned}\tag{3.121c}$$

where $\widehat{\boldsymbol{\varepsilon}}_h=\boldsymbol{\varepsilon}_h^{\boldsymbol{q}}-\tau\left(\varepsilon_h^v-\varepsilon_h^\lambda\right)\boldsymbol{n}$.

Proof. Substituting the exact solution $(\boldsymbol{q}, v)$ to eq. (3.1) into the space-time HDG method eq. (3.11), we find:

$$\begin{aligned}
&-\left(\boldsymbol{q}, f_n\partial_t\boldsymbol{r}_h\right)_{\mathcal{T}^n}-\left(\boldsymbol{q}, \boldsymbol{r}_h f_n'\right)_{\mathcal{T}^n}+\langle\boldsymbol{q}, \boldsymbol{r}_h f_n\rangle_{\mathcal{F}_\Omega^n(t_{n+1})}\\
&\qquad+\left(v, f_n\nabla\cdot\boldsymbol{r}_h\right)_{\mathcal{T}^n}-\langle v, \boldsymbol{r}_h\cdot\boldsymbol{n} f_n\rangle_{\mathcal{F}_\mathcal{Q}^n}=\langle\boldsymbol{q}, \boldsymbol{r}_h f_n\rangle_{\mathcal{F}_\Omega^n(t_n)},
\end{aligned}\tag{3.122a}$$

$$-\left(w_h, f_n\nabla\cdot\boldsymbol{q}\right)_{\mathcal{T}^n}=0,\tag{3.122b}$$

$$\begin{aligned}
&\langle\boldsymbol{q}\cdot\boldsymbol{n}, \mu_h f_n\rangle_{\mathcal{F}_\mathcal{Q}^n}-\langle v, f_n\partial_t\mu_h\rangle_{\mathcal{F}_\mathcal{S}^n}-\langle v, \mu_h f_n'\rangle_{\mathcal{F}_\mathcal{S}^n}+\langle\!\langle v, \mu_h f_n\rangle\!\rangle_{\partial\mathcal{E}_\mathcal{S}^n(t_{n+1})}\\
&\qquad=\langle\!\langle v, \mu_h f_n\rangle\!\rangle_{\partial\mathcal{E}_\mathcal{S}^n(t_n)}.
\end{aligned}\tag{3.122c}$$

Subtracting now (3.11) from (3.122), we obtain

$$\begin{aligned}
&-\left(\boldsymbol{q}-\boldsymbol{q}_h, f_n\partial_t\boldsymbol{r}_h\right)_{\mathcal{T}^n}-\left(\boldsymbol{q}-\boldsymbol{q}_h, \boldsymbol{r}_h f_n'\right)_{\mathcal{T}^n}+\langle\boldsymbol{q}-\boldsymbol{q}_h, \boldsymbol{r}_h f_n\rangle_{\mathcal{F}_\Omega^n(t_{n+1})}\\
&\qquad+\left(v-v_h, f_n\nabla\cdot\boldsymbol{r}_h\right)_{\mathcal{T}^n}-\langle v-\lambda_h, \boldsymbol{r}_h\cdot\boldsymbol{n} f_n\rangle_{\mathcal{F}_\mathcal{Q}^n}=\langle\boldsymbol{q}-\boldsymbol{q}_h^-, \boldsymbol{r}_h f_n\rangle_{\mathcal{F}_\Omega^n(t_n)},
\end{aligned}\tag{3.123a}$$

$$-\left(w_h f_n, \nabla\cdot(\boldsymbol{q}-\boldsymbol{q}_h)\right)_{\mathcal{T}^n} - \langle \tau\left(v_h-\lambda_h\right), w_h f_n\rangle_{\mathcal{F}^n_{\mathcal{Q}}} = 0, \tag{3.123b}$$

$$\begin{aligned}\langle\left(\boldsymbol{q}-\boldsymbol{q}_h\right)\cdot\boldsymbol{n} + \tau\left(v_h-\lambda_h\right), \mu_h f_n\rangle_{\mathcal{F}^n_{\mathcal{Q}}} - \langle v-\lambda_h, f_n\partial_t\mu_h\rangle_{\mathcal{F}^n_{\mathcal{S}}}\\ - \langle v-\lambda_h, \mu_h f_n'\rangle_{\mathcal{F}^n_{\mathcal{S}}} + \langle\!\langle v-\lambda_h, \mu_h f_n\rangle\!\rangle_{\partial\mathcal{E}^n_{\mathcal{S}}(t_{n+1})} = \langle\!\langle v-\lambda_h^-, \mu_h f_n\rangle\!\rangle_{\partial\mathcal{E}^n_{\mathcal{S}}(t_n)}.\end{aligned} \tag{3.123c}$$

We next split the numerical errors as $\boldsymbol{q}-\boldsymbol{q}_h = \boldsymbol{q}-\boldsymbol{\Pi_V q}+\boldsymbol{\varepsilon}_h^{\boldsymbol{q}}$, $\boldsymbol{q}-\boldsymbol{q}_h^- = \boldsymbol{q}-\boldsymbol{\Pi_{V^-}q}+\boldsymbol{\varepsilon}_h^{\boldsymbol{q}^-}$, $v-v_h = v-\Pi_W v+\varepsilon_h^v$, $v-\lambda_h = v-P_M^{f_n}v+\varepsilon_h^\lambda$ and $v-\lambda_h^- = v-P_{M^-}^{f_{n-1}}v+\varepsilon_h^{\lambda^-}$. Note also that

$$\begin{aligned}\boldsymbol{q}-\widehat{\boldsymbol{q}}_h &= \boldsymbol{q}-\boldsymbol{q}_h-\tau\left(\lambda_h-v_h\right)\boldsymbol{n} = \boldsymbol{q}-\boldsymbol{q}_h-\tau\left(v-v_h-v+\lambda_h\right)\boldsymbol{n}\\ &= \boldsymbol{\varepsilon}_h^{\boldsymbol{q}}-\tau\left(\varepsilon_h^v-\varepsilon_h^\lambda\right)\boldsymbol{n}+\boldsymbol{q}-\boldsymbol{\Pi_V q}-\tau\left(v-\Pi_W v-\left(v-P_M^{f_n}v\right)\right)\boldsymbol{n}\\ &= \widehat{\boldsymbol{\varepsilon}}_h+\boldsymbol{q}-\boldsymbol{\Pi_V q}-\tau\left(v-\Pi_W v-\left(v-P_M^{f_n}v\right)\right)\boldsymbol{n}.\end{aligned} \tag{3.124}$$

We will write eq. (3.123) in terms of the projection and approximation errors.

Consider first eq. (3.123a):

$$\begin{aligned}&-\left(\boldsymbol{\varepsilon}_h^{\boldsymbol{q}}, f_n\partial_t\boldsymbol{r}_h\right)_{\mathcal{T}^n} - \left(\boldsymbol{\varepsilon}_h^{\boldsymbol{q}}, \boldsymbol{r}_h f_n'\right)_{\mathcal{T}^n} + \langle\boldsymbol{\varepsilon}_h^{\boldsymbol{q}}, \boldsymbol{r}_h f_n\rangle_{\mathcal{F}^n_\Omega(t_{n+1})} + \left(\varepsilon_h^v, f_n\nabla\cdot\boldsymbol{r}_h\right)_{\mathcal{T}^n}\\ &\qquad - \langle\varepsilon_h^\lambda, \boldsymbol{r}_h\cdot\boldsymbol{n} f_n\rangle_{\mathcal{F}^n_{\mathcal{Q}}}\\ &= -\left(\boldsymbol{\Pi_V q}-\boldsymbol{q}, f_n\partial_t\boldsymbol{r}_h\right)_{\mathcal{T}^n} - \left(\boldsymbol{\Pi_V q}-\boldsymbol{q}, \boldsymbol{r}_h f_n'\right)_{\mathcal{T}^n} + \langle\boldsymbol{\Pi_V q}-\boldsymbol{q}, \boldsymbol{r}_h f_n\rangle_{\mathcal{F}^n_\Omega(t_{n+1})}\\ &\qquad + \left(\Pi_W v-v, f_n\nabla\cdot\boldsymbol{r}_h\right)_{\mathcal{T}^n} - \langle P_M^{f_n}v-v, \boldsymbol{r}_h\cdot\boldsymbol{n} f_n\rangle_{\mathcal{F}^n_{\mathcal{Q}}}\\ &\qquad + \langle\boldsymbol{\varepsilon}_h^{\boldsymbol{q}^-}, \boldsymbol{r}_h f_n\rangle_{\mathcal{F}^n_\Omega(t_n)} - \langle\boldsymbol{\Pi_{V^-}q}-\boldsymbol{q}, \boldsymbol{r}_h f_n\rangle_{\mathcal{F}^n_\Omega(t_n)},\end{aligned} \tag{3.125}$$

which simplifies to

$$\begin{aligned}&-\left(\boldsymbol{\varepsilon}_h^{\boldsymbol{q}}, f_n\partial_t\boldsymbol{r}_h\right)_{\mathcal{T}^n} - \left(\boldsymbol{\varepsilon}_h^{\boldsymbol{q}}, \boldsymbol{r}_h f_n'\right)_{\mathcal{T}^n} + \langle\boldsymbol{\varepsilon}_h^{\boldsymbol{q}}, \boldsymbol{r}_h f_n\rangle_{\mathcal{F}^n_\Omega(t_{n+1})}\\ &\qquad + \left(\varepsilon_h^v, f_n\nabla\cdot\boldsymbol{r}_h\right)_{\mathcal{T}^n} - \langle\varepsilon_h^\lambda, \boldsymbol{r}_h\cdot\boldsymbol{n} f_n\rangle_{\mathcal{F}^n_{\mathcal{Q}}} = -\left(\boldsymbol{\Pi_V q}-\boldsymbol{q}, f_n\partial_t\boldsymbol{r}_h\right)_{\mathcal{T}^n}\\ &\qquad\qquad - \left(\boldsymbol{\Pi_V q}-\boldsymbol{q}, \boldsymbol{r}_h f_n'\right)_{\mathcal{T}^n} + \langle\boldsymbol{\Pi_V q}-\boldsymbol{q}, \boldsymbol{r}_h f_n\rangle_{\mathcal{F}^n_\Omega(t_{n+1})}\\ &\qquad\qquad + \langle\boldsymbol{\varepsilon}_h^{\boldsymbol{q}^-}, \boldsymbol{r}_h f_n\rangle_{\mathcal{F}^n_\Omega(t_n)} - \langle\boldsymbol{\Pi_{V^-}q}-\boldsymbol{q}, \boldsymbol{r}_h f_n\rangle_{\mathcal{F}^n_\Omega(t_n)},\end{aligned} \tag{3.126}$$

using the properties of the projections Π_W and $P_M^{f_n}$. This proves eq. (3.121a).

We consider next eq. (3.123b). Integrating eq. (3.123b) by parts in space,

$$\left(\boldsymbol{q}-\boldsymbol{q}_h, f_n\nabla w_h\right)_{\mathcal{T}^n} - \langle\left(\boldsymbol{q}-\boldsymbol{q}_h\right)\cdot\boldsymbol{n} - \tau\left(\lambda_h-v_h\right), w_h f_n\rangle_{\mathcal{F}^n_{\mathcal{Q}}} = 0. \tag{3.127}$$

We next write this equation in terms of the projection and approximation errors:

$$\begin{aligned}\left(\boldsymbol{\varepsilon}_h^{\boldsymbol{q}}, f_n\nabla w_h\right)_{\mathcal{T}^n} - \langle\widehat{\boldsymbol{\varepsilon}}_h\cdot\boldsymbol{n}, w_h f_n\rangle_{\mathcal{F}_{\mathcal{Q}}^n}&\\ = \left(\boldsymbol{\Pi_V q}-\boldsymbol{q}, f_n\nabla w_h\right)_{\mathcal{T}^n} - \langle\tau\left(P_M^{f_n}v - v\right), w_h f_n\rangle_{\mathcal{F}_{\mathcal{Q}}^n}&\\ - \langle(\boldsymbol{\Pi_V q}-\boldsymbol{q})\cdot\boldsymbol{n} - \tau\left(\Pi_W v - v\right), w_h f_n\rangle_{\mathcal{F}_{\mathcal{Q}}^n}.&\end{aligned} \tag{3.128}$$

Using the properties of the projections Π_h and $P_M^{f_n}$, we obtain

$$\left(\boldsymbol{\varepsilon}_h^{\boldsymbol{q}}, f_n\nabla w_h\right)_{\mathcal{T}^n} - \langle\widehat{\boldsymbol{\varepsilon}}_h\cdot\boldsymbol{n}, w_h f_n\rangle_{\mathcal{F}_{\mathcal{Q}}^n} = 0, \tag{3.129}$$

proving eq. (3.121b).

Finally, we write eq. (3.123c) in terms of the projection and approximation errors:

$$\begin{aligned}\langle\widehat{\boldsymbol{\varepsilon}}_h\cdot\boldsymbol{n},\mu_h f_n\rangle_{\mathcal{F}_{\mathcal{Q}}^n} - \langle\varepsilon_h^\lambda, f_n\partial_t\mu_h\rangle_{\mathcal{F}_{\mathcal{S}}^n} - \langle\varepsilon_h^\lambda,\mu_h f_n'\rangle_{\mathcal{F}_{\mathcal{S}}^n} + \langle\!\langle\varepsilon_h^\lambda,\mu_h f_n\rangle\!\rangle_{\partial\mathcal{E}_{\mathcal{S}}^n(t_{n+1})}&\\ = \langle(\boldsymbol{\Pi_V q}-\boldsymbol{q})\cdot\boldsymbol{n} - \tau\left(\Pi_W v - v\right),\mu_h f_n\rangle_{\mathcal{F}_{\mathcal{Q}}^n} + \langle\tau\left(P_M^{f_n}v - v\right),\mu_h f_n\rangle_{\mathcal{F}_{\mathcal{Q}}^n}&\\ - \langle P_M^{f_n}v - v, f_n\partial_t\mu_h\rangle_{\mathcal{F}_{\mathcal{S}}^n} - \langle P_M^{f_n}v - v,\mu_h f_n'\rangle_{\mathcal{F}_{\mathcal{S}}^n} + \langle\!\langle P_M^{f_n}v - v,\mu_h f_n\rangle\!\rangle_{\partial\mathcal{E}_{\mathcal{S}}^n(t_{n+1})}&\\ + \langle\!\langle\varepsilon_h^{\lambda-},\mu_h f_n\rangle\!\rangle_{\partial\mathcal{E}_{\mathcal{S}}^n(t_n)} - \langle\!\langle P_{M^-}^{f_{n-1}}v - v,\mu_h f_n\rangle\!\rangle_{\partial\mathcal{E}_{\mathcal{S}}^n(t_n)}.&\end{aligned} \tag{3.130}$$

Using the properties of the projections Π_h and $P_M^{f_n}$, we obtain

$$\begin{aligned}\langle\widehat{\boldsymbol{\varepsilon}}_h\cdot\boldsymbol{n},\mu_h f_n\rangle_{\mathcal{F}_{\mathcal{Q}}^n} - \langle\varepsilon_h^\lambda, f_n\partial_t\mu_h\rangle_{\mathcal{F}_{\mathcal{S}}^n} - \langle\varepsilon_h^\lambda,\mu_h f_n'\rangle_{\mathcal{F}_{\mathcal{S}}^n} + \langle\!\langle\varepsilon_h^\lambda,\mu_h f_n\rangle\!\rangle_{\partial\mathcal{E}_{\mathcal{S}}^n(t_{n+1})}&\\ = \langle\!\langle\varepsilon_h^{\lambda-},\mu_h f_n\rangle\!\rangle_{\partial\mathcal{E}_{\mathcal{S}}^n(t_n)} + \langle\!\langle P_M^{f_n}v - v,\mu_h f_n\rangle\!\rangle_{\partial\mathcal{E}_{\mathcal{S}}^n(t_{n+1})}&\\ - \langle\!\langle P_{M^-}^{f_{n-1}}v - v,\mu_h f_n\rangle\!\rangle_{\partial\mathcal{E}_{\mathcal{S}}^n(t_n)},&\end{aligned} \tag{3.131}$$

proving eq. (3.121c). □

Next, we prove a bound for the projection errors.

Lemma 3.11. *The following bound holds for the projection errors:*

$$\begin{aligned}\tfrac{\alpha}{2}\left\|\boldsymbol{\varepsilon}_h^{\boldsymbol{q}}\right\|_{f_n,\mathcal{T}^n}^2 + \tfrac{\alpha}{2}\left\|\varepsilon_h^\lambda\right\|_{f_n,\mathcal{F}_{\mathcal{S}}^n}^2 + e^{-\alpha\Delta t}\left\|\boldsymbol{\varepsilon}_h^{\boldsymbol{q}}\right\|_{\mathcal{F}_\Omega^n(t_{n+1})}^2 + e^{-\alpha\Delta t}\left\|\varepsilon_h^\lambda\right\|_{\partial\mathcal{E}_{\mathcal{S}}^n(t_{n+1})}^2&\\ \leq \left\|\boldsymbol{\varepsilon}_h^{\boldsymbol{q}-}\right\|_{\mathcal{F}_\Omega^n(t_n)}^2 + \left\|\varepsilon_h^{\lambda-}\right\|_{\partial\mathcal{E}_{\mathcal{S}}^n(t_n)}^2 + C\Delta t^{-2}\left\|\boldsymbol{q}-\boldsymbol{\Pi_V q}\right\|_{f_n,\mathcal{T}^n}^2&\\ + C\left\|\boldsymbol{\Pi_V q}-\boldsymbol{q}\right\|_{f_n,\mathcal{T}^n}^2 + C\Delta t^{-1}\left\|\boldsymbol{\Pi_V q}-\boldsymbol{q}\right\|_{f_n,\mathcal{F}_\Omega^n(t_{n+1})}^2&\\ + C\Delta t^{-1}\left\|\boldsymbol{\Pi}_{\boldsymbol{V}^-}\boldsymbol{q}-\boldsymbol{q}\right\|_{f_n,\mathcal{F}_\Omega^n(t_n)}^2 + C\Delta t^{-1}\left\|P_M^{f_n}v - v\right\|_{f_n,\partial\mathcal{E}_{\mathcal{S}}^n(t_{n+1})}^2&\\ + C\Delta t^{-1}\left\|P_{M^-}^{f_{n-1}}v - v\right\|_{f_n,\partial\mathcal{E}_{\mathcal{S}}^n(t_n)}^2.&\end{aligned} \tag{3.132}$$

Proof. Take $\boldsymbol{r}_h = \boldsymbol{\varepsilon}_h^{\boldsymbol{q}}$ in eq. (3.121a), $w_h = \varepsilon_h^v$ in eq. (3.121b) and $\mu_h = \varepsilon_h^\lambda$ in eq. (3.121c). Adding the resulting equations we obtain

$$\begin{aligned}
&-\left(\boldsymbol{\varepsilon}_h^{\boldsymbol{q}}, f_n\partial_t\boldsymbol{\varepsilon}_h^{\boldsymbol{q}}\right)_{\mathcal{T}^n} - \left(f_n'\boldsymbol{\varepsilon}_h^{\boldsymbol{q}}, \boldsymbol{\varepsilon}_h^{\boldsymbol{q}}\right)_{\mathcal{T}^n} + \langle f_n\boldsymbol{\varepsilon}_h^{\boldsymbol{q}}, \boldsymbol{\varepsilon}_h^{\boldsymbol{q}}\rangle_{\mathcal{F}_\Omega^n(t_{n+1})}\\
&+\left(\varepsilon_h^v, f_n\nabla\cdot\boldsymbol{\varepsilon}_h^{\boldsymbol{q}}\right)_{\mathcal{T}^n} - \langle\varepsilon_h^\lambda, \boldsymbol{\varepsilon}_h^{\boldsymbol{q}}\cdot\boldsymbol{n}f_n\rangle_{\mathcal{F}_\mathcal{Q}^n} + \left(\boldsymbol{\varepsilon}_h^{\boldsymbol{q}}, f_n\nabla\varepsilon_h^v\right)_{\mathcal{T}^n} - \langle\widehat{\boldsymbol{\varepsilon}}_h\cdot\boldsymbol{n}, \varepsilon_h^v f_n\rangle_{\mathcal{F}_\mathcal{Q}^n}\\
&+\langle\widehat{\boldsymbol{\varepsilon}}_h\cdot\boldsymbol{n}, \varepsilon_h^\lambda f_n\rangle_{\mathcal{F}_\mathcal{Q}^n} - \langle\varepsilon_h^\lambda, f_n\partial_t\varepsilon_h^\lambda\rangle_{\mathcal{F}_\mathcal{S}^n} - \langle f_n'\varepsilon_h^\lambda, \varepsilon_h^\lambda\rangle_{\mathcal{F}_\mathcal{S}^n} + \langle\!\langle f_n\varepsilon_h^\lambda, \varepsilon_h^\lambda\rangle\!\rangle_{\partial\mathcal{E}_\mathcal{S}^n(t_{n+1})}\\
=&\langle\boldsymbol{\varepsilon}_h^{\boldsymbol{q}-}, \boldsymbol{\varepsilon}_h^{\boldsymbol{q}}f_n\rangle_{\mathcal{F}_\Omega^n(t_n)} + \langle\!\langle\varepsilon_h^{\lambda-}, \varepsilon_h^\lambda f_n\rangle\!\rangle_{\partial\mathcal{E}_\mathcal{S}^n(t_n)}\\
&-\left(\boldsymbol{\Pi}_{\boldsymbol{V}}\boldsymbol{q}-\boldsymbol{q}, f_n\partial_t\boldsymbol{\varepsilon}_h^{\boldsymbol{q}}\right)_{\mathcal{T}^n} - \left(\boldsymbol{\Pi}_{\boldsymbol{V}}\boldsymbol{q}-\boldsymbol{q}, \boldsymbol{\varepsilon}_h^{\boldsymbol{q}}f_n'\right)_{\mathcal{T}^n}\\
&+\langle\boldsymbol{\Pi}_{\boldsymbol{V}}\boldsymbol{q}-\boldsymbol{q}, \boldsymbol{\varepsilon}_h^{\boldsymbol{q}}f_n\rangle_{\mathcal{F}_\Omega^n(t_{n+1})} - \langle\boldsymbol{\Pi}_{\boldsymbol{V}^-}\boldsymbol{q}-\boldsymbol{q}, \boldsymbol{\varepsilon}_h^{\boldsymbol{q}}f_n\rangle_{\mathcal{F}_\Omega^n(t_n)}\\
&+\langle\!\langle P_M^{f_n}v - v, \varepsilon_h^\lambda f_n\rangle\!\rangle_{\partial\mathcal{E}_\mathcal{S}^n(t_{n+1})} - \langle\!\langle P_{M^-}^{f_{n-1}}v - v, \varepsilon_h^\lambda f_n\rangle\!\rangle_{\partial\mathcal{E}_\mathcal{S}^n(t_n)}.
\end{aligned} \tag{3.133}$$

Applying integration by parts with respect to time on the first and ninth terms, integration by parts with respect to space on the sixth term, and expanding out some terms:

$$\begin{aligned}
&-\tfrac{1}{2}\left(f_n'\boldsymbol{\varepsilon}_h^{\boldsymbol{q}}, \boldsymbol{\varepsilon}_h^{\boldsymbol{q}}\right)_{\mathcal{T}^n} + \tfrac{1}{2}\langle f_n\boldsymbol{\varepsilon}_h^{\boldsymbol{q}}, \boldsymbol{\varepsilon}_h^{\boldsymbol{q}}\rangle_{\mathcal{F}_\Omega^n(t_{n+1})} + \tfrac{1}{2}\langle f_n\boldsymbol{\varepsilon}_h^{\boldsymbol{q}}, \boldsymbol{\varepsilon}_h^{\boldsymbol{q}}\rangle_{\mathcal{F}_\Omega^n(t_n)}\\
&+\langle\tau\left(\varepsilon_h^v - \varepsilon_h^\lambda\right), f_n\left(\varepsilon_h^v - \varepsilon_h^\lambda\right)\rangle_{\mathcal{F}_\mathcal{Q}^n} - \tfrac{1}{2}\langle f_n'\varepsilon_h^\lambda, \varepsilon_h^\lambda\rangle_{\mathcal{F}_\mathcal{S}^n} + \tfrac{1}{2}\langle\!\langle f_n\varepsilon_h^\lambda, \varepsilon_h^\lambda\rangle\!\rangle_{\partial\mathcal{E}_\mathcal{S}^n(t_{n+1})}\\
&+\tfrac{1}{2}\langle\!\langle f_n\varepsilon_h^\lambda, \varepsilon_h^\lambda\rangle\!\rangle_{\partial\mathcal{E}_\mathcal{S}^n(t_n)}\\
=&\langle\boldsymbol{\varepsilon}_h^{\boldsymbol{q}-}, \boldsymbol{\varepsilon}_h^{\boldsymbol{q}}f_n\rangle_{\mathcal{F}_\Omega^n(t_n)} + \langle\!\langle\varepsilon_h^{\lambda-}, \varepsilon_h^\lambda f_n\rangle\!\rangle_{\partial\mathcal{E}_\mathcal{S}^n(t_n)} - \left(\boldsymbol{\Pi}_{\boldsymbol{V}}\boldsymbol{q}-\boldsymbol{q}, f_n\partial_t\boldsymbol{\varepsilon}_h^{\boldsymbol{q}}\right)_{\mathcal{T}^n}\\
&-\left(\boldsymbol{\Pi}_{\boldsymbol{V}}\boldsymbol{q}-\boldsymbol{q}, \boldsymbol{\varepsilon}_h^{\boldsymbol{q}}f_n'\right)_{\mathcal{T}^n} + \langle\boldsymbol{\Pi}_{\boldsymbol{V}}\boldsymbol{q}-\boldsymbol{q}, \boldsymbol{\varepsilon}_h^{\boldsymbol{q}}f_n\rangle_{\mathcal{F}_\Omega^n(t_{n+1})} - \langle\boldsymbol{\Pi}_{\boldsymbol{V}^-}\boldsymbol{q}-\boldsymbol{q}, \boldsymbol{\varepsilon}_h^{\boldsymbol{q}}f_n\rangle_{\mathcal{F}_\Omega^n(t_n)}\\
&+\langle\!\langle P_M^{f_n}v - v, \varepsilon_h^\lambda f_n\rangle\!\rangle_{\partial\mathcal{E}_\mathcal{S}^n(t_{n+1})} - \langle\!\langle P_{M^-}^{f_{n-1}}v - v, \varepsilon_h^\lambda f_n\rangle\!\rangle_{\partial\mathcal{E}_\mathcal{S}^n(t_n)}.
\end{aligned} \tag{3.134}$$

Moving the first two terms on the right hand side to the left hand side, we obtain

$$\begin{aligned}
&-\tfrac{1}{2}\left(f_n'\boldsymbol{\varepsilon}_h^{\boldsymbol{q}}, \boldsymbol{\varepsilon}_h^{\boldsymbol{q}}\right)_{\mathcal{T}^n} + \tfrac{1}{2}\langle f_n\boldsymbol{\varepsilon}_h^{\boldsymbol{q}}, \boldsymbol{\varepsilon}_h^{\boldsymbol{q}}\rangle_{\mathcal{F}_\Omega^n(t_{n+1})} + \tfrac{1}{2}\langle f_n\boldsymbol{\varepsilon}_h^{\boldsymbol{q}}, \boldsymbol{\varepsilon}_h^{\boldsymbol{q}}\rangle_{\mathcal{F}_\Omega^n(t_n)}\\
&-\langle\boldsymbol{\varepsilon}_h^{\boldsymbol{q}-}, \boldsymbol{\varepsilon}_h^{\boldsymbol{q}}f_n\rangle_{\mathcal{F}_\Omega^n(t_n)} + \langle\tau\left(\varepsilon_h^v - \varepsilon_h^\lambda\right), f_n\left(\varepsilon_h^v - \varepsilon_h^\lambda\right)\rangle_{\mathcal{F}_\mathcal{Q}^n} - \tfrac{1}{2}\langle f_n'\varepsilon_h^\lambda, \varepsilon_h^\lambda\rangle_{\mathcal{F}_\mathcal{S}^n}\\
&+\tfrac{1}{2}\langle\!\langle f_n\varepsilon_h^\lambda, \varepsilon_h^\lambda\rangle\!\rangle_{\partial\mathcal{E}_\mathcal{S}^n(t_{n+1})} + \tfrac{1}{2}\langle\!\langle f_n\varepsilon_h^\lambda, \varepsilon_h^\lambda\rangle\!\rangle_{\partial\mathcal{E}_\mathcal{S}^n(t_n)} - \langle\!\langle\varepsilon_h^{\lambda-}, \varepsilon_h^\lambda f_n\rangle\!\rangle_{\partial\mathcal{E}_\mathcal{S}^n(t_n)}\\
=&-\left(\boldsymbol{\Pi}_{\boldsymbol{V}}\boldsymbol{q}-\boldsymbol{q}, f_n\partial_t\boldsymbol{\varepsilon}_h^{\boldsymbol{q}}\right)_{\mathcal{T}^n}\\
&-\left(\boldsymbol{\Pi}_{\boldsymbol{V}}\boldsymbol{q}-\boldsymbol{q}, \boldsymbol{\varepsilon}_h^{\boldsymbol{q}}f_n'\right)_{\mathcal{T}^n} + \langle\boldsymbol{\Pi}_{\boldsymbol{V}}\boldsymbol{q}-\boldsymbol{q}, \boldsymbol{\varepsilon}_h^{\boldsymbol{q}}f_n\rangle_{\mathcal{F}_\Omega^n(t_{n+1})} - \langle\boldsymbol{\Pi}_{\boldsymbol{V}^-}\boldsymbol{q}-\boldsymbol{q}, \boldsymbol{\varepsilon}_h^{\boldsymbol{q}}f_n\rangle_{\mathcal{F}_\Omega^n(t_n)}\\
&+\langle\!\langle P_M^{f_n}v - v, \varepsilon_h^\lambda f_n\rangle\!\rangle_{\partial\mathcal{E}_\mathcal{S}^n(t_{n+1})} - \langle\!\langle P_{M^-}^{f_{n-1}}v - v, \varepsilon_h^\lambda f_n\rangle\!\rangle_{\partial\mathcal{E}_\mathcal{S}^n(t_n)}.
\end{aligned} \tag{3.135}$$

Notice that

$$\begin{aligned}
&\tfrac{1}{2}\langle f_n\boldsymbol{\varepsilon}_h^{\boldsymbol{q}}, \boldsymbol{\varepsilon}_h^{\boldsymbol{q}}\rangle_{\mathcal{F}_\Omega^n(t_n)} - \langle\boldsymbol{\varepsilon}_h^{\boldsymbol{q}-}, \boldsymbol{\varepsilon}_h^{\boldsymbol{q}}f_n\rangle_{\mathcal{F}_\Omega^n(t_n)}\\
&\quad= \tfrac{1}{2}\langle\boldsymbol{\varepsilon}_h^{\boldsymbol{q}} - \boldsymbol{\varepsilon}_h^{\boldsymbol{q}-}, \boldsymbol{\varepsilon}_h^{\boldsymbol{q}}f_n\rangle_{\mathcal{F}_\Omega^n(t_n)} - \tfrac{1}{2}\langle\boldsymbol{\varepsilon}_h^{\boldsymbol{q}-}, \boldsymbol{\varepsilon}_h^{\boldsymbol{q}}f_n\rangle_{\mathcal{F}_\Omega^n(t_n)}\\
&\quad= \tfrac{1}{2}\langle\boldsymbol{\varepsilon}_h^{\boldsymbol{q}} - \boldsymbol{\varepsilon}_h^{\boldsymbol{q}-}, \left(\boldsymbol{\varepsilon}_h^{\boldsymbol{q}} - \boldsymbol{\varepsilon}_h^{\boldsymbol{q}-}\right)f_n\rangle_{\mathcal{F}_\Omega^n(t_n)} - \tfrac{1}{2}\langle\boldsymbol{\varepsilon}_h^{\boldsymbol{q}-}, \boldsymbol{\varepsilon}_h^{\boldsymbol{q}-}f_n\rangle_{\mathcal{F}_\Omega^n(t_n)}.
\end{aligned} \tag{3.136}$$

Similarly,

$$\begin{aligned}&\tfrac{1}{2}\langle\!\langle f_n\varepsilon_h^\lambda, \varepsilon_h^\lambda\rangle\!\rangle_{\partial\mathcal{E}_\mathcal{S}^n(t_n)} - \langle\!\langle \varepsilon_h^{\lambda-}, \varepsilon_h^\lambda f_n\rangle\!\rangle_{\partial\mathcal{E}_\mathcal{S}^n(t_n)}\\ &= \tfrac{1}{2}\langle\!\langle \varepsilon_h^\lambda - \varepsilon_h^{\lambda-}, (\varepsilon_h^\lambda - \varepsilon_h^{\lambda-})\, f_n\rangle\!\rangle_{\partial\mathcal{E}_\mathcal{S}^n(t_n)} - \tfrac{1}{2}\langle\!\langle \varepsilon_h^{\lambda-}, \varepsilon_h^{\lambda-} f_n\rangle\!\rangle_{\partial\mathcal{E}_\mathcal{S}^n(t_n)}.\end{aligned} \tag{3.137}$$

Substituting these expressions in eq. (3.135) and rearranging terms, we obtain

$$\begin{aligned}&-\tfrac{1}{2}\left(f_n'\boldsymbol{\varepsilon}_h^{\boldsymbol{q}}, \boldsymbol{\varepsilon}_h^{\boldsymbol{q}}\right)_{\mathcal{T}^n} + \tfrac{1}{2}\langle f_n\boldsymbol{\varepsilon}_h^{\boldsymbol{q}}, \boldsymbol{\varepsilon}_h^{\boldsymbol{q}}\rangle_{\mathcal{F}_\Omega^n(t_{n+1})} + \tfrac{1}{2}\langle \boldsymbol{\varepsilon}_h^{\boldsymbol{q}} - \boldsymbol{\varepsilon}_h^{\boldsymbol{q}-}, (\boldsymbol{\varepsilon}_h^{\boldsymbol{q}} - \boldsymbol{\varepsilon}_h^{\boldsymbol{q}-})\, f_n\rangle_{\mathcal{F}_\Omega^n(t_n)}\\ &+ \langle \tau\left(\varepsilon_h^v - \varepsilon_h^\lambda\right), f_n\left(\varepsilon_h^v - \varepsilon_h^\lambda\right)\rangle_{\mathcal{F}_\mathcal{Q}^n} - \tfrac{1}{2}\langle f_n'\varepsilon_h^\lambda, \varepsilon_h^\lambda\rangle_{\mathcal{F}_\mathcal{S}^n} + \tfrac{1}{2}\langle\!\langle f_n\varepsilon_h^\lambda, \varepsilon_h^\lambda\rangle\!\rangle_{\partial\mathcal{E}_\mathcal{S}^n(t_{n+1})}\\ &+ \tfrac{1}{2}\langle\!\langle \varepsilon_h^\lambda - \varepsilon_h^{\lambda-}, (\varepsilon_h^\lambda - \varepsilon_h^{\lambda-})\, f_n\rangle\!\rangle_{\partial\mathcal{E}_\mathcal{S}^n(t_n)}\\ =&\tfrac{1}{2}\langle \boldsymbol{\varepsilon}_h^{\boldsymbol{q}-}, \boldsymbol{\varepsilon}_h^{\boldsymbol{q}-} f_n\rangle_{\mathcal{F}_\Omega^n(t_n)} + \tfrac{1}{2}\langle\!\langle \varepsilon_h^{\lambda-}, \varepsilon_h^{\lambda-} f_n\rangle\!\rangle_{\partial\mathcal{E}_\mathcal{S}^n(t_n)}\\ &-\left(\boldsymbol{\Pi}_{\boldsymbol{V}}\boldsymbol{q} - \boldsymbol{q}, f_n\partial_t\boldsymbol{\varepsilon}_h^{\boldsymbol{q}}\right)_{\mathcal{T}^n}\\ &-\left(\boldsymbol{\Pi}_{\boldsymbol{V}}\boldsymbol{q} - \boldsymbol{q}, \boldsymbol{\varepsilon}_h^{\boldsymbol{q}} f_n'\right)_{\mathcal{T}^n} + \langle \boldsymbol{\Pi}_{\boldsymbol{V}}\boldsymbol{q} - \boldsymbol{q}, \boldsymbol{\varepsilon}_h^{\boldsymbol{q}} f_n\rangle_{\mathcal{F}_\Omega^n(t_{n+1})} - \langle \boldsymbol{\Pi}_{\boldsymbol{V}-}\boldsymbol{q} - \boldsymbol{q}, \boldsymbol{\varepsilon}_h^{\boldsymbol{q}} f_n\rangle_{\mathcal{F}_\Omega^n(t_n)}\\ &+ \langle\!\langle P_M^{f_n} v - v, \varepsilon_h^\lambda f_n\rangle\!\rangle_{\partial\mathcal{E}_\mathcal{S}^n(t_{n+1})} - \langle\!\langle P_{M^-}^{f_{n-1}} v - v, \varepsilon_h^\lambda f_n\rangle\!\rangle_{\partial\mathcal{E}_\mathcal{S}^n(t_n)}.\end{aligned} \tag{3.138}$$

Recall that $f_n = e^{-\alpha(t-t_n)}$, where $\alpha > 0$ is constant, and so $f_n' = -\alpha f_n$. Moreover, $f_n(t_n) = 1$ and $f_n(t_{n+1}) = e^{-\alpha\Delta t}$. With these definitions and by the Cauchy–Schwarz inequality applied to the right hand side of eq. (3.138), we obtain

$$\begin{aligned}&\tfrac{\alpha}{2}\left\|\boldsymbol{\varepsilon}_h^{\boldsymbol{q}}\right\|_{f_n,\mathcal{T}^n}^2 + \tfrac{\alpha}{2}\left\|\varepsilon_h^\lambda\right\|_{f_n,\mathcal{F}_\mathcal{S}^n}^2 + \tfrac{e^{-\alpha\Delta t}}{2}\left\|\boldsymbol{\varepsilon}_h^{\boldsymbol{q}}\right\|_{\mathcal{F}_\Omega^n(t_{n+1})}^2 + \tfrac{e^{-\alpha\Delta t}}{2}\left\|\varepsilon_h^\lambda\right\|_{\partial\mathcal{E}_\mathcal{S}^n(t_{n+1})}^2\\ \le&\tfrac{1}{2}\left\|\boldsymbol{\varepsilon}_h^{\boldsymbol{q}-}\right\|_{\mathcal{F}_\Omega^n(t_n)}^2 + \tfrac{1}{2}\left\|\varepsilon_h^{\lambda-}\right\|_{\partial\mathcal{E}_\mathcal{S}^n(t_n)}^2\\ &+ \left\|\boldsymbol{q} - \boldsymbol{\Pi}_{\boldsymbol{V}}\boldsymbol{q}\right\|_{f_n,\mathcal{T}^n}\left\|\partial_t\boldsymbol{\varepsilon}_h^{\boldsymbol{q}}\right\|_{f_n,\mathcal{T}^n} + \alpha\left\|\boldsymbol{\Pi}_{\boldsymbol{V}}\boldsymbol{q} - \boldsymbol{q}\right\|_{f_n,\mathcal{T}^n}\left\|\boldsymbol{\varepsilon}_h^{\boldsymbol{q}}\right\|_{f_n,\mathcal{T}^n}\\ &+ \left\|\boldsymbol{\Pi}_{\boldsymbol{V}}\boldsymbol{q} - \boldsymbol{q}\right\|_{f_n,\mathcal{F}_\Omega^n(t_{n+1})}\left\|\boldsymbol{\varepsilon}_h^{\boldsymbol{q}}\right\|_{f_n,\mathcal{F}_\Omega^n(t_{n+1})} + \left\|\boldsymbol{\Pi}_{\boldsymbol{V}-}\boldsymbol{q} - \boldsymbol{q}\right\|_{f_n,\mathcal{F}_\Omega^n(t_n)}\left\|\boldsymbol{\varepsilon}_h^{\boldsymbol{q}}\right\|_{f_n,\mathcal{F}_\Omega^n(t_n)}\\ &+ \left\|P_M^{f_n} v - v\right\|_{f_n,\partial\mathcal{E}_\mathcal{S}^n(t_{n+1})}\left\|\varepsilon_h^\lambda\right\|_{f_n,\partial\mathcal{E}_\mathcal{S}^n(t_{n+1})} + \left\|P_{M^-}^{f_{n-1}} v - v\right\|_{f_n,\partial\mathcal{E}_\mathcal{S}^n(t_n)}\left\|\varepsilon_h^\lambda\right\|_{f_n,\partial\mathcal{E}_\mathcal{S}^n(t_n)}.\end{aligned} \tag{3.139}$$

Note that, by eq. (3.42b) and eq. (3.42a),

$$\begin{aligned}\left\|\boldsymbol{\varepsilon}_h^{\boldsymbol{q}}\right\|_{f_n,\mathcal{F}_\Omega^n(t_n)} &\le C\Delta t^{-1/2}\left\|\boldsymbol{\varepsilon}_h^{\boldsymbol{q}}\right\|_{f_n,\mathcal{T}^n},\\ \left\|\varepsilon_h^\lambda\right\|_{f_n,\partial\mathcal{E}_\mathcal{S}^n(t_n)} &\le C\Delta t^{-1/2}\left\|\varepsilon_h^\lambda\right\|_{f_n,\mathcal{F}_\mathcal{S}^n}.\end{aligned} \tag{3.140}$$

Furthermore, combining a standard inverse inequality and using equivalence of the norms $\|\cdot\|_\mathcal{K}$ and $\|\cdot\|_{f_n,\mathcal{K}}$ we also have

$$\left\|\partial_t\boldsymbol{\varepsilon}_h^{\boldsymbol{q}}\right\|_{f_n,\mathcal{T}^n} \le C\Delta t^{-1}\left\|\boldsymbol{\varepsilon}_h^{\boldsymbol{q}}\right\|_{f_n,\mathcal{T}^n}. \tag{3.141}$$

Using eq. (3.140) and eq. (3.141) for the right hand side of eq. (3.139) and multiplying by 2,

$$
\begin{aligned}
&\alpha \left\|\boldsymbol{\varepsilon}_h^{\boldsymbol{q}}\right\|_{f_n,\mathcal{T}^n}^2 + \alpha \left\|\varepsilon_h^{\lambda}\right\|_{f_n,\mathcal{F}_{\mathcal{S}}^n}^2 + e^{-\alpha\Delta t} \left\|\boldsymbol{\varepsilon}_h^{\boldsymbol{q}}\right\|_{\mathcal{F}_{\Omega}^n(t_{n+1})}^2 + e^{-\alpha\Delta t} \left\|\varepsilon_h^{\lambda}\right\|_{\partial\mathcal{E}_{\mathcal{S}}^n(t_{n+1})}^2 \\
&\leq \left\|\boldsymbol{\varepsilon}_h^{\boldsymbol{q}^-}\right\|_{\mathcal{F}_{\Omega}^n(t_n)}^2 + \left\|\varepsilon_h^{\lambda^-}\right\|_{\partial\mathcal{E}_{\mathcal{S}}^n(t_n)}^2 \\
&\quad + C\Delta t^{-1} \left\|\boldsymbol{q} - \boldsymbol{\Pi}_{\boldsymbol{V}}\boldsymbol{q}\right\|_{f_n,\mathcal{T}^n} \left\|\boldsymbol{\varepsilon}_h^{\boldsymbol{q}}\right\|_{f_n,\mathcal{T}^n} + 2\alpha \left\|\boldsymbol{\Pi}_{\boldsymbol{V}}\boldsymbol{q} - \boldsymbol{q}\right\|_{f_n,\mathcal{T}^n} \left\|\boldsymbol{\varepsilon}_h^{\boldsymbol{q}}\right\|_{f_n,\mathcal{T}^n} \\
&\quad + C\Delta t^{-1/2} \left\|\boldsymbol{\Pi}_{\boldsymbol{V}}\boldsymbol{q} - \boldsymbol{q}\right\|_{f_n,\mathcal{F}_{\Omega}^n(t_{n+1})} \left\|\boldsymbol{\varepsilon}_h^{\boldsymbol{q}}\right\|_{f_n,\mathcal{T}^n} \\
&\quad + C\Delta t^{-1/2} \left\|\boldsymbol{\Pi}_{\boldsymbol{V}^-}\boldsymbol{q} - \boldsymbol{q}\right\|_{f_n,\mathcal{F}_{\Omega}^n(t_n)} \left\|\boldsymbol{\varepsilon}_h^{\boldsymbol{q}}\right\|_{f_n,\mathcal{T}^n} \\
&\quad + C\Delta t^{-1/2} \left\|P_M^{f_n} v - v\right\|_{f_n,\partial\mathcal{E}_{\mathcal{S}}^n(t_{n+1})} \left\|\varepsilon_h^{\lambda}\right\|_{f_n,\mathcal{F}_{\mathcal{S}}^n} \\
&\quad + C\Delta t^{-1/2} \left\|P_{M^-}^{f_{n-1}} v - v\right\|_{f_n,\partial\mathcal{E}_{\mathcal{S}}^n(t_n)} \left\|\varepsilon_h^{\lambda}\right\|_{f_n,\mathcal{F}_{\mathcal{S}}^n} .
\end{aligned}
\tag{3.142}
$$

Applying Young's inequality to the right hand side of eq. (3.142), we obtain

$$
\begin{aligned}
&\alpha \left\|\boldsymbol{\varepsilon}_h^{\boldsymbol{q}}\right\|_{f_n,\mathcal{T}^n}^2 + \alpha \left\|\varepsilon_h^{\lambda}\right\|_{f_n,\mathcal{F}_{\mathcal{S}}^n}^2 + e^{-\alpha\Delta t} \left\|\boldsymbol{\varepsilon}_h^{\boldsymbol{q}}\right\|_{\mathcal{F}_{\Omega}^n(t_{n+1})}^2 + e^{-\alpha\Delta t} \left\|\varepsilon_h^{\lambda}\right\|_{\partial\mathcal{E}_{\mathcal{S}}^n(t_{n+1})}^2 \\
&\leq \left\|\boldsymbol{\varepsilon}_h^{\boldsymbol{q}^-}\right\|_{\mathcal{F}_{\Omega}^n(t_n)}^2 + \left\|\varepsilon_h^{\lambda^-}\right\|_{\partial\mathcal{E}_{\mathcal{S}}^n(t_n)}^2 + \frac{C}{4\delta_1}\Delta t^{-2} \left\|\boldsymbol{q} - \boldsymbol{\Pi}_{\boldsymbol{V}}\boldsymbol{q}\right\|_{f_n,\mathcal{T}^n}^2 + \delta_1 \left\|\boldsymbol{\varepsilon}_h^{\boldsymbol{q}}\right\|_{f_n,\mathcal{T}^n}^2 \\
&\quad + \frac{C}{4\delta_1} \left\|\boldsymbol{\Pi}_{\boldsymbol{V}}\boldsymbol{q} - \boldsymbol{q}\right\|_{f_n,\mathcal{T}^n}^2 + \delta_1 \left\|\boldsymbol{\varepsilon}_h^{\boldsymbol{q}}\right\|_{f_n,\mathcal{T}^n}^2 + \frac{C}{4\delta_1}\Delta t^{-1} \left\|\boldsymbol{\Pi}_{\boldsymbol{V}}\boldsymbol{q} - \boldsymbol{q}\right\|_{f_n,\mathcal{F}_{\Omega}^n(t_{n+1})}^2 \\
&\quad + \delta_1 \left\|\boldsymbol{\varepsilon}_h^{\boldsymbol{q}}\right\|_{f_n,\mathcal{T}^n}^2 + \frac{C}{4\delta_1}\Delta t^{-1} \left\|\boldsymbol{\Pi}_{\boldsymbol{V}^-}\boldsymbol{q} - \boldsymbol{q}\right\|_{f_n,\mathcal{F}_{\Omega}^n(t_n)}^2 + \delta_1 \left\|\boldsymbol{\varepsilon}_h^{\boldsymbol{q}}\right\|_{f_n,\mathcal{T}^n}^2 \\
&\quad + \frac{C}{4\delta_2}\Delta t^{-1} \left\|P_M^{f_n} v - v\right\|_{f_n,\partial\mathcal{E}_{\mathcal{S}}^n(t_{n+1})}^2 + \delta_2 \left\|\varepsilon_h^{\lambda}\right\|_{f_n,\mathcal{F}_{\mathcal{S}}^n}^2 \\
&\quad + \frac{C}{4\delta_2}\Delta t^{-1} \left\|P_{M^-}^{f_{n-1}} v - v\right\|_{f_n,\partial\mathcal{E}_{\mathcal{S}}^n(t_n)}^2 + \delta_2 \left\|\varepsilon_h^{\lambda}\right\|_{f_n,\mathcal{F}_{\mathcal{S}}^n}^2 ,
\end{aligned}
\tag{3.143}
$$

where $\delta_1, \delta_2 > 0$ are free to choose constants. Collecting terms,

$$
\begin{aligned}
&(\alpha - 4\delta_1) \left\|\boldsymbol{\varepsilon}_h^{\boldsymbol{q}}\right\|_{f_n,\mathcal{T}^n}^2 + (\alpha - 2\delta_2) \left\|\varepsilon_h^{\lambda}\right\|_{f_n,\mathcal{F}_{\mathcal{S}}^n}^2 + e^{-\alpha\Delta t} \left\|\boldsymbol{\varepsilon}_h^{\boldsymbol{q}}\right\|_{\mathcal{F}_{\Omega}^n(t_{n+1})}^2 + e^{-\alpha\Delta t} \left\|\varepsilon_h^{\lambda}\right\|_{\partial\mathcal{E}_{\mathcal{S}}^n(t_{n+1})}^2 \\
&\leq \left\|\boldsymbol{\varepsilon}_h^{\boldsymbol{q}^-}\right\|_{\mathcal{F}_{\Omega}^n(t_n)}^2 + \left\|\varepsilon_h^{\lambda^-}\right\|_{\partial\mathcal{E}_{\mathcal{S}}^n(t_n)}^2 + C\Delta t^{-2} \left\|\boldsymbol{q} - \boldsymbol{\Pi}_{\boldsymbol{V}}\boldsymbol{q}\right\|_{f_n,\mathcal{T}^n}^2 \\
&\quad + C \left\|\boldsymbol{\Pi}_{\boldsymbol{V}}\boldsymbol{q} - \boldsymbol{q}\right\|_{f_n,\mathcal{T}^n}^2 + C\Delta t^{-1} \left\|\boldsymbol{\Pi}_{\boldsymbol{V}}\boldsymbol{q} - \boldsymbol{q}\right\|_{f_n,\mathcal{F}_{\Omega}^n(t_{n+1})}^2 \\
&\quad + C\Delta t^{-1} \left\|\boldsymbol{\Pi}_{\boldsymbol{V}^-}\boldsymbol{q} - \boldsymbol{q}\right\|_{f_n,\mathcal{F}_{\Omega}^n(t_n)}^2 + C\Delta t^{-1} \left\|P_M^{f_n} v - v\right\|_{f_n,\partial\mathcal{E}_{\mathcal{S}}^n(t_{n+1})}^2 \\
&\quad + C\Delta t^{-1} \left\|P_{M^-}^{f_{n-1}} v - v\right\|_{f_n,\partial\mathcal{E}_{\mathcal{S}}^n(t_n)}^2 .
\end{aligned}
\tag{3.144}
$$

The result follows by choosing $\delta_1 = \alpha/8$ and $\delta_2 = \alpha/4$. □

Remark 3.1. *If* $(\boldsymbol{q}, v) \in [H^{(s_t,s_s)}(\mathcal{E}^n)]^2 \times H^{(s_t,s_s)}(\mathcal{E}^n)$, *with* $1 < s_t \leq p+1$ *and* $1 \leq s_s \leq p+1$, *then combining Lemma 3.11, Corollary 3.1 and Lemma 3.9 gives the following leading order terms*

$$\begin{aligned}
&\tfrac{\alpha}{2} \left\|\boldsymbol{\varepsilon}_h^{\boldsymbol{q}}\right\|^2_{f_n,\mathcal{T}^n} + \tfrac{\alpha}{2} \left\|\varepsilon_h^{\lambda}\right\|^2_{f_n,\mathcal{F}_{\mathcal{S}}^n} + e^{-\alpha\Delta t} \left\|\boldsymbol{\varepsilon}_h^{\boldsymbol{q}}\right\|^2_{\mathcal{F}_{\Omega}^n(t_{n+1})} + e^{-\alpha\Delta t} \left\|\varepsilon_h^{\lambda}\right\|^2_{\partial\mathcal{E}_{\mathcal{S}}^n(t_{n+1})} \\
&\qquad \leq \left\|\boldsymbol{\varepsilon}_h^{\boldsymbol{q}^-}\right\|^2_{\mathcal{F}_{\Omega}^n(t_n)} + \left\|\varepsilon_h^{\lambda^-}\right\|^2_{\partial\mathcal{E}_{\mathcal{S}}^n(t_n)} \\
&\qquad\quad + C\left(\Delta t^{-2} h^{2s_s} + \Delta t^{2s_t-2}\right) \|\boldsymbol{q}\|^2_{H^{(s_t,s_s)}(\mathcal{E}^n)} \\
&\qquad\quad + C\left(\Delta t^{-2} h^{2s_s} + \Delta t^{2s_t-2}\right) \|v\|^2_{H^{(s_t,s_s)}(\mathcal{E}^n)} \\
&\qquad\quad + C\left(\Delta t^{-2} h^{2s_s} + \Delta t^{2s_t-2}\right) \|v\|^2_{H^{(s_t,s_s)}(\partial\mathcal{E}_{\mathcal{S}}^n)},
\end{aligned} \tag{3.145}$$

where $h = \max_{\mathcal{K}} h_K$.

To prove the *a priori* error estimates we will use the following lemma:

Lemma 3.12. *Let* $A_n, B_n, D_n \geq 0$ *for all* $n = 0, 1, \cdots N-1$, *and* $\alpha > 0$. *Moreover, assume that there exists a constant* $C \geq 0$ *such that* $C\Delta t B_n \leq A_n$ *for all* n. *If* $B_0 = 0$, $(N-1)\Delta t = T$ *and*

$$A_n + e^{-\alpha\Delta t} B_n \leq B_{n-1} + D_n, \tag{3.146}$$

then,

$$A_n \leq C \sum_{i=1}^{n} D_i, \tag{3.147}$$

where $C > 0$ *depends on* α *and* T.

Proof. Since $C\Delta t B_n \leq A_n$, by eq. (3.146), we have

$$\left(C\Delta t + e^{-\alpha\Delta t}\right) B_n \leq B_{n-1} + D_n. \tag{3.148}$$

Let $\gamma = C\Delta t + e^{-\alpha\Delta t}$. By induction, we have the following

$$\begin{aligned}
B_n &\leq \gamma^{-1} B_{n-1} + \gamma^{-1} D_n \\
&\leq \gamma^{-2} B_{n-2} + \gamma^{-2} D_{n-1} + \gamma^{-1} D_n \\
&\leq \gamma^{-3} B_{n-3} + \gamma^{-3} D_{n-2} + \gamma^{-2} D_{n-1} + \gamma^{-1} D_n \\
&\vdots \\
&\leq \sum_{i=1}^{n} \gamma^{i-n-1} D_i,
\end{aligned} \tag{3.149}$$

where we used that $B_0 = 0$. Note that $-n \leq i - n - 1 \leq -1$, $i \in \{1, \ldots, n\}$. This implies that if $\gamma \geq 1$ then $\gamma^{i-n-1} \leq \gamma^{-1} \leq 1$ while if $\gamma < 1$ then $\gamma^{i-n-1} \leq \gamma^{-n}$. We next bound γ^{-n}. Note that

$$e^{-\alpha \Delta t} \leq C_1 \Delta t + e^{-\alpha \Delta t} = \gamma. \tag{3.150}$$

Since $n \leq N-1$, we have that $\gamma^{-n} \leq e^{\alpha n \Delta t} \leq e^{\alpha T} \leq C_2$. Therefore $\gamma^{i-n-1} \leq \max\{1, C_2\} = C$.

We may therefore bound B_n in eq. (3.149) as:

$$B_n \leq C \sum_{i=1}^{n} D_i. \tag{3.151}$$

In order to obtain the final result, recall that, by eq. (3.146), we have the following:

$$A_n \leq B_{n-1} + D_n. \tag{3.152}$$

Using eq. (3.151) we obtain

$$A_n \leq C \sum_{i=1}^{n-1} D_i + D_n \leq C \sum_{i=1}^{n} D_i, \tag{3.153}$$

which completes the proof. □

The following theorem gives the final error bounds.

Theorem 3.4. *Let $h = \max_{K \in \mathcal{T}^n} h_K$. Assume that the spatial shape-regularity condition eq. (3.21) holds and that the triangulation $\mathcal{T}^n$ does not have any hanging nodes. Suppose that $(\boldsymbol{q}, v)$ solves eq. (3.1), with $\boldsymbol{q} \in [H^{(s_t, s_s)}(\mathcal{E}^n)]^2$ and $v \in H^{(s_t, s_s)}(\mathcal{E}^n)$, with $1/2 < s_t \leq p+1$ and $1 \leq s_s \leq p+1$. Then we have the following estimates:*

$$\begin{aligned} &\sum_{n=0}^{N-1} \left\| \boldsymbol{q} - \boldsymbol{q}_h \right\|_{f_n, \mathcal{T}^n} + \sum_{n=0}^{N-1} \left\| v - \lambda_h \right\|_{f_n, \mathcal{F}_S^n} \\ &\quad \leq C \left(\Delta t^{-1} h^{s_s} + \Delta t^{s_t - 1} \right) \| \boldsymbol{q} \|_{H^{(s_t, s_s)}(\mathcal{E}^n)} \\ &\quad + C \left(\Delta t^{-1} h^{s_s} + \Delta t^{s_t - 1} \right) \| v \|_{H^{(s_t, s_s)}(\mathcal{E}^n)} \\ &\quad + C \left(\Delta t^{-1} h^{s_s} + \Delta t^{s_t - 1} \right) \| v \|_{H^{(s_t, s_s)}(\partial \mathcal{E}_S^n)}, \end{aligned} \tag{3.154}$$

where $C > 0$ depends on α and the final time T.

Proof. Let

$$\begin{aligned} A_n &= \tfrac{\alpha}{2} \left\|\boldsymbol{\varepsilon}_h^{\boldsymbol{q}}\right\|_{f_n,\mathcal{T}^n}^2 + \tfrac{\alpha}{2} \left\|\varepsilon_h^{\lambda}\right\|_{f_n,\mathcal{F}_{\mathcal{S}}^n}^2, \\ B_n &= \left\|\boldsymbol{\varepsilon}_h^{\boldsymbol{q}}\right\|_{\mathcal{F}_{\Omega}^n(t_{n+1})}^2 + \left\|\varepsilon_h^{\lambda}\right\|_{\partial\mathcal{E}_{\mathcal{S}}^n(t_{n+1})}^2. \end{aligned} \tag{3.155}$$

Note that

$$B_{n-1} = \left\|\boldsymbol{\varepsilon}_h^{\boldsymbol{q}}\right\|_{\mathcal{F}_{\Omega}^{n-1}(t_n)}^2 + \left\|\varepsilon_h^{\lambda}\right\|_{\partial\mathcal{E}_{\mathcal{S}}^{n-1}(t_n)}^2 = \left\|\boldsymbol{\varepsilon}_h^{\boldsymbol{q}-}\right\|_{\mathcal{F}_{\Omega}^n(t_n)}^2 + \left\|\varepsilon_h^{\lambda-}\right\|_{\partial\mathcal{E}_{\mathcal{S}}^n(t_n)}^2. \tag{3.156}$$

By eq. (3.42b) and the equivalence of the norms $\|\cdot\|_{\mathcal{K}}$ and $\|\cdot\|_{f_n,\mathcal{K}}$, we have the following:

$$C\Delta t B_n \leq \left\|\boldsymbol{\varepsilon}_h^{\boldsymbol{q}}\right\|_{\mathcal{T}^n}^2 + \left\|\varepsilon_h^{\lambda}\right\|_{\mathcal{F}_{\mathcal{S}}^n}^2 \leq C A_n. \tag{3.157}$$

Moreover, let D_n be defined as follows:

$$\begin{aligned} D_n =& C\left(\Delta t^{-2} h^{2s_s} + \Delta t^{2s_t-2}\right) \|\boldsymbol{q}\|_{H^{(s_t,s_s)}(\mathcal{E}^n)}^2 \\ &+ C\left(\Delta t^{-2} h^{2s_s} + \Delta t^{2s_t-2}\right) \|v\|_{H^{(s_t,s_s)}(\mathcal{E}^n)}^2 \\ &+ C\left(\Delta t^{-2} h^{2s_s} + \Delta t^{2s_t-2}\right) \|v\|_{H^{(s_t,s_s)}(\partial\mathcal{E}_{\mathcal{S}}^n)}^2. \end{aligned} \tag{3.158}$$

With these definitions, Lemma 3.12 gives the following bound for the projection errors:

$$\begin{aligned} &\tfrac{\alpha}{2} \left\|\boldsymbol{\varepsilon}_h^{\boldsymbol{q}}\right\|_{f_n,\mathcal{T}^n}^2 + \tfrac{\alpha}{2} \left\|\varepsilon_h^{\lambda}\right\|_{f_n,\mathcal{F}_{\mathcal{S}}^n}^2 \\ &\quad\leq C\left(\Delta t^{-2} h^{2s_s} + \Delta t^{2s_t-2}\right) \sum_{k=0}^{n} \|\boldsymbol{q}\|_{H^{(s_t,s_s)}(\mathcal{E}^k)}^2 \\ &\quad+ C\left(\Delta t^{-2} h^{2s_s} + \Delta t^{2s_t-2}\right) \sum_{k=0}^{n} \|v\|_{H^{(s_t,s_s)}(\mathcal{E}^k)}^2 \\ &\quad+ C\left(\Delta t^{-2} h^{2s_s} + \Delta t^{2s_t-2}\right) \sum_{k=0}^{n} \|v\|_{H^{(s_t,s_s)}(\partial\mathcal{E}_{\mathcal{S}}^k)}^2. \end{aligned} \tag{3.159}$$

Summing over all time slabs, we obtain:

$$\begin{aligned} &\tfrac{\alpha}{2} \sum_{n=0}^{N-1} \left\|\boldsymbol{\varepsilon}_h^{\boldsymbol{q}}\right\|_{f_n,\mathcal{T}^n}^2 + \tfrac{\alpha}{2} \sum_{n=0}^{N-1} \left\|\varepsilon_h^{\lambda}\right\|_{f_n,\mathcal{F}_{\mathcal{S}}^n}^2 \\ &\quad\leq C(N-1)\left(\Delta t^{-2} h^{2s_s} + \Delta t^{2s_t-2}\right) \|\boldsymbol{q}\|_{H^{(s_t,s_s)}(\mathcal{E})}^2 \\ &\quad+ C(N-1)\left(\Delta t^{-2} h^{2s_s} + \Delta t^{2s_t-2}\right) \|v\|_{H^{(s_t,s_s)}(\mathcal{E})}^2 \\ &\quad+ C(N-1)\left(\Delta t^{-2} h^{2s_s} + \Delta t^{2s_t-2}\right) \|v\|_{H^{(s_t,s_s)}(\partial\mathcal{E}_{\mathcal{S}})}^2. \end{aligned} \tag{3.160}$$

By the triangle inequality note that

$$\begin{aligned}\sum_{n=0}^{N-1}\|\boldsymbol{q}-\boldsymbol{q}_h\|_{f_n,\mathcal{T}^n} &\leq \sum_{n=0}^{N-1}\|\boldsymbol{q}-\boldsymbol{\Pi}_{\boldsymbol{V}}\boldsymbol{q}\|_{f_n,\mathcal{T}^n}+\sum_{n=0}^{N-1}\|\boldsymbol{\varepsilon}_h^{\boldsymbol{q}}\|_{f_n,\mathcal{T}^n}\,,\\ \sum_{n=0}^{N-1}\|v-\lambda_h\|_{f_n,\mathcal{F}_{\mathcal{S}}^n} &\leq \sum_{n=0}^{N-1}\|v-P_M^{f_n}v\|_{f_n,\mathcal{F}_{\mathcal{S}}^n}+\sum_{n=0}^{N-1}\|\varepsilon_h^{\lambda}\|_{f_n,\mathcal{F}_{\mathcal{S}}^n}\,.\end{aligned} \tag{3.161}$$

The result follows by Lemma 3.9 and eq. (3.160). □

Remark 3.2. *Assuming* $\boldsymbol{q}\in\left[H^{(p+1,p+1)}(\mathcal{E})\right]^2$ *and* $v\in H^{(p+1,p+1)}(\mathcal{E})$*, the error estimates in Theorem 3.4 give the following leading order terms:*

$$\sum_{n=0}^{N-1}\|\boldsymbol{q}-\boldsymbol{q}_h\|_{f_n,\mathcal{T}^n}+\sum_{n=0}^{N-1}\|v-\lambda_h\|_{f_n,\mathcal{F}_{\mathcal{S}}^n}\leq C\left(\Delta t^{-1}h^{p+1}+\Delta t^{p}\right). \tag{3.162}$$

3.5 Numerical results

In this section we verify the theoretical results of the previous sections. The space-time HDG method for the linear free-surface problem eq. (3.1) is implemented using the modular finite-element method (MFEM) library [25]. The linear systems of algebraic equations are solved by the direct solver MUMPS [4, 5] through PETSc [7, 9]. We will consider the same test cases as in Chapter 2.

3.5.1 Linear waves in an unbounded domain

We consider the time harmonic linear free-surface waves example in an unbounded domain. We consider the domain $\Omega=[-1,\,1]\times[-1,\,0]$ and apply periodic boundary conditions at $x_1=-1$ and $x_1=1$. As in section 2.4.3, the analytical solution to this problem is given by

$$\phi(\boldsymbol{x},t)=A\cosh(k(x_2+1))\cos(\omega t-kx_1), \tag{3.163a}$$
$$\zeta(x_1,t)=-\partial_t\phi(x_1,0,t)=A\omega\cosh(k)\sin(\omega t-kx_1), \tag{3.163b}$$

where $\omega^2=k\tanh(k)$.

We take $k=2\pi$ and A such that the maximum amplitude of the wave height is 0.05. In table 3.1, table 3.2, and table 3.3 we show the approximation errors and convergence

rates for the velocity $\boldsymbol{q}_h$ on the entire space-time domain $\mathcal{E}$ and for the free-surface height λ_h on the entire free-surface boundary $\partial\mathcal{E}_\mathcal{S}$. We test convergence in space, in time, and in space-time separately.

We first test convergence in space. To ensure the spatial error dominates over the temporal error we take a small time step $\Delta t = 10^{-5}$ when $p = 1$ and $\Delta t = 10^{-4}$ when $p = 2$. We compute the error after 200 (when $p = 1$) or 20 (when $p = 2$) time steps. As observed in table 3.1, the error is of order $\mathcal{O}(h^{p+1})$.

We next consider convergence in time. For this we compute up to a final time $T = 1$. To ensure that the temporal error dominates over the spatial error we use a mesh consisting of 73728 elements when $p = 1$ and 36864 elements when $p = 2$. We observe in table 3.2 that the error is of order $\mathcal{O}(\Delta t^{p+1})$.

We note that the rates of convergence in space and time separately are better than predicted from remark 3.2. We now consider convergence in space-time in which we refine the spatial mesh and time step simultaneously. We compute the solution up to a final time of $T = 1$. The initial time step is $\Delta t = 0.25$ and the initial mesh has 18 elements. We observe in table 3.3 that the error is of order $\mathcal{O}(\Delta t^p + h^p)$, as expected from our analysis, see remark 3.2.

Finally, we consider a case where h is fixed so that the spatial mesh consists of 1152 triangles and the number of global degrees-of-freedom is 13920. We take $p = 1$ and solve the problem up to a final time $T = 1$. From remark 3.2, we see that if h is fixed, eventually the dominant term in the error will be of order $\mathcal{O}(\Delta t^{-1} h^{p+1})$, which results in divergence of the solution. This effect can be observed in table 3.4 where the errors start to increase after three levels of refinement in time. Unlike standard time stepping methods, for space-time methods Δt has to be chosen carefully depending on its relation to the spatial mesh size h.

Table 3.1: Spatial rates of convergence for linear waves in an unbounded domain, see section 3.5.1.

		$\boldsymbol{q}_h$		λ_h	
	DOFs	$L^2(\mathcal{E})$-error	Order	$L^2(\partial\mathcal{E}_\mathcal{S})$-error	Order
	228	1.1e-3	-	2.5e-2	-
$p=1$	888	3.2e-4	1.7	1.4e-2	0.9
	3504	8.5e-5	1.9	3.4e-3	2.0
	13920	2.2e-5	2.0	8.2e-4	2.1
	55488	5.4e-6	2.0	1.9e-4	2.1
	486	4.0e-4	-	1.5e-3	-
$p=2$	1890	6.0e-5	2.7	2.3e-4	2.8
	7452	7.9e-6	2.9	3.5e-5	2.7
	29592	1.0e-6	3.0	4.8e-6	2.9

Table 3.2: Time rates of convergence for linear waves in an unbounded domain, see section 3.5.1.

		$\boldsymbol{q}_h$		λ_h	
	Δt	$L^2(\mathcal{E})$-error	Order	$L^2(\partial\mathcal{E}_\mathcal{S})$-error	Order
	1	1.7e-2	-	1.7e-2	-
$p=1$	1/2	5.1e-3	1.8	5.1e-3	1.8
	1/4	1.2e-3	2.1	1.2e-3	2.1
	1/8	3.0e-4	2.0	3.0e-4	2.0
	1/16	8.2e-5	1.9	7.9e-5	1.9
	1	3.8e-3	-	3.8e-3	-
$p=2$	1/2	4.8e-4	3.0	4.8e-4	3.0
	1/4	5.9e-5	3.0	5.9e-5	3.0
	1/8	7.5e-6	3.0	7.5e-6	3.0
	1/16	1.6e-6	2.3	1.3e-6	2.5

Table 3.3: Space-time rates of convergence for linear waves in an unbounded domain, see section 3.5.1.

		$\boldsymbol{q}_h$		λ_h	
	DOFs	$L^2(\mathcal{E})$-error	Order	$L^2(\partial\mathcal{E}_\mathcal{S})$-error	Order
	228	3.5e-2	-	3.4e-2	-
$p=1$	888	1.7e-2	1.1	1.5e-2	1.2
	3504	7.2e-3	1.2	5.9e-3	1.3
	13920	3.2e-3	1.2	2.7e-3	1.2
	55488	1.5e-3	1.1	1.3e-3	1.1
	486	1.6e-2	-	1.3e-2	-
$p=2$	1890	3.4e-3	2.2	2.3e-3	2.5
	7452	6.7e-4	2.4	4.4e-4	2.4
	29592	1.4e-4	2.3	9.8e-5	2.2
	117936	3.1e-5	2.2	2.4e-5	2.1

Table 3.4: Time rates of convergence for a coarse mesh for linear waves in an unbounded domain, see section 3.5.1.

	$\boldsymbol{q}_h$		λ_h	
Δt	$L^2(\mathcal{E})$-error	Order	$L^2(\partial\mathcal{E}_\mathcal{S})$-error	Order
1	1.8e-2	-	1.8e-2	-
1/2	5.3e-3	1.7	5.2e-3	1.8
1/4	1.8e-3	1.6	1.5e-3	1.8
1/8	1.4e-3	0.3	9.9e-4	0.6
1/16	2.0e-3	-0.5	1.5e-3	-0.6
1/32	3.2e-3	-0.7	2.6e-3	-0.8
1/64	5.6e-3	-0.8	5.0e-3	-0.9
1/128	1.0e-2	-0.9	9.5e-3	-0.9
1/256	1.8e-2	-0.8	1.8e-2	-0.9

3.5.2 Simulation of water waves in a water tank

In this example we consider waves generated by a piston-type wavemaker. This test case is proposed in [88]. In this case we consider the spatial domain $\Omega = [0, 10] \times [-1, 0]$. We apply homogeneous Neumann boundary conditions on $x_1 = 10$ and $x_2 = -1$. The wave maker is located on the left side of the domain, i.e., at $x_1 = 0$, where the boundary condition is given by

$$\boldsymbol{q} \cdot \boldsymbol{n} = T(t), \tag{3.164}$$

where $T(t) = a \sin(ft)$ with $a = 0.05$ the amplitude of the wave and $f = 1.8138$ the frequency of the wave. We compute the solution for $t \in [0, 53.4]$ and take $\Delta t = 0.2$. The mesh consists of 512 prismatic elements which are constructed by extruding spatial triangles in the time direction. Figure 3.3 shows the free-surface elevation or wave height at different time levels for polynomial orders $p = 1$, $p = 2$ and $p = 3$. At time $t = 4$, the first wave leaves the wave maker which is located at $x_1 = 0$. At $t = 25.8$ the waves reach the right wall of the water tank. At time $t = 53.4$, waves have hit the right wall and have started traveling in the opposite direction. We furthermore note that the discretization is less diffusive as the polynomial degree increases.

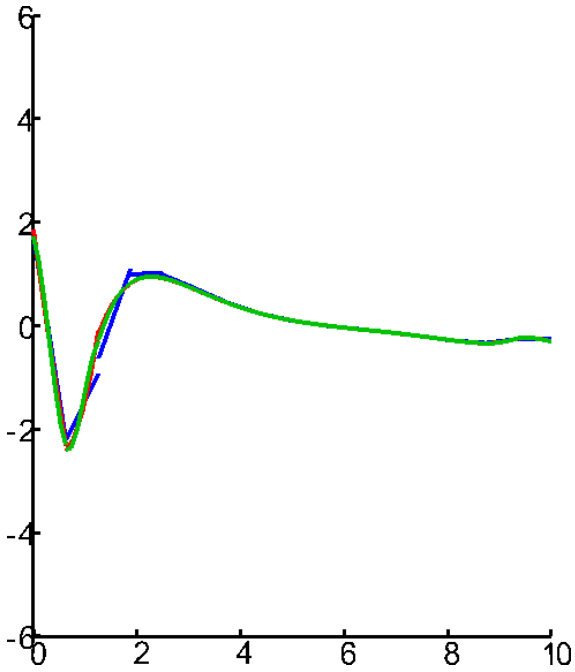

(a) Free-surface elevation at $t = 4$.

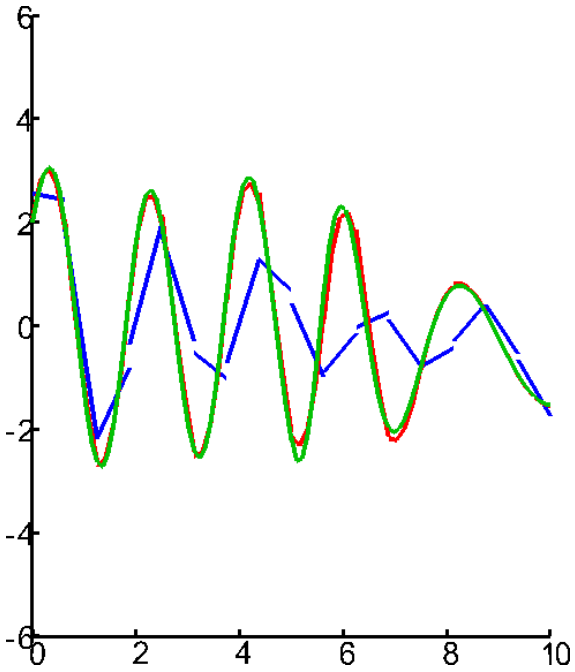

(b) Free-surface elevation at $t = 25.8$.

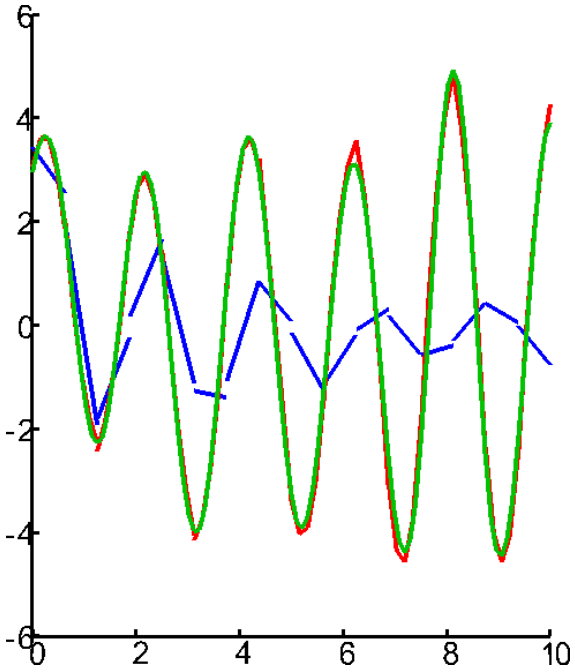

(c) Free-surface elevation at $t = 53.4$.

Figure 3.3: Simulation of water waves in a water tank, see section 3.5.2. The free-surface elevation at different time levels for polynomial degree $p = 1$ (blue line), $p = 2$ (red line), and $p = 3$ (green line).

Chapter 4

A space-time hybridizable/embedded discontinuous Galerkin method for nonlinear free-surface waves

In this Chapter we consider the nonlinear water wave problem eq. (4.3). This problem requires a discretization that can handle time-dependent domains and moving meshes. For this, we present a novel interface-tracking space-time hybridizable/embedded discontinuous Galerkin method with a level set approach for the numerical solution of the two-fluid Navier–Stokes equations. The Navier–Stokes equations are solved with a space-time HDG method that is point-wise divergence-free and $H(\mathrm{div})$-conforming, which implies exact mass conservation. For the level set equation we use a space-time EDG method which allows straightforward updating of the mesh without having to rely on smoothing techniques that could potentially lead to instabilities, as was shown in [2].

The space-time HDG method used for the two-fluid incompressible flow problem is *compatible* with the space-time EDG method for the level set equation, i.e., given the discrete velocity the space-time EDG method is able to preserve the constant solution. We remark that for discontinuous Galerkin methods compatibility is a stronger statement than local conservation of the flow field [22]. It was furthermore shown in [22] that if a method is not compatible it may produce erroneous solutions.

We first recast eq. (1.36) in a space-time setting and introduce the notation that will be used in this chapter.

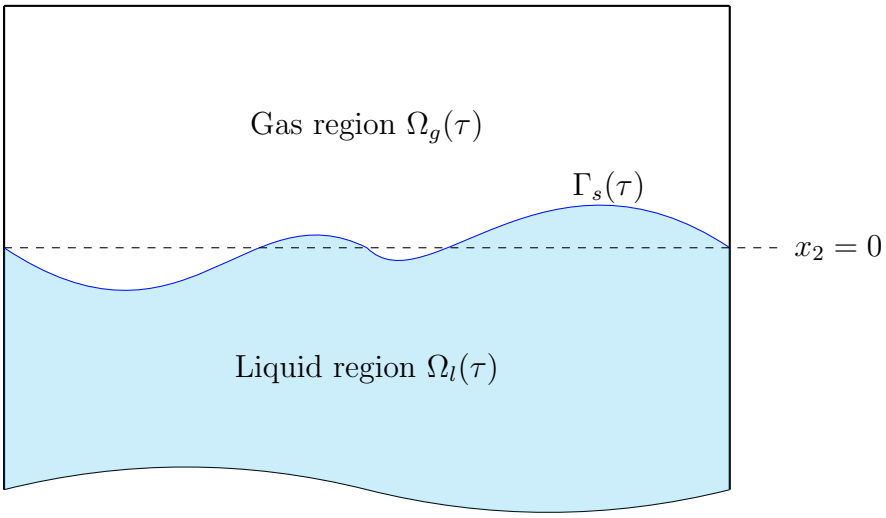

Figure 4.1: A description of the two-fluid flow domain $\Omega \subset \mathbb{R}^2$ at time $t = \tau$.

4.1 The space-time incompressible two-fluid flow model

Let $\Omega \subset \mathbb{R}^2$ be a bounded domain and let $I = (0, t_N]$ be the time interval of interest. Furthermore, let $\mathcal{E} := \Omega \times I \subset \mathbb{R}^3$ denote the space-time domain. We assume that the space-time domain $\mathcal{E}$ is divided into two non-overlapping polygonal regions, $\mathcal{E}_l$ and $\mathcal{E}_g$ such that $\mathcal{E} = \mathcal{E}_l \cup \mathcal{E}_g$. In what follows, $\mathcal{E}_l$ and $\mathcal{E}_g$ represent, respectively, the liquid and gas regions of the space-time domain. Let $x = (x_1, x_2)$, then the liquid and gas regions at a particular time level τ are denoted by $\Omega_l(\tau) := \{(x,t) \in \mathcal{E}_l \ : \ t = \tau\}$ and $\Omega_g(\tau) := \{(x,t) \in \mathcal{E}_g \ : \ t = \tau\}$. Note that the spatial domains Ω_l and Ω_g are *time-dependent*.

The space-time interface between the liquid and gas regions is defined as

$$\mathcal{S} := \left\{(x,t) \in \mathcal{E} \ : \ x_2 = \zeta(x_1, t)\right\}, \tag{4.1}$$

where $\zeta(x_1, t)$ is the wave height. We will denote the interface at time level τ by $\Gamma_s(\tau) := \{(x,t) \in \mathcal{S} \ : \ t = \tau\}$. A plot of the domain at time level τ is given in fig. 4.1.

The position of the interface eq. (4.1) is not known a priori. To find its position we introduce the level set function $\phi(t,x) = \zeta(t, x_1) - x_2$ and the Heaviside function $H(\phi)$ which is defined by

$$H(\phi) = \begin{cases} 1 & \text{if } \phi > 0, \\ 0 & \text{if } \phi < 0. \end{cases} \tag{4.2}$$

We note that the interface corresponds to the zero level set, $\phi = 0$.

Let k be a subscript to denote a liquid ($k = l$) or a gas ($k = g$) property. Then given the dynamic viscosities $\mu_k \in \mathbb{R}^+$, the constant densities $\rho_k \in \mathbb{R}^+$, and the constant acceleration due to gravity g, the space-time formulation of the incompressible two-fluid flow model for the velocity $u : \mathcal{E} \to \mathbb{R}^2$ and pressure $p : \mathcal{E} \to \mathbb{R}$ is given by

$$\rho\left(\partial_t u + u \cdot \nabla u\right) + \nabla p - \mu \Delta u = -\rho g e_2 \qquad \text{in } \mathcal{E}, \tag{4.3a}$$

$$\nabla \cdot u = 0 \qquad \text{in } \mathcal{E}, \tag{4.3b}$$

$$\partial_t \phi + u \cdot \nabla \phi = 0 \qquad \text{in } \mathcal{E}, \tag{4.3c}$$

where e_2 is the unit vector in the x_2-direction and

$$u = u_g + (u_l - u_g)H(\phi), \qquad p = p_g + (p_l - p_g)H(\phi), \tag{4.4a}$$

$$\rho = \rho_g + (\rho_l - \rho_g)H(\phi), \qquad \mu = \mu_g + (\mu_l - \mu_g)H(\phi). \tag{4.4b}$$

Let $\Omega_0 := \{(x,t) \in \partial\mathcal{E} \ : \ t = 0\}$ and similarly $\Omega_N := \{(x,t) \in \partial\mathcal{E} \ : \ t = t_N\}$. Then the boundary of the space-time domain $\mathcal{E}$ is partitioned such that $\partial\mathcal{E} = \partial\mathcal{E}^D \cup \partial\mathcal{E}^N \cup \Omega_0 \cup \Omega_N$, where there is no overlap between the four sets. Here, $\partial\mathcal{E}^D$ and $\partial\mathcal{E}^N$ denote, respectively, the Dirichlet and Neumann parts of the space-time boundary. The space-time outward unit normal vector to $\partial\mathcal{E}$ is denoted by (n_t, n), with $n_t \in \mathbb{R}$ the temporal component and $n \in \mathbb{R}^2$ the spatial component. We will define the inflow boundary $\partial\mathcal{E}^-$ as the portion of $\partial\mathcal{E}^N$ on which $n_t + u \cdot n < 0$. The outflow boundary is then defined as $\partial\mathcal{E}^+ := \partial\mathcal{E}^N \backslash \partial\mathcal{E}^-$. We prescribe the following boundary and initial conditions:

$$u = 0 \qquad \text{on } \partial\mathcal{E}^D, \tag{4.5a}$$

$$\left[n_t + u \cdot n - \max\left(n_t + u \cdot n, 0\right)\right] u + \left(p\mathbb{I} - \mu\nabla u\right) n = f \qquad \text{on } \partial\mathcal{E}^N, \tag{4.5b}$$

$$u(x,0) = u_0(x) \qquad \text{in } \Omega_0, \tag{4.5c}$$

$$-(n_t + u \cdot n)\phi = r \qquad \text{on } \partial\mathcal{E}^-, \tag{4.5d}$$

$$\phi(x,0) = \phi_0(x) \qquad \text{in } \Omega_0, \tag{4.5e}$$

where the boundary data $f : \partial\mathcal{E}^N \to \mathbb{R}^d$ and $r : \partial\mathcal{E}^- \to \mathbb{R}$, and the divergence-free initial condition $u_0 : \Omega_0 \to \mathbb{R}^d$ are given. Furthermore, $\phi_0(x) := \zeta_0(x_1) - x_2$ with $\zeta_0(x_1)$ the given initial wave height. Here, $\mathbb{I}$ is the 2×2 identity matrix.

We remark that the two-fluid problem assumes a no-slip and a dynamic boundary condition on the interface, i.e.,

$$u_l = u_g \qquad \text{on } \mathcal{S}, \tag{4.6a}$$

$$\left(p_l\mathbb{I} - \mu_l\nabla u_l\right) n_s = \left(p_g\mathbb{I} - \mu_g\nabla u_g\right) n_s \qquad \text{on } \mathcal{S}, \tag{4.6b}$$

respectively, where n_s is the normal vector on the interface $\Gamma_s(t)$ pointing outwards from $\Omega_l(t)$.

4.2 The space-time hybridizable/embedded discontinuous Galerkin method

In this section we will introduce the space-time discretization for the two-fluid problem eqs. (4.3) and (4.5). In particular we will introduce a space-time HDG for the momentum and mass eqs. (4.3a) and (4.3b) coupled to a space-time EDG discretization of the level set equation eq. (4.3c).

4.2.1 Space-time notation

We will use notation similar to for example [38]. For this we first partition the time interval I into time levels $0 = t_0 < t_1 < t_2 < \ldots < t_N$ and denote the n^{th} time interval by $I_n = (t_n, t_{n+1})$. The length of each time interval is denoted by $\Delta t = t_{n+1} - t_n$ and we denote the n^{th} space-time slab as $\mathcal{E}^n := \mathcal{E} \cap \left(\mathbb{R}^2 \times I_n\right)$. Define $\Omega_n := \{(x,t) \in \mathcal{E} : t = t_n\}$. The boundary of a space-time slab, $\partial\mathcal{E}^n$, can then be divided into Ω_n, Ω_{n+1}, and $\mathcal{Q}_{\mathcal{E}}^n := \partial\mathcal{E}^n \backslash (\Omega_{n+1} \cup \Omega_n)$.

Following [37, 38] we consider a tetrahedral space-time mesh which is constructed as follows. First, the triangular spatial mesh of Ω_n is extruded to the new time level t_{n+1} according to the domain deformation prescribed by the wave height. (Note that the wave height is not known a priori and so, as we will describe in section 4.3, an iterative procedure is used to find the final approximation to the domain at time level t_{n+1}.) Each element of this prismatic space-time mesh is then subdivided into three tetrahedrons. We denote the space-time triangulation in space-time slab $\mathcal{E}^n$ by $\mathcal{T}^n := \{\mathcal{K}\}$. The space-time elements $\mathcal{K} \in \mathcal{T}^n$ that lie in the liquid region of the space-time slab form the triangulation $\mathcal{T}_l^n$. $\mathcal{T}_g^n$ is defined similarly but for the gas region. The triangulation of the whole space-time domain $\mathcal{E}$ is denoted by $\mathcal{T} := \cup_n \mathcal{T}^n$.

The boundary of a space-time tetrahedron $\mathcal{K}_j \in \mathcal{T}^n$ is denoted by $\partial\mathcal{K}_j$ and the outward unit space-time normal vector on the boundary of $\mathcal{K}_j \in \mathcal{T}^n$ is given by $(n_t^{\mathcal{K}_j}, n^{\mathcal{K}_j})$. The boundary $\partial\mathcal{K}_j$ consists of at most one face that belongs to a time level (on which $|n_t^{\mathcal{K}_j}| = 1$). We denote this face by K_j^n if $n_t^{\mathcal{K}_j} = -1$ and by K_j^{n+1} if $n_t^{\mathcal{K}_j} = 1$. The remaining faces of $\partial\mathcal{K}_j$ are denoted by $\mathcal{Q}_{\mathcal{K}_j}^n := \partial\mathcal{K}_j \backslash K_j^n$. or $\mathcal{Q}_{\mathcal{K}_j}^n := \partial\mathcal{K}_j \backslash K_j^{n+1}$. In the remainder of this

Chapter we will drop the sub- and superscript notation when referring to the space-time normal vector and the space-time cell wherever no confusion will occur.

In a space-time slab $\mathcal{E}^n$, the set of all faces for which $|n_t| \neq 1$ is denoted by $\mathcal{F}^n$ while the union of these faces is denoted by Γ^n. By $\mathcal{F}_{\mathcal{S}}^n$ we denote all the faces in $\mathcal{F}^n$ that lie on the interface $\mathcal{S}$. Similarly, the set of all faces in $\mathcal{F}^n$ that lie on the boundary of the space-time domain is denoted by $\mathcal{F}_B^n$. The remaining set of (interior) faces is denoted by $\mathcal{F}_I^n$. Then $\mathcal{F}^n = \mathcal{F}_I^n \cup \mathcal{F}_{\mathcal{S}}^n \cup \mathcal{F}_B^n$. Furthermore, we will denote the set of faces that lie on a Neumann boundary, $\partial\mathcal{E}^N \cap \partial\mathcal{E}^n$, by $\mathcal{F}_N^n$.

On each space-time slab $\mathcal{E}^n$ we consider the following discontinuous finite element spaces on $\mathcal{T}^n$:

$$V_h^n := \left\{ v_h \in \left[L^2(\mathcal{T}^n)\right]^2 : v_h|_{\mathcal{K}} \in \left[P^k(\mathcal{K})\right]^2, \forall \mathcal{K} \in \mathcal{T}^n \right\}, \tag{4.7a}$$

$$Q_h^n := \left\{ q_h \in L^2(\mathcal{T}^n) : q_h|_{\mathcal{K}} \in P^{k-1}(\mathcal{K}), \forall \mathcal{K} \in \mathcal{T}^n \right\}, \tag{4.7b}$$

$$M_h^n := \left\{ m_h \in L^2(\mathcal{T}^n) : m_h|_{\mathcal{K}} \in P^k(\mathcal{K}), \forall \mathcal{K} \in \mathcal{T}^n \right\}, \tag{4.7c}$$

where $P^l(D)$ denotes the space of polynomials of degree l on a domain D. Additionally, we consider the following facet finite element spaces:

$$\bar{V}_h^n := \left\{ \bar{v}_h \in \left[L^2(\mathcal{F}^n)\right]^2 : \bar{v}_h|_{\mathcal{F}} \in \left[P^k(\mathcal{F})\right]^2, \forall \mathcal{F} \in \mathcal{F}^n, \bar{v}_h = 0 \text{ on } \partial\mathcal{E}^D \cap \partial\mathcal{E}^n \right\}, \tag{4.8a}$$

$$\bar{Q}_h^n := \left\{ \bar{q}_h \in L^2(\mathcal{F}^n) : \bar{q}_h|_{\mathcal{F}} \in P^k(\mathcal{F}), \forall \mathcal{F} \in \mathcal{F}^n \right\}, \tag{4.8b}$$

$$\bar{M}_h^n := \left\{ \bar{m}_h \in L^2(\mathcal{F}^n) : \bar{m}_h|_{\mathcal{F}} \in P^k(\mathcal{F}), \forall \mathcal{F} \in \mathcal{F}^n \right\} \cap C(\Gamma^n). \tag{4.8c}$$

Note that the facet velocity field in $\bar{V}_h^n$ and facet pressure field in $\bar{Q}_h^n$ are discontinuous while the facet level set field in $\bar{M}_h^n$ is continuous. We note that the left and right traces of a function $u_h \in V_h^n$ at an interior facet $\mathcal{F} \in \mathcal{F}_I^n \cup \mathcal{F}_S^n$ are denoted by u_h^l and u_h^r. In general, $u_h^l \neq u_h^r$, so it will be useful to introduce the jump operator $[\![u_h \cdot n]\!] = u_h^l \cdot n^l + u_h^r \cdot n^r$. On a boundary facet $\mathcal{F} \in \mathcal{F}_B^n$, the jump operator is defined as $[\![u_h \cdot n]\!] = u_h \cdot n$. Analogous definitions apply for functions in Q_h^n.

To simplify the notation, we introduce $X_h^{v,n} := V_h^n \times \bar{V}_h^n$, $X_h^{q,n} = Q_h^n \times \bar{Q}_h^n$, $X_h^n = X_h^{v,n} \times X_h^{q,n}$, and $X_h^{m,n} = M_h^n \times \bar{M}_h^n$. Function pairs in $X_h^{v,n}$, $X_h^{q,n}$, and $X_h^{m,n}$ will be denoted by boldface, e.g., $\boldsymbol{v}_h = (v_h, \bar{v}_h) \in X_h^{v,n}$, $\boldsymbol{q}_h = (q_h, \bar{q}_h) \in X_h^{q,n}$ and $\boldsymbol{m}_h = (m_h, \bar{m}_h) \in X_h^{m,n}$.

We will make use of the $H(\mathrm{div}; D)$ space, where $D \subset \mathbb{R}^d$, which is defined as

$$H(\mathrm{div}; D) = \left\{ u \in \left[L^2(D)\right]^d : \nabla \cdot u \in L^2(D) \right\}. \tag{4.9}$$

4.2.2 Discretization of the momentum and mass equations

An exactly mass conserving space-time HDG discretization for the single-phase Navier–Stokes equations was introduced in [37, 38]. Here we modify this discretization to take into account that the density and viscosity may be discontinuous across elements (see eq. (4.4b)).

Since the density and viscosity is constant on each element $\mathcal{K} \in \mathcal{T}^n$ we define $\rho_{\mathcal{K}} = \rho_g$ if $\mathcal{K} \in \mathcal{T}_g^n$ and $\rho_{\mathcal{K}} = \rho_l$ if $\mathcal{K} \in \mathcal{T}_l^n$ (and $\mu_{\mathcal{K}}$ is defined similarly).

First, we focus on eq. (4.3a). Note that since $\nabla \cdot u = 0$, we can write $u \cdot \nabla u = \nabla \cdot (u \otimes u)$, where, $\otimes$ denotes the outer product. For two vectors $a \in \mathbb{R}^n$ and $b \in \mathbb{R}^m$, $a \otimes b \in \mathbb{R}^{n \times m}$ with elements $\left(a \otimes b\right)_{ij} = a_i b_j$. Multiply by a test function $v_h \in V_h^n$ integrate over a space-time element $\mathcal{K} \in \mathcal{T}^n$ and replace u by $u_h \in V_h^n$ and p by $p_h \in Q_h^n$. Sum over all space-time elements in $\mathcal{E}^n$ to obtain

$$\sum_{\mathcal{K} \in \mathcal{T}_h} \int_{\mathcal{K}} \rho_{\mathcal{K}} \left(\partial_t u_h \cdot v_h + \nabla \cdot (u_h \otimes u_h) \cdot v_h \right) \mathrm{d}x \, \mathrm{d}t + \sum_{\mathcal{K} \in \mathcal{T}^n} \int_{\mathcal{K}} \nabla p_h \cdot v_h \, \mathrm{d}x \, \mathrm{d}t$$
$$- \sum_{\mathcal{K} \in \mathcal{T}^n} \int_{\mathcal{K}} \mu_{\mathcal{K}} \Delta u_h \cdot v_h \, \mathrm{d}x \, \mathrm{d}t = - \sum_{\mathcal{K} \in \mathcal{T}^n} \int_{\mathcal{K}} \rho_{\mathcal{K}} g e_2 \cdot v_h \, \mathrm{d}x \, \mathrm{d}t. \quad (4.10)$$

Applying integration by parts in both space-time, we obtain

$$- \sum_{\mathcal{K} \in \mathcal{T}_h} \int_{\mathcal{K}} \rho_{\mathcal{K}} \left(u_h \cdot \partial_t v_h + (u_h \otimes u_h) : \nabla v_h \right) \mathrm{d}x \, \mathrm{d}t + \sum_{\mathcal{K} \in \mathcal{T}^n} \int_{\partial \mathcal{K}} H_{\mathcal{K}}(\boldsymbol{u}_h, u_h; \rho_{\mathcal{K}}, n_t, n) \cdot v_h \, \mathrm{d}s$$
$$- \sum_{\mathcal{K} \in \mathcal{T}^n} \int_{\mathcal{K}} p_h \nabla \cdot v_h \, \mathrm{d}x \, \mathrm{d}t + \sum_{\mathcal{K} \in \mathcal{T}^n} \int_{\mathcal{K}} \mu_{\mathcal{K}} \nabla u_h : \nabla v_h \, \mathrm{d}x \, \mathrm{d}t$$
$$+ \sum_{\mathcal{K} \in \mathcal{T}^n} \int_{\mathcal{Q}_{\mathcal{K}}} \widehat{\sigma}_h n \cdot v_h \, \mathrm{d}s = - \sum_{\mathcal{K} \in \mathcal{T}^n} \int_{\mathcal{K}} \rho_{\mathcal{K}} g e_2 \cdot v_h \, \mathrm{d}x \, \mathrm{d}t. \quad (4.11)$$

Here we have introduced the space-time upwind numerical flux $H_{\mathcal{K}}(\boldsymbol{u}_h, u_h; \rho_{\mathcal{K}}, n_t, n)$ and the diffusive numerical flux $\widehat{\sigma}_h$. The upwind flux is defined as

$$H_{\mathcal{K}}(\boldsymbol{u}_h, u_h; \rho_{\mathcal{K}}, n_t, n) = \begin{cases} \widehat{\rho}_{\mathcal{K}}(n_t + u_h \cdot n)(u_h + \lambda(\bar{u}_h - u_h)) & \text{on } \mathcal{Q}_{\mathcal{K}}, \\ \rho_{\mathcal{K}} u_h n_t & \text{on } K^{n+1}, \\ \rho_{\mathcal{K}} u_h^- n_t & \text{on } K^n, \end{cases} \quad (4.12)$$

where $\lambda = 1$ if $n_t + u \cdot n < 0$ and $\lambda = 0$ otherwise, and $u_h^- = \lim_{\epsilon \to 0} u_h(t_n - \epsilon, x)$ for $n > 0$. When $n = 0$ then u_h^- is the projection of the initial condition u_0 into $V_h^0 \cap H(\mathrm{div}; \Omega_0)$ such

that it is exactly divergence-free. Here, $\widehat{\rho}_{\mathcal{K}} = (\rho_{\mathcal{K}} + \rho_{\mathcal{K}^-})/2$, where $\mathcal{K}^-$ is the neighboring element to $\mathcal{K}$ that shares a facet on $\mathcal{Q}_{\mathcal{K}}$. We consider an interior penalty-type diffusive numerical flux

$$\widehat{\sigma}_h = -\mu_{\mathcal{K}} \nabla u_h + \bar{p}_h \mathbb{I} + \frac{\mu_{\mathcal{K}} \alpha}{h_{\mathcal{K}}} (u_h - \bar{u}_h) \otimes n, \tag{4.13}$$

where $\alpha > 0$ is a penalty parameter that has to be large enough to ensure stability [46]. Substituting these definitions in eq. (4.11), we obtain

$$\begin{aligned}
&- \sum_{\mathcal{K} \in \mathcal{T}_h} \int_{\mathcal{K}} \rho_{\mathcal{K}} \left(u_h \cdot \partial_t v_h + (u_h \otimes u_h) : \nabla v_h \right) \mathrm{d}x \, \mathrm{d}t + \sum_{\mathcal{K} \in \mathcal{T}^n} \int_{K^{n+1}} \rho_{\mathcal{K}} u_h \cdot v_h \, \mathrm{d}x \\
&\quad + \sum_{\mathcal{K} \in \mathcal{T}^n} \int_{\mathcal{Q}_{\mathcal{K}}} \widehat{\rho}_{\mathcal{K}} (n_t + u_h \cdot n)(u_h + \lambda(\bar{u}_h - u_h)) \cdot v_h \, \mathrm{d}s - \sum_{\mathcal{K} \in \mathcal{T}^n} \int_{\mathcal{K}} p_h \nabla \cdot v_h \, \mathrm{d}x \, \mathrm{d}t \\
&\quad + \sum_{\mathcal{K} \in \mathcal{T}^n} \int_{\mathcal{K}} \mu_{\mathcal{K}} \nabla u_h : \nabla v_h \, \mathrm{d}x \, \mathrm{d}t + \sum_{\mathcal{K} \in \mathcal{T}^n} \int_{\mathcal{Q}_{\mathcal{K}}} \bar{p}_h v_h \cdot n \, \mathrm{d}s - \sum_{\mathcal{K} \in \mathcal{T}^n} \int_{\mathcal{Q}_{\mathcal{K}}} \mu_{\mathcal{K}} \frac{\partial u_h}{\partial n} \cdot v_h \, \mathrm{d}s \\
&\quad - \sum_{\mathcal{K} \in \mathcal{T}^n} \int_{\mathcal{Q}_{\mathcal{K}}} \mu_{\mathcal{K}} \frac{\partial v_h}{\partial n} \cdot (u_h - \bar{u}_h) \, \mathrm{d}s + \sum_{\mathcal{K} \in \mathcal{T}^n} \int_{\mathcal{Q}_{\mathcal{K}}} \frac{\mu_{\mathcal{K}} \alpha}{h_{\mathcal{K}}} (u_h - \bar{u}_h) \cdot v_h \, \mathrm{d}s \\
&\quad = - \sum_{\mathcal{K} \in \mathcal{T}^n} \int_{\mathcal{K}} \rho_{\mathcal{K}} g e_2 \cdot v_h \, \mathrm{d}x \, \mathrm{d}t + \sum_{\mathcal{K} \in \mathcal{T}^n} \int_{K^n} \rho_{\mathcal{K}} u_h^- \cdot v_h \, \mathrm{d}x.
\end{aligned} \tag{4.14}$$

The last term on the left-hand side of eq. (4.14) is consistent and usually added for symmetry of the diffusive terms. To obtain a consistent discretization, we add the following term to the left-hand side of eq. (4.14)

$$\sum_{\mathcal{K} \in \mathcal{T}^n} \int_{\mathcal{Q}_{\mathcal{K}}} \left(\rho_{\mathcal{K}} - \widehat{\rho}_{\mathcal{K}} \right) \left(n_t + w \cdot n \right) u_h \cdot v_h \, \mathrm{d}s. \tag{4.15}$$

Now, we move on to eq. (4.3b). Multiply by a test function $q_h \in Q_h^n$, integrate over a space-time element $\mathcal{K} \in \mathcal{T}^n$ and replace u by $u_h \in V_h^n$. Sum over all space-time elements in $\mathcal{E}^n$ to obtain

$$\sum_{\mathcal{K} \in \mathcal{T}^n} \int_{\mathcal{K}} \nabla \cdot u_h q_h \, \mathrm{d}x \, \mathrm{d}t = 0. \tag{4.16}$$

Integrating by parts twice, and introducing the numerical flux $\widehat{u}_h \cdot n = \bar{u}_h \cdot n$ in the first integration by parts, we get

$$\sum_{\mathcal{K} \in \mathcal{T}^n} \int_{\mathcal{K}} \nabla \cdot u_h q_h \, \mathrm{d}x \, \mathrm{d}t - \sum_{\mathcal{K} \in \mathcal{T}^n} \int_{\mathcal{Q}_{\mathcal{K}}} (u_h - \bar{u}_h) \cdot n q_h \, \mathrm{d}s = 0. \tag{4.17}$$

In addition to eq. (4.14) and eq. (4.17), we introduce an equation that imposes that the sum of the space-time normal components of the numerical fluxes $H_{\mathcal{K}}(\boldsymbol{u}_h, u_h; \rho_{\mathcal{K}}, n_t, n)$ and $\widehat{\sigma}_h$ is single-valued on the faces of the mesh:

$$
\begin{aligned}
-\sum_{\mathcal{K}\in\mathcal{T}^n}\int_{\mathcal{Q}_{\mathcal{K}}}\widehat{\rho}_{\mathcal{K}}(n_t+u_h\cdot n)(u_h+\lambda(\bar{u}_h-u_h))\cdot\bar{v}_h\,\mathrm{d}s-\sum_{\mathcal{K}\in\mathcal{T}^n}\int_{\mathcal{Q}_{\mathcal{K}}}\bar{p}_h\bar{v}_h\cdot n\,\mathrm{d}s\\
+\sum_{\mathcal{K}\in\mathcal{T}^n}\int_{\mathcal{Q}_{\mathcal{K}}}\mu_{\mathcal{K}}\frac{\partial u_h}{\partial n}\cdot\bar{v}_h\,\mathrm{d}s-\sum_{\mathcal{K}\in\mathcal{T}^n}\int_{\mathcal{Q}_{\mathcal{K}}}\frac{\mu_{\mathcal{K}}\alpha}{h_{\mathcal{K}}}(u_h-\bar{u}_h)\cdot\bar{v}_h\,\mathrm{d}s\\
+\int_{\partial\mathcal{E}^+}\rho_{\mathcal{K}}(n_t+\bar{u}_h\cdot n)\bar{u}_h\cdot\bar{v}_h\,\mathrm{d}s=-\sum_{\mathcal{F}\in\mathcal{F}_N^n}\int_{\mathcal{F}}f\cdot\bar{v}_h\,\mathrm{d}s.
\end{aligned}
\tag{4.18}
$$

Collecting eq. (4.14), eq. (4.17) and eq. (4.18), the space-time HDG discretization for the momentum and mass equations eqs. (4.3a) and (4.3b) is given by: find $(\boldsymbol{u}_h, \boldsymbol{p}_h) \in X_h^n$ such that

$$
\begin{aligned}
&t_h^n(\boldsymbol{u}_h,\boldsymbol{u}_h,\boldsymbol{v}_h)+a_h^n(\boldsymbol{u}_h,\boldsymbol{v}_h)+b_h^n(\boldsymbol{p}_h,\boldsymbol{v}_h)-b_h^n(\boldsymbol{q}_h,\boldsymbol{u}_h)\\
&\qquad=-\sum_{\mathcal{K}\in\mathcal{T}^n}\int_{\mathcal{K}}\rho_{\mathcal{K}}ge_2\cdot v_h\,\mathrm{d}x\,\mathrm{d}t-\sum_{\mathcal{F}\in\mathcal{F}_N^n}\int_{\mathcal{F}}f\cdot\bar{v}_h\,\mathrm{d}s+\int_{\Omega_n}\rho_{\mathcal{K}}u_h^-\cdot v_h\,\mathrm{d}x,
\end{aligned}
\tag{4.19}
$$

for all $(\boldsymbol{v}_h, \boldsymbol{q}_h) \in X_h^n$. The convective trilinear form is given by

$$
\begin{aligned}
t_h^n(\boldsymbol{w};\boldsymbol{u},\boldsymbol{v}):=&-\sum_{\mathcal{K}\in\mathcal{T}^n}\int_{\mathcal{K}}\rho_{\mathcal{K}}\left(u\cdot\partial_t v+u\otimes w:\nabla v\right)\mathrm{d}x\,\mathrm{d}t+\sum_{\mathcal{K}\in\mathcal{T}^n}\int_{K^{n+1}}\rho_{\mathcal{K}}u\cdot v\,\mathrm{d}x\\
&+\sum_{\mathcal{K}\in\mathcal{T}^n}\int_{\mathcal{Q}_{\mathcal{K}}}\widehat{\rho}_{\mathcal{K}}\left(n_t+w\cdot n\right)\left(u+\lambda\left(\bar{u}-u\right)\right)\cdot\left(v-\bar{v}\right)\mathrm{d}s\\
&+\int_{\partial\mathcal{E}^+}\rho_{\mathcal{K}}\left(n_t+\bar{w}\cdot n\right)\bar{u}\cdot\bar{v}\,\mathrm{d}s+\sum_{\mathcal{K}\in\mathcal{T}^n}\int_{\mathcal{Q}_{\mathcal{K}}}\left(\rho_{\mathcal{K}}-\widehat{\rho}_{\mathcal{K}}\right)\left(n_t+w\cdot n\right)u\cdot v\,\mathrm{d}s,
\end{aligned}
\tag{4.20}
$$

and the bilinear forms are given by

$$
\begin{aligned}
a_h^n(\boldsymbol{u},\boldsymbol{v}):=&\sum_{\mathcal{K}\in\mathcal{T}^n}\int_{\mathcal{K}}\mu_{\mathcal{K}}\nabla u:\nabla v\,\mathrm{d}x\,\mathrm{d}t+\sum_{\mathcal{K}\in\mathcal{T}^n}\int_{\mathcal{Q}_{\mathcal{K}}}\frac{\mu_{\mathcal{K}}\alpha}{h_{\mathcal{K}}}\left(u-\bar{u}\right)\cdot\left(v-\bar{v}\right)\mathrm{d}s \qquad (4.21a)\\
&-\sum_{\mathcal{K}\in\mathcal{T}^n}\int_{\mathcal{Q}_{\mathcal{K}}}\mu_{\mathcal{K}}\left[\left(u-\bar{u}\right)\cdot\tfrac{\partial v}{\partial n}+\tfrac{\partial u}{\partial n}\cdot\left(v-\bar{v}\right)\right]\mathrm{d}s,\\
b_h^n(\boldsymbol{p},\boldsymbol{v}):=&-\sum_{\mathcal{K}\in\mathcal{T}^n}\int_{\mathcal{K}}p\nabla\cdot v\,\mathrm{d}x\,\mathrm{d}t+\sum_{\mathcal{K}\in\mathcal{T}^n}\int_{\mathcal{Q}_{\mathcal{K}}}\left(v-\bar{v}\right)\cdot n\bar{p}\,\mathrm{d}s. \qquad (4.21b)
\end{aligned}
$$

To find the solution of the nonlinear discrete problem eq. (4.19), we use a Picard iteration scheme: in every space-time slab, given $(\boldsymbol{u}_h^k, \boldsymbol{p}_h^k)$ we seek a solution $(\boldsymbol{u}_h^{k+1}, \boldsymbol{p}_h^{k+1})$ to the linear discrete problem

$$\begin{aligned} t_h^n(\boldsymbol{u}_h^k; \boldsymbol{u}_h^{k+1}, \boldsymbol{v}_h) + a_h^n(\boldsymbol{u}_h^{k+1}, \boldsymbol{v}_h) + b_h^n(\boldsymbol{p}_h^{k+1}, \boldsymbol{v}_h) - b_h^n(\boldsymbol{q}_h, \boldsymbol{u}_h^{k+1}) \\ = -\sum_{\mathcal{K}\in\mathcal{T}^n} \int_{\mathcal{K}} \rho_{\mathcal{K}} g e_2 \cdot v_h \,\mathrm{d}x\,\mathrm{d}t - \sum_{\mathcal{F}\in\mathcal{F}_N^n} \int_{\mathcal{F}} f \cdot \bar{v}_h \,\mathrm{d}s + \int_{\Omega_n} \rho_{\mathcal{K}} u_h^- \cdot v_h \,\mathrm{d}x, \end{aligned} \tag{4.22}$$

for all $(\boldsymbol{v}_h, \boldsymbol{q}_h) \in X_h^n$ and for $k = 0, 1, 2, \ldots$ until the following stopping criterium is met:

$$\max\left\{ \frac{\|u_h^k - u_h^{k-1}\|_\infty}{\|u_h^k - u_h^0\|_\infty}, \frac{\|p_h^k - p_h^{k-1}\|_\infty}{\|p_h^k - p_h^0\|_\infty} \right\} < \varepsilon_{u,p}, \tag{4.23}$$

where $\varepsilon_{u,p}$ is a user given parameter. We then set $(\boldsymbol{u}_h, \boldsymbol{p}_h) = (\boldsymbol{u}_h^{k+1}, \boldsymbol{p}_h^{k+1})$.

4.2.3 Discretization of the level set equation

The space-time EDG discretization for the level set equation eq. (4.3c) is based on the space-time discretization presented in [45]: In each space-time slab $\mathcal{E}^n$, for $n = 0, 1, \ldots, N-1$, given u find $\boldsymbol{\Phi}_h \in X_h^{m,n}$ such that

$$c_h(\boldsymbol{\Phi}_h, \boldsymbol{m}_h; u) = \sum_{\mathcal{K}\in\mathcal{T}^n} \int_{K^n} \phi_h^- m_h \,\mathrm{d}x + \int_{\partial\mathcal{E}^-} r\bar{m}_h \,\mathrm{d}s \qquad \forall \boldsymbol{m}_h \in X_h^{m,n}, \tag{4.24}$$

where $\phi_h^- = \lim_{\epsilon\to 0} \phi_h(t_n - \epsilon, x)$ for $n > 0$. When $n = 0$ ϕ_h^- is the projection of the initial condition ϕ_0 into M_h^0. The bilinear form is given by

$$\begin{aligned} c_h(\boldsymbol{\Phi}, \boldsymbol{m}; u) = &-\sum_{\mathcal{K}\in\mathcal{T}^n} \int_{\mathcal{K}} (\phi\partial_t m + \phi u \cdot \nabla m) \,\mathrm{d}x\,\mathrm{d}t + \sum_{\mathcal{K}\in\mathcal{T}^n} \int_{K^{n+1}} \phi m \,\mathrm{d}x \\ &+ \sum_{\mathcal{K}\in\mathcal{T}^n} \int_{\mathcal{Q}_{\mathcal{K}}} (n_t + u \cdot n) \left(\phi + \lambda\left(\bar{\phi} - \phi\right)\right)(m - \bar{m}) \,\mathrm{d}s + \int_{\partial\mathcal{E}^+} (n_t + u \cdot n)\bar{\phi}\bar{m} \,\mathrm{d}s. \end{aligned} \tag{4.25}$$

4.2.4 Properties of the discretization

In this section we discuss properties of the space-time HDG/EDG discretization, eqs. (4.19) and (4.24), of the two-fluid flow model. We start by showing that the discretization conserves mass exactly. Note that the discrete version of the mass conservation equation

eq. (4.3b) is

$$\sum_{K\in\mathcal{T}_h}\int_{\mathcal{K}} q_h\nabla\cdot u_h\,\mathrm{d}x\,\mathrm{d}t+\sum_{K\in\mathcal{T}_h}\int_{\mathcal{Q}_{\mathcal{K}}}(u_h-\bar{u}_h)\cdot n\bar{q}_h\,\mathrm{d}s=0. \tag{4.26}$$

Therefore, in order to obtain exact mass conservation, we require (i) that $\nabla\cdot u_h=0$ point-wise, i.e., for all $(x,t)\in\mathcal{K}\in\mathcal{T}$, and (ii) that $[\![u_h\cdot n]\!]=0$ on all interior faces. The following proposition shows these two properties.

Proposition 4.1 (Exact mass conservation)**.** *If $\boldsymbol{u}_h\in X_h^{v,n}$ satisfy eqs. (4.19) and (4.24) then u_h is exactly divergence free, i.e., $\nabla\cdot u_h=0$ for all $(x,t)\in\mathcal{K}\in\mathcal{T}^n$ and $u_h\in H(\mathrm{div};\mathcal{E}^n)$.*

Proof. The proof follows that of [38, Prop. 1] and included here only for completeness.

First, we show that $\nabla\cdot u_h=0$ for all $(x,t)\in\mathcal{K}\in\mathcal{T}$. First, note that $(\nabla\cdot u_h)\in Q_h^n$. Take $v_h=0$, $\bar{v}_h=0$, $\bar{q}_h=0$ and $q_h=\nabla\cdot u_h$ in eq. (4.19) to obtain

$$\sum_{K\in\mathcal{T}_h}\int_{\mathcal{K}}(\nabla\cdot u_h)^2\,\mathrm{d}x\,\mathrm{d}t=0. \tag{4.27}$$

It follows that $\nabla\cdot u_h=0$ for all $(x,t)\in\mathcal{K}\in\mathcal{T}$.

To show that $u_h\in H(\mathrm{div};\mathcal{E}^n)$, note that $((u_h-\bar{u}_h)\cdot n)\in\bar{Q}_h^n$. Take $\bar{v}_h=0$, $q_h=0$ and $\bar{q}_h=[\![(u_h-\bar{u}_h)\cdot n]\!]$ in eq. (4.19) to obtain

$$\sum_{\mathcal{F}\in\mathcal{F}_I^n\cup\mathcal{F}_S^n}\int_{\mathcal{F}}[\![(u_h-\bar{u}_h)\cdot n]\!]^2\,\mathrm{d}s+\sum_{\mathcal{F}\in\mathcal{F}_B^n}\int_{\mathcal{F}}\big((u_h-\bar{u}_h)\cdot n\big)^2\,\mathrm{d}s=0. \tag{4.28}$$

Since $\bar{u}_h$ is single-valued on interior facets, we simplify this equation to

$$\sum_{\mathcal{F}\in\mathcal{F}_I^n\cup\mathcal{F}_S^n}\int_{\mathcal{F}}[\![u_h\cdot n]\!]^2\,\mathrm{d}s+\sum_{\mathcal{F}\in\mathcal{F}_B^n}\int_{\mathcal{F}}\big((u_h-\bar{u}_h)\cdot n\big)^2\,\mathrm{d}s=0. \tag{4.29}$$

We see that $u_h\cdot n$ is single-valued on interior facets, and $u_h\cdot n=\bar{u}_h\cdot n$ on boundary facets, i.e., $u_h\in H(\mathrm{div};\mathcal{E}^n)$, see [42, Lemma 4.11]. □

It was shown in [22] for different flow/transport discretizations that loss of accuracy and/or loss of global conservation may occur if a discretization is not compatible. (Note that the compatibility for discontinuous Galerkin methods is a stronger statement than local conservation of the flow field [22].) The next result shows that since u_h is exactly divergence free, the space-time HDG discretization of the two-fluid model eq. (4.19) and the space-time EDG discretization of the level-set equation eq. (4.24) are compatible.

Proposition 4.2 (Compatibility)**.** *If $u_h \in V_h^n$ is the velocity solution to the space-time HDG discretization eq. (4.19), then the space-time EDG discretization eq. (4.24) is: (i) globally conservative; and (ii) able to preserve the constant solution.*

Proof. We first note that global conservation of the EDG discretization was shown in [87]. To show that the space-time EDG discretization eq. (4.24) is able to preserve the constant solution we present a space-time extension of the discussion in [13, Section 3.4]. For this, let the boundary and initial conditions in eqs. (4.5d) and (4.5e) be given by, respectively, $\phi_0(x) = \psi$ and $r = -(n_t + u_h \cdot n)\psi$, where ψ is a constant. Consider now the first space-time slab $\mathcal{E}^0$. The constant $\mathbf{\Phi}_h = (\psi, \psi)$ is preserved by eq. (4.24) if and only if

$$c_h((\psi,\psi), \boldsymbol{m}_h; u_h) = \sum_{\mathcal{K}\in\mathcal{T}^0} \int_{K^n} \psi m_h \,\mathrm{d}x - \int_{\partial\mathcal{E}^-} (n_t + u_h \cdot n)\psi \bar{m}_h \,\mathrm{d}s \qquad \forall \boldsymbol{m}_h \in X_h^{m,n}. \tag{4.30}$$

If $\psi = 0$ it is clear that eq. (4.30) holds. Consider therefore the case that $\psi \neq 0$. Writing out the left hand side, dividing both sides by ψ, and integrating by parts in time, we find that eq. (4.30) is equivalent to

$$\begin{aligned} -\sum_{\mathcal{K}\in\mathcal{T}^0} \int_{\mathcal{K}} u_h \cdot \nabla m_h \,\mathrm{d}x\,\mathrm{d}t - \sum_{\mathcal{K}\in\mathcal{T}^0} \int_{\mathcal{Q}_\mathcal{K}} n_t m_h \,\mathrm{d}s + \sum_{\mathcal{K}\in\mathcal{T}^0} \int_{\mathcal{Q}_\mathcal{K}} (n_t + u_h \cdot n)\,(m_h - \bar{m}_h)\,\mathrm{d}s \\ + \int_{\partial\mathcal{E}^+} (n_t + u_h \cdot n)\bar{m}_h \,\mathrm{d}s = 0, \end{aligned} \tag{4.31}$$

for all $\boldsymbol{m}_h \in X_h^{m,n}$. Using that $\nabla \cdot (u_h m_h) = u_h \cdot \nabla m_h + m_h \nabla \cdot u_h$ on each element $\mathcal{K}$, integration by parts in space, single-valuedness of $\bar{m}_h$ and $u_h \cdot n$ on interior facets (by Proposition 4.1), we find that the constant $\mathbf{\Phi}_h = (\psi, \psi)$ is preserved by eq. (4.24) if and only if

$$\sum_{\mathcal{K}\in\mathcal{T}^0} \int_{\mathcal{K}} m_h \nabla \cdot u_h \,\mathrm{d}x\,\mathrm{d}t = 0. \tag{4.32}$$

The result follows since $\nabla \cdot u_h = 0$ by Proposition 4.1. □

We emphasize that compatibility in Proposition 4.2 between the space-time HDG discretization eq. (4.19) and the space-time EDG discretization eq. (4.24) is a direct consequence of Proposition 4.1, i.e., that $\nabla \cdot u_h = 0$ pointwise and that $u_h \cdot n$ is continuous across element boundaries. A discretization that does not satisfy Proposition 4.1 may not be compatible with eq. (4.24).

We end this section by showing consistency of the space-time HDG/EDG discretization.

Proposition 4.3 (Consistency)**.** *Let $u(x,t)$, $p(x,t)$, and $\phi(x,t)$ be the smooth solution to the two-fluid model, eqs. (4.3) and (4.5). Let $\boldsymbol{u} = (u,u)$, $\boldsymbol{p} = (p,p)$, and $\boldsymbol{\Phi} = (\phi,\phi)$. Then*

$$\begin{aligned} &t_h^n(\boldsymbol{u},\boldsymbol{u},\boldsymbol{v}_h) + a_h^n(\boldsymbol{u},\boldsymbol{v}_h) + b_h^n(\boldsymbol{p},\boldsymbol{v}_h) - b_h^n(\boldsymbol{q},\boldsymbol{u}_h) \\ &\quad = -\sum_{\mathcal{K}\in\mathcal{T}^n}\int_{\mathcal{K}} \rho_{\mathcal{K}} g e_2 \cdot v_h \,\mathrm{d}x\,\mathrm{d}t - \sum_{\mathcal{F}\in\mathcal{F}_N^n}\int_{\mathcal{F}} f\cdot\bar{v}_h \,\mathrm{d}s + \int_{\Omega_n} \rho_{\mathcal{K}} u\cdot v_h \,\mathrm{d}x \qquad \forall(\boldsymbol{v}_h,\boldsymbol{q}_h)\in X_h^n, \end{aligned} \tag{4.33}$$

and

$$c_h(\boldsymbol{\Phi},\boldsymbol{m}_h;u) = \sum_{\mathcal{K}\in\mathcal{T}^n}\int_{K^n}\phi m_h \,\mathrm{d}x + \int_{\partial\mathcal{E}^-} r\bar{m}_h \,\mathrm{d}s \qquad \forall \boldsymbol{m}_h \in X_h^{m,n}. \tag{4.34}$$

Proof. We first show eq. (4.33). By definition eq. (4.20), integration by parts, and using that $\widehat{\rho}_{\mathcal{K}}$, u and $\bar{v}_h$ are single-valued on faces, we find

$$\begin{aligned} t_h^n(\boldsymbol{u};\boldsymbol{u},\boldsymbol{v}_h) = \sum_{\mathcal{K}\in\mathcal{T}^n}\int_{\mathcal{K}} \rho_{\mathcal{K}}\left(\partial_t u + u\cdot\nabla u\right)\cdot v_h \,\mathrm{d}x\,\mathrm{d}t + \sum_{\mathcal{K}\in\mathcal{T}^n}\int_{K^n}\rho_{\mathcal{K}} u\cdot v_h\,\mathrm{d}x \\ - \int_{\partial\mathcal{E}^-}\rho_{\mathcal{K}}\left(n_t + u\cdot n\right) u\cdot\bar{v}_h\,\mathrm{d}s. \end{aligned} \tag{4.35}$$

Similarly, by definition eq. (4.21a) and integration by parts,

$$a_h^n(\boldsymbol{u},\boldsymbol{v}_h) = -\sum_{\mathcal{K}\in\mathcal{T}^n}\int_{\mathcal{K}}\mu_{\mathcal{K}}\Delta u\cdot v_h\,\mathrm{d}x\,\mathrm{d}t + \sum_{\mathcal{K}\in\mathcal{T}^n}\int_{\mathcal{Q}_{\mathcal{K}}}\mu_{\mathcal{K}}\frac{\partial u}{\partial n}\cdot\bar{v}_h\,\mathrm{d}s, \tag{4.36}$$

and by definition eq. (4.21b), integration by parts, and using that $\nabla\cdot u = 0$,

$$b_h^n(\boldsymbol{p},\boldsymbol{v}_h) - b_h^n(\boldsymbol{q}_h,\boldsymbol{u}) = \sum_{\mathcal{K}\in\mathcal{T}^n}\int_{\mathcal{K}}\nabla p\cdot v_h\,\mathrm{d}x\,\mathrm{d}t - \sum_{\mathcal{K}\in\mathcal{T}^n}\int_{\mathcal{Q}_{\mathcal{K}}}\bar{v}_h\cdot np\,\mathrm{d}s. \tag{4.37}$$

Combining eqs. (4.35) to (4.37), we obtain

$$\begin{aligned} &t_h^n(\boldsymbol{u};\boldsymbol{u},\boldsymbol{v}_h) + a_h^n(\boldsymbol{u},\boldsymbol{v}_h) + b_h^n(\boldsymbol{p},\boldsymbol{v}_h) - b_h^n(\boldsymbol{q}_h,\boldsymbol{u}) \\ &\quad = \sum_{\mathcal{K}\in\mathcal{T}^n}\int_{\mathcal{K}}\rho_{\mathcal{K}}\left[\left(\partial_t u + u\cdot\nabla u\right) + \nabla p - \mu_{\mathcal{K}}\Delta u\right]\cdot v_h\,\mathrm{d}x\,\mathrm{d}t + \sum_{\mathcal{K}\in\mathcal{T}^n}\int_{K^n}\rho_{\mathcal{K}} u\cdot v_h\,\mathrm{d}x \\ &\qquad - \sum_{\mathcal{K}\in\mathcal{T}^n}\int_{\mathcal{Q}_{\mathcal{K}}}\left(p\mathbb{I} - \mu_{\mathcal{K}}\nabla u\right) n\cdot\bar{v}_h\,\mathrm{d}s - \int_{\partial\mathcal{E}^-}\rho_{\mathcal{K}}\left(n_t + u\cdot n\right) u\cdot\bar{v}_h\,\mathrm{d}s. \end{aligned} \tag{4.38}$$

The last two terms may be combined using that $\bar{v}_h = 0$ on $\partial\mathcal{E}^D$ and the single-valuedness of $(p\mathbb{I} - \mu_\mathcal{K}\nabla u)\, n$ on element boundaries:

$$\begin{aligned} t_h^n(\boldsymbol{u}; \boldsymbol{u}, \boldsymbol{v}_h) + a_h^n(\boldsymbol{u}, \boldsymbol{v}_h) + b_h^n(\boldsymbol{p}, \boldsymbol{v}_h) - b_h^n(\boldsymbol{q}_h, \boldsymbol{u}) \\ = \sum_{\mathcal{K}\in\mathcal{T}^n} \int_\mathcal{K} \rho_\mathcal{K} \left[(\partial_t u + u \cdot \nabla u) + \nabla p - \mu_\mathcal{K} \Delta u \right] \cdot v_h \,\mathrm{d}x \,\mathrm{d}t + \int_{\Omega_n} \rho_\mathcal{K} u \cdot v_h \,\mathrm{d}x \\ - \int_{\partial\mathcal{E}^N} \left(\left[n_t + u \cdot n - \max\left(n_t + u \cdot n, 0\right) \right] u + \left(p\mathbb{I} - \mu\nabla u\right) n \right) \cdot \bar{v}_h \,\mathrm{d}s. \end{aligned} \tag{4.39}$$

Equation (4.33) follows using eq. (4.3a) and eq. (4.5b).

We next show eq. (4.34). By definition eq. (4.25), integration by parts, and using that ϕ, $\bar{m}_h$, and u are single-valued on faces, we find

$$c_h(\boldsymbol{\Phi}, \boldsymbol{m}_h; u) = \sum_{\mathcal{K}\in\mathcal{T}^n} \int_\mathcal{K} \left(\partial_t \phi + u \cdot \nabla\phi\right) m_h \,\mathrm{d}x \,\mathrm{d}t + \sum_{\mathcal{K}\in\mathcal{T}^n} \int_{K^n} \phi m_h \,\mathrm{d}x - \int_{\partial\mathcal{E}^-} \left(n_t + u \cdot n\right) \phi \bar{m}_h \,\mathrm{d}s. \tag{4.40}$$

Equation (4.34) follows using eqs. (4.3c) and (4.5d). □

4.3 The solution algorithm

In this section we describe how we iteratively solve the discretization of the two-fluid model and the level set equation, and how we update the mesh in each space-time slab.

4.3.1 Coupling discretization and mesh deformation

Given the level set function ϕ_h from space-time slab $\mathcal{E}^{n-1}$ we create an initial mesh for the space-time slab $\mathcal{E}^n$. Using Picard iterations we solve the space-time HDG discretization eq. (4.22) for the momentum and mass equations until we satisfy eq. (4.23). The velocity solution to the space-time HDG discretization is then used in the space-time EDG discretization eq. (4.24) to update the level set function. With this level set function we update the mesh. We continue updating the mesh and solving the space-time HDG and EDG discretizations in space-time slab $\mathcal{E}^n$ until the following stopping criterium is met:

$$\frac{\|\phi_h^{n,m} - \phi_h^{n,m-1}\|_\infty}{\|\phi_h^{n,m} - \phi_h^{n,0}\|_\infty} < \varepsilon_\phi, \tag{4.41}$$

where ε_ϕ is a user given parameter and $\phi_h^{n,m}$ is the approximation to ϕ_h after m iterations in the n^{th} space-time slab. The algorithm is described in Algorithm 1.

Algorithm 1 Coupling the discretization and mesh deformation

Initialize the flow properties and the level set function.
Set $n = 0$, $t_n = 0$.
while $t_n < t_N$ **do**
  Set $m = 0$.
  Create an initial space-time mesh for space-time slab $\mathcal{E}^n$ given $\phi_h^{n,m}$.
  while $\phi_h^{n,m}$ *does not satisfy eq.* (4.41) **do**
    Solve the space-time HDG discretization eq. (4.19) using Picard iterations eq. (4.22).
    Given $u_h^{n,m}$ from the previous step, solve the level set equation eq. (4.24) to obtain $\phi^{n,m+1}$.
    Modify the space-time mesh according to $\phi^{n,m+1}$.
  end
  Set $u_h^n = u_h^{n,m+1}$, $p_h^n = p_h^{n,m+1}$, $\phi_h^n = \phi_h^{n,m+1}$, and $t_n = t_{n+1}$.
end

4.3.2 Mesh deformation

Recall that the shape of the subdomains $\Omega_l(t)$ and $\Omega_g(t)$ depends on the position of the free-surface $\Gamma_s(t)$. Once the discrete level set function ϕ_h is obtained by solving eq. (4.24), the wave height must be obtained in order to update the mesh nodes. Traditionally, using standard discontinuous Galerkin methods for free-surface problems, the approximation to the wave height is discontinuous. This implies that the free-surface of the domain is not well defined and a postprocessing of the free-surface is required to address this [31, 84]. This mesh smoothing, however, may require extra stabilization terms (see [2]).

Using the space-time embedded discontinuous Galerkin method eq. (4.24) for the level set function, mesh smoothing is not required. This is because the facet approximation to the level set function $\bar{\phi}_h$ is continuous on the mesh skeleton, see eq. (4.8c). We therefore avoid any smoothing of the mesh that may lead to instabilities while maintaining all the conservation properties that discontinuous Galerkin methods provide.

We next describe how to obtain the wave height from the level set function and subsequently how to move the mesh nodes. We first note that $\bar{\phi}_h$ is the trace of an H^1 function. Denoting by M_h^c the space of functions of M_h which are continuous on $\mathcal{E}^n$, we denote by

ϕ_h^c the function in M_h^c that coincides with $\bar{\phi}_h$ on the element boundaries. We note that it is computationally cheap to find ϕ_h^c because it can be found element-wise. By definition $\phi(t, x_1, x_2) = \zeta(t, x_1) - x_2$ and so an approximation to the wave height, ζ_h, can be obtained by evaluating ϕ_h^c at $x_2 = 0$.

Once we have obtained ζ_h we update mesh nodes as follows. Let $(x_{1,i}^0, x_{2,i}^0)$ denote the coordinates of node i of the undisturbed mesh ($\zeta_h = 0$), and let $(x_{1,i}^k, x_{2,i}^k)$ denote the coordinates of the node i at time t_k. Denote by $T_b(x_1)$ ($B_b(x_1)$) the maximum (minimum) x_2 value in Ω on the vertical direction through x_1. Then:

- If $x_{2,i}^0 < 0$,

$$x_{2,i}^{k+1} = x_{2,i}^0 + \gamma_i^k \zeta_h(t_{k+1}, x_{1,i}^k) \quad \text{where } \gamma_i^k = \frac{B_b(x_{1,i}^k) + x_{2,i}^0}{B_b(x_{1,i}^k)}. \tag{4.42}$$

- If $x_{2,i}^0 > 0$,

$$x_{2,i}^{k+1} = x_{2,i}^0 + \gamma_i^k \zeta_h(t_{k+1}, x_{1,i}^k) \quad \text{where } \gamma_i^k = \frac{T_b(x_{1,i}^k) - x_{2,i}^0}{T_b(x_{1,i}^k)}. \tag{4.43}$$

4.4 Numerical results

All the simulations in this section were implemented using the Modular Finite Element Method (MFEM) library [25]. Furthermore, as is common with interior penalty type discretizations, we set the penalty parameter to $\alpha = 10k^2$ [68].

4.4.1 Sloshing in a water tank

We consider a small-amplitude periodic wave that is allowed to oscillate freely in a rectangular tank with length that is twice the depth of the still water level. The computational domain is $\Omega = [-1, 1] \times [-1, 0.2]$. Initially the fluid is at rest and the wave has a profile given by

$$\zeta_0(x_1) = 0.01 \cos\left(\kappa(x_1 + 0.5)\right), \tag{4.44}$$

where $\kappa = 2\pi$ is the wave period. An analytical solution to the linearized free-surface flow problem is given in [89]; given a high enough Reynolds number and assuming a negligible

influence of the finite depth of the tank, the analytic wave height ζ_{ref} is given by

$$\frac{\zeta_{\text{ref}}(x_1,t)}{\zeta_0(x_1)} = 1 - \frac{1}{1+4\nu^2\kappa^2/g}\left[1 - e^{-2\nu\kappa^2 t}\left(\cos(\sqrt{\kappa g}t) + 2\nu\kappa^2\frac{\sin(\sqrt{\kappa g}t)}{\sqrt{\kappa g}}\right)\right], \tag{4.45}$$

where ν is the kinematic viscosity of the liquid which is set to $\nu = 1/2000$. The densities are $\rho_l = 1000$ and $\rho_g = 1$, and the viscosities $\mu_l = 0.5$, $\mu_g = 1/2000$. We consider two meshes, a structured mesh with 1152 spatial triangles (3452 space-time tetrahedra), and a finer mesh with 2756 spatial triangles (8268 space-time tetrahedra) that is more refined around the free-surface. At $x_2 = -1$ we apply no-slip boundary conditions, and at $x_2 = 0.2$ we apply a homogeneous Neumann boundary conditions. The polynomial degree is $k = 2$ and the time step is $\Delta t = 0.02$. In fig. 4.2 we show the wave height elevation at the middle of the tank ($x_1 = 0$) with the analytical solution and with the numerical method described in algorithm 1 with the two meshes described above. We see that for the coarser mesh there is some discrepancy with the analytical solution. However, for the finer mesh, there is a better agreement with eq. (4.45).

To show how the mesh moves with the interface, in fig. 4.3 we plot the mesh and wave height at times $t = 0$ and $t = 3.86$.

4.4.2 Waves generated by a submerged obstacle

In this example, we consider waves in a channel generated by a submerged cylinder. The computational domain is $\Omega = [-1, 2] \times [-0.75, 0.5]$ and the initial wave height is $\zeta = 0$. A cylinder of radius 0.1 is located at $(0, -0.25)$. See fig. 4.4.

On the left, top and bottom boundaries of the domain we impose $u = [1, 0]^T$ whereas on the right boundary of the domain we impose a homogeneous Neumann boundary condition. On the boundary of the circle, homogeneous Dirichlet boundary conditions are imposed. Moreover, $\boldsymbol{u}_0(x) = [1, 0]^T$. For the level set function, we set $r = 0$ at the inflow part of the boundary ($x = -0.75$). The densities are set to $\rho_l = 1000$, $\rho_g = 1$ and the viscosities are set to $\mu_l = 1/200$ and $\mu_g = 1/200$. In fig. 4.5 we show the velocity magnitude at different moments in time. For visualization purposes, we plot only the liquid domain $\Omega_l(t)$. The wave continues to oscillate in a similar way until about time $t = 8$ when the oscillations become less pronounced. Figure 4.6 shows the velocity streamlines behind the cylinder at different moments in time. We see that the vortices oscillate up and down. In [33], a similar test case was presented. In that case, the submerged obstacle is a box instead of a cylinder. We see that the wave and the streamlines behind the obstacle show a similar behavior.

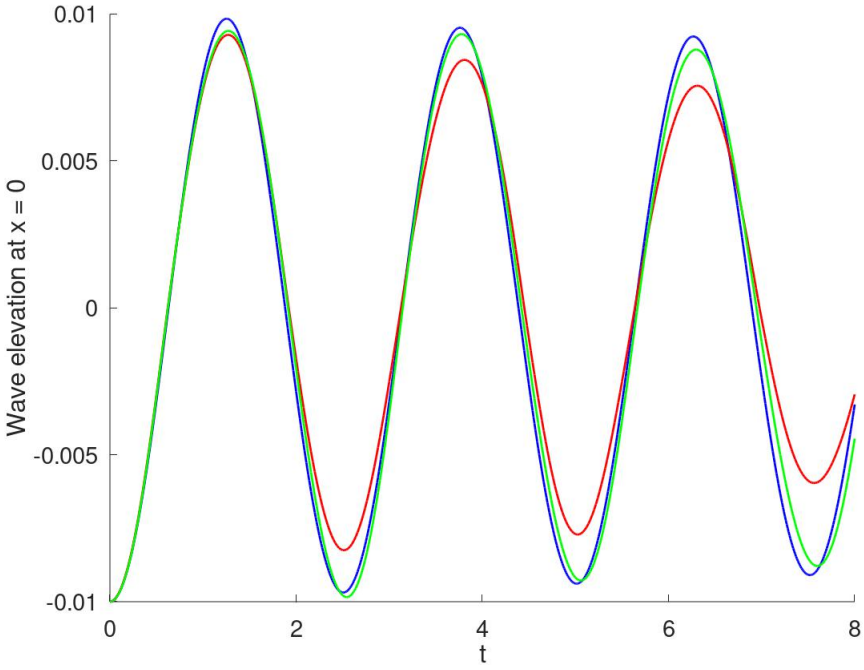

Figure 4.2: Wave elevation at $x = 0$ with the anaytical solution eq. (4.45) (blue line), coarser mesh (red line) and finer mesh (green line) for the test case section 4.4.1.

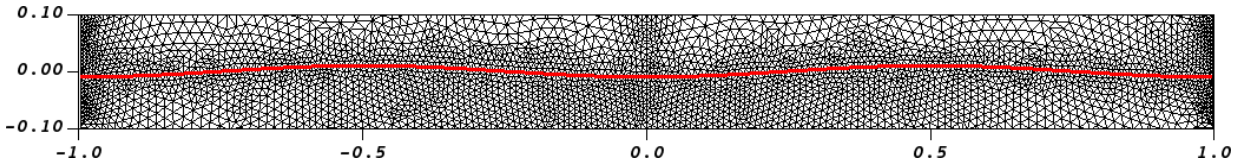

(a) Spatial mesh and wave height at $t = 0$.

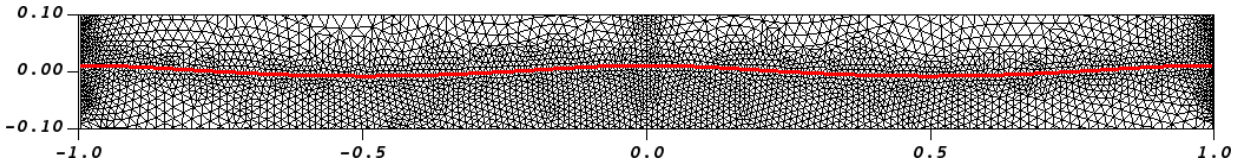

(b) Spatial mesh and wave height at $t = 3.86$

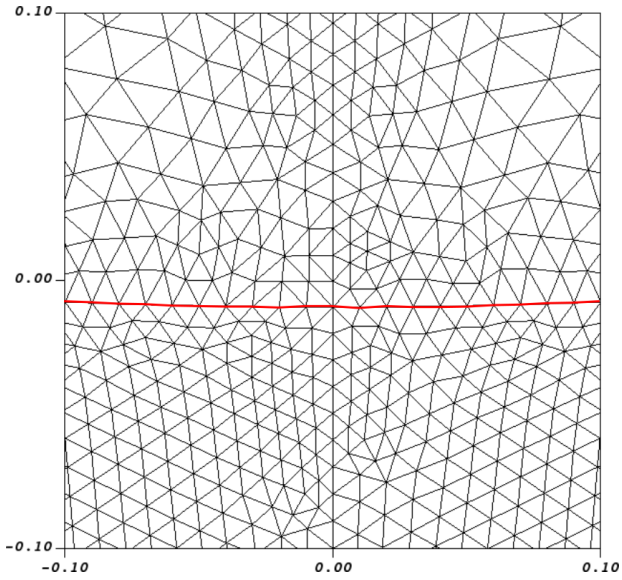

(c) Spatial mesh and wave height at $t = 0$.

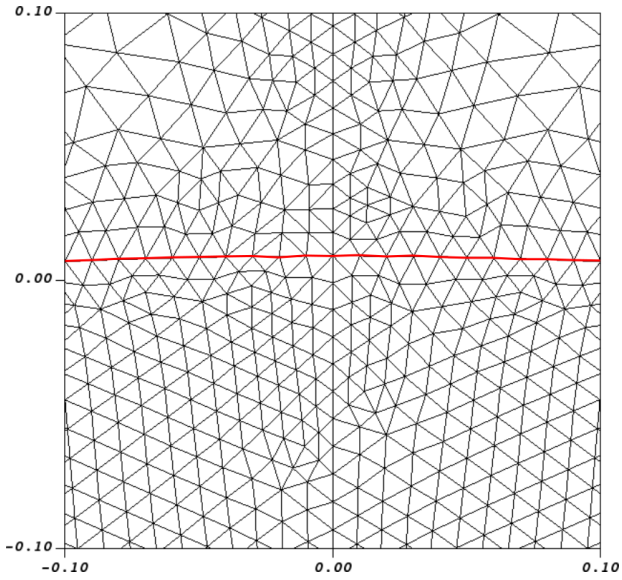

(d) Spatial mesh and wave height at $t = 3.86$

Figure 4.3: The spatial mesh at two instances in time for the test case described in section 4.4.1. The top two figures are an extract of the mesh in $[-1, 1] \times [-0.1, 0.1]$. The bottom two figures zoom into the region $[-0.1, 0.1] \times [-0.1, 0.1]$. We indicate the wave height in all figures in red. Note that the mesh conforms to the interface.

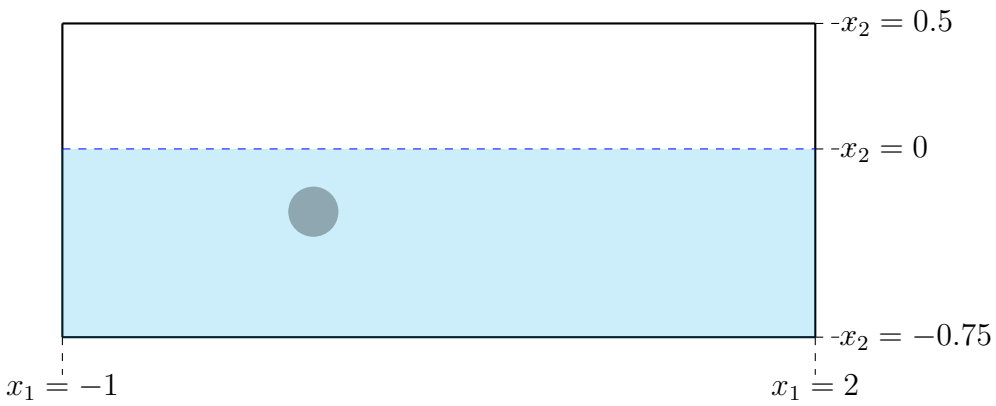

Figure 4.4: Depiction of the flow domain $\Omega \subset \mathbb{R}^2$ for the test case in section 4.4.2.

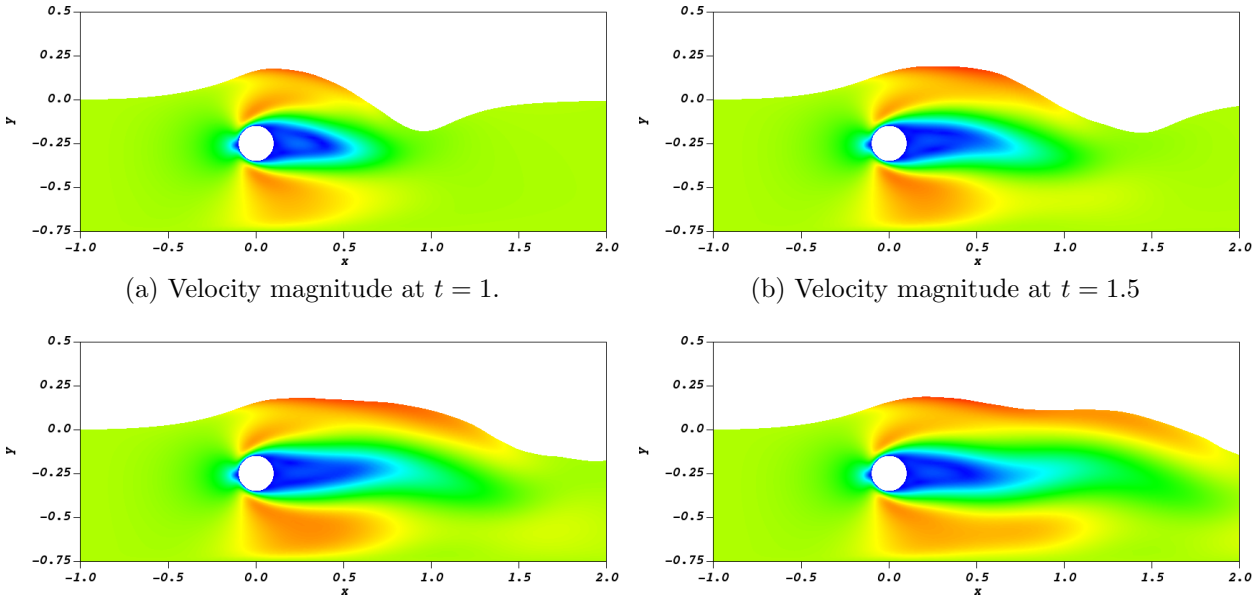

(a) Velocity magnitude at $t = 1$.

(b) Velocity magnitude at $t = 1.5$

(c) Velocity magnitude at $t = 2$.

(d) Velocity magnitude at $t = 2.5$

Figure 4.5: Velocity magnitude in the liquid domain $\Omega_l(t)$ at different moments in time for the test case described in section 4.4.2.

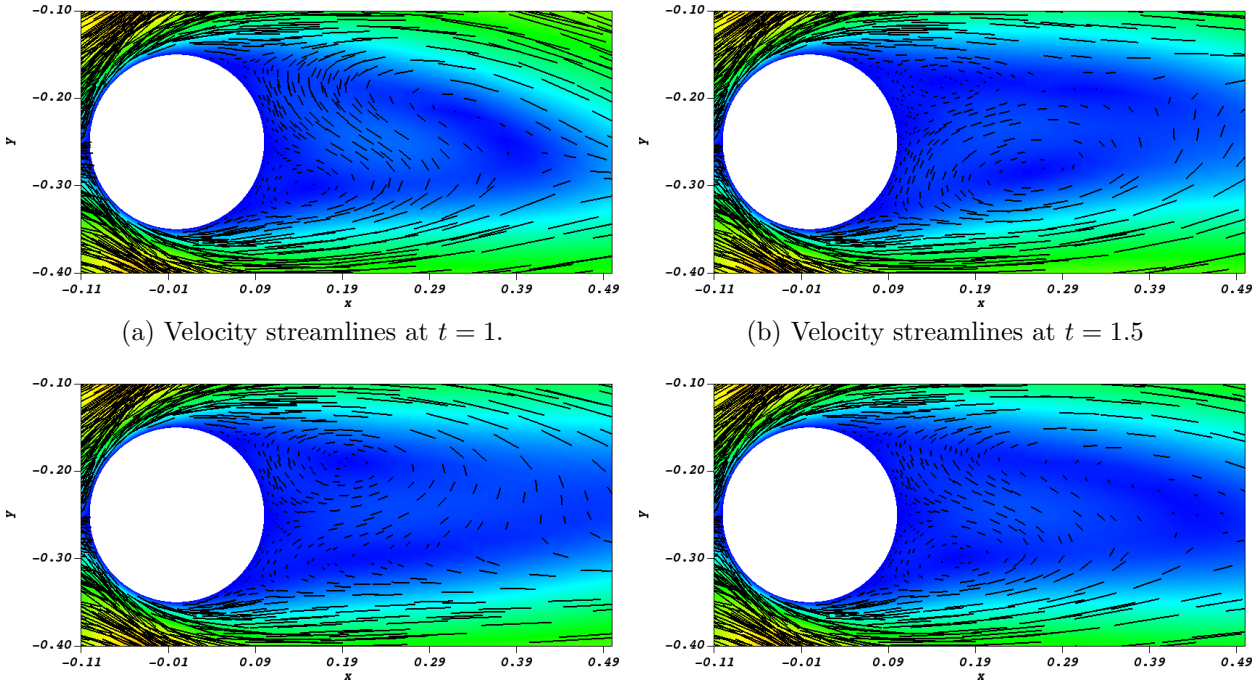

(a) Velocity streamlines at $t = 1$.

(b) Velocity streamlines at $t = 1.5$

(c) Velocity streamlines at $t = 2$.

(d) Velocity streamlines at $t = 2.5$

Figure 4.6: Velocity streamlines behind the cylinder at different moments in time for the test case described in section 4.4.2.

Chapter 5

Conclusions

In this thesis, we have presented novel analyses and techniques for the solution of free-surface problems with space-time hybridizable discontinuous Galerkin methods. In Chapter 2 we presented an HDG method for the linear free-surface problem with a second order BDF time stepper. We compared our results to those of [82] in which a DG method is used for the same problem, and we conclude that due to our mixed formulation, we can obtain a better approximation to the velocity of the fluid and superconvergence of the velocity potential.

In Chapter 3, we introduced and analyzed a novel space-time HDG method for the linear free-surface problem. In contrast to some analyses of space-time methods, e.g. [12], we obtained error estimates in which the dependency on the spatial mesh size and the time step is explicit. To achieve this, we derived anisotropic space-time analysis tools. We presented numerical results that demonstrate the validity of our analysis. The space-time analysis tools developed in this thesis can be used and extended to other problems and discretizations.

A novel interface-tracking space-time HDG/EDG level set method for the two-fluid Navier–Stokes equations was developed in Chapter 4. The space-time HDG method applied to the Navier–Stokes equations is $H(\mathrm{div})$-conforming and produces point-wise divergence-free velocity fields. This results in a scheme that is locally mass conserving. Since the mesh conforms to the interface, there is no smoothing of the flow properties, as it is usually done in level set methods [33, 53, 54]. A continuous approximation to the wave height was obtained by a space-time EDG method. This allowed us to move the mesh according to the interface without relying on smoothing techniques that could result in instabilities.

For future projects, it would be interesting to apply the space-time HDG/EDG method

in Chapter 4 to more general two-phase flows where topological changes are allowed. This would involve defining a projection of the solution from one domain to another ideally without loss of accuracy. This extension would allow for more general applications, such as a bubble rising in a column, dam braking, etc. The next step would be to consider fluid-structure interaction with free-surface flows as done in [85]. For such an application, a discretization for the solid structure has to be developed first. In terms of analysis, we could explore if the analysis in Chapter 3 can be extended to linear partial differential equations on moving domains.

References

[1] V. Aizinger and C. Dawson. A discontinuous Galerkin method for two-dimensional flow and transport in shallow water. *Adv. Water Resour.*, 25:67–84, 2002.

[2] V. Aizinger and C. Dawson. The local discontinuous Galerkin method for three-dimensional shallow water flow. *Comput. Methods Appl. Mech. Engrg.*, 196:734–746, 2006.

[3] V. R. Ambati and O. Bokhove. Space-time discontinuous Galerkin finite element method for shallow water flows. *J. Comput. Appl. Math.*, 204:452–462, 2007.

[4] P. R. Amestoy, A. Guermouche, J.-Y. L'Excellent, and S. Pralet. Hybrid scheduling for the parallel solution of linear systems. *Parallel Comput.*, 32(2):136–156, 2006.

[5] P.R. Amestoy, I.S. Duff, J.-Y. L'Excellent, and J. Koster. A fully asynchronous multifrontal solver using distributed dynamic scheduling. *SIAM J. Matrix Anal. & Appl.*, 23(1):15–41, 2001.

[6] D. N. Arnold, F. Brezzi, B. Cockburn, and L. D. Marini. Unified analysis of discontinuous galerkin methods for elliptic problems. *SIAM J. Numer. Anal.*, 39(5):1749–1779, 2002.

[7] Satish Balay, Shrirang Abhyankar, Mark F. Adams, Jed Brown, Peter Brune, Kris Buschelman, Lisandro Dalcin, Victor Eijkhout, William D. Gropp, Dinesh Kaushik, Matthew G. Knepley, Lois Curfman McInnes, Karl Rupp, Barry F. Smith, Stefano Zampini, Hong Zhang, and Hong Zhang. PETSc users manual. Technical Report ANL-95/11 - Revision 3.7, Argonne National Laboratory, 2016.

[8] Satish Balay, Shrirang Abhyankar, Mark F. Adams, Jed Brown, Peter Brune, Kris Buschelman, Lisandro Dalcin, Victor Eijkhout, William D. Gropp, Dinesh Kaushik, Matthew G. Knepley, Lois Curfman McInnes, Karl Rupp, Barry F. Smith, Stefano

Zampini, Hong Zhang, and Hong Zhang. PETSc Web page. http://www.mcs.anl.gov/petsc, 2016.

[9] Satish Balay, William D. Gropp, Lois Curfman McInnes, and Barry F. Smith. Efficient management of parallelism in object oriented numerical software libraries. In E. Arge, A. M. Bruaset, and H. P. Langtangen, editors, *Modern Software Tools in Scientific Computing*, pages 163–202. , Birkhäuser Press, 1997.

[10] E. Bezchlebová, V. Dolejší, M. Feistauer, and P. Sváček. Numerical simulation of two-phase flow of immiscible fluids by the finite element, discontinuous Galerkin and level-set methods. *Adv. Comput. Math.*, 45(4):1993–2018, 2019.

[11] S. Brenner and L. R. Scott. *The Mathematical Theory of Finite Element Methods*, volume 15. Springer–Verlag New York, 2008.

[12] A. Cangiani, Z. Dong, and E. H. Georgoulis. *hp*-version space-time discontinuous Galerkin methods for parabolic problems on prismatic meshes. *SIAM J. Sci. Comput.*, 39(4):A1251–A1279, 2017.

[13] A. Cesmelioglu and S. Rhebergen. A compatible embedded-hybridized discontinuous Galerkin method for the Stokes–Darcy-transport problem. 2020. Submitted.

[14] Y. C. Chang, T. Y. Hou, B. Merriman, and S. Osher. A level set formulation of Eulerian interface capturing methods for incompressible fluid flows. *J. Comput. Phys.*, 124:449–464, 1996.

[15] P. G. Ciarlet. *The Finite Element Method for Elliptic Problems*. SIAM, 2002.

[16] B. Cockburn, B. Dong, and J. Guzmán. A superconvergent LDG-hybridizable Galerkin method for second-order elliptic problems. *Math. Comp.*, 77:887–1916, 2008.

[17] B. Cockburn, B. Dong, J. Guzmán, M. Restelli, and R. Sacco. A hybridizable discontinuous Galerkin method for steady-state convection-diffusion-reaction problems. *SIAM J. Sci. Comput.*, 31(5):3827–3846, 2009.

[18] B. Cockburn, J. Gopalakrishnan, and R. Lazarov. Unified hybridization of discontinuous Galerkin, mixed, and continuous Galerkin methods for second order elliptic problems. *SIAM J. Numer. Anal.*, 47:1319–1365, 2009.

[19] B. Cockburn, J. Gopalakrishnan, and F.-J. Sayas. A projection-based error analysis of HDG methods. *Math. Comp.*, 79:1351–1367, 2010.

[20] B. Cockburn, J. Guzmán, S.-C. Soon, and H. K. Stolarski. An analysis of the embedded discontinuous Galerkin method for second-order elliptic problems. *SIAM J. Numer. Anal.*, 47:2686–2707, 2009.

[21] B. Cockburn and V. Quenneville-Bélair. Uniform-in-time superconvergence of the HDG methods for the acoustic wave equation. *Math. Comp.*, 83:65–85, 2014.

[22] C. Dawson, S. Sun, and M. F. Wheeler. Compatible algorithms for coupled flow and transport. *Comput. Methods Appl. Mech. Engrg.*, 193(23-26):2565–2580, 2004.

[23] L. Debnath. *Nonlinear Water Waves*. Academic Press, Inc., 1994.

[24] D. A. Di Pietro and A. Ern. *Mathematical Aspects of Discontinuous Galerkin Methods*, volume 69 of *Mathématiques et Applications*. Springer-Verlag Berlin Heidelberg, 2012.

[25] V. A. Dobrev, T. V. Kolev, et al. MFEM: Modular finite element methods. http://mfem.org, 2020.

[26] C. Frantzis and D. G. E. Grigoriadis. An efficient method for two-fluid incompressible flows appropriate for the immersed boundary method. *J. Comput. Phys.*, 376:28–53, 2019.

[27] D. A. French. A space-time finite element method for the wave equation. *Comput. Methods Appl. Mech. Engrg.*, 107:145–157, 1993.

[28] D. A. French and T. E. Peterson. A continuous space-time finite element method for the wave equation. *Math. Comp.*, 65:491–506, 1996.

[29] G. Fu. An explicit divergence-free DG method for incompressible flow. *Comput. Methods Appl. Mech. Engrg.*, 345:502–517, 2019.

[30] G. Fu. Arbitrary Lagrangian–Eulerian hybridizable discontinuous Galerkin methods for incompressible flow with moving boundaries and interfaces. *Comput. Meth. Appl. Mech. Engrg.*, 367, 2020.

[31] E. Gagarina, V. R. Ambati, J. J. W. van der Vegt, and O. Bokhove. Variational space-time (dis)continuous Galerkin method for nonlinear free surface water waves. *J. Comput. Phys.*, 275:459–483, 2014.

[32] E. H. Georgoulis. *Discontinuous Galerkin methods on shape-regular and anisotropic meshes*. D.Phil. Thesis, University of Oxford, 2003.

[33] J. Grooss and J. S. Hesthaven. A level set discontinuous galerkin method for free surface flows. *Comput. Methods Appl. Mech. Engrg.*, 195:3406–3429, 2006.

[34] H. Guillard and C. Farhat. On the significance of the geometric conservation law for flow computations on moving meshes. *Comput. Methods Appl. Mech. Engrg.*, 190:1467–1482, 2000.

[35] I. Güler, M. Behr, and T. Tezduyar. Parallel finite element computation of free-surface flows. *Comput. Mech.*, 23:117–123, 1999.

[36] S. Güzey, B. Cockburn, and H. Stolarski. The embedded discontinuous Galerkin methods: Application to linear shells problems. *Internat. J. Numer. Methods Engrg.*, 70:757–790, 2007.

[37] T. L. Horvath and S. Rhebergen. A locally conservative and energy-stable finite element method for the Navier–Stokes problem on time-dependent domains. *Int. J. Numer. Meth. Fluids*, 89(12):519–532, 2019.

[38] T. L. Horvath and S. Rhebergen. An exactly mass conserving space-time embedded-hybridized discontinuous Galerkin method for the Navier-Stokes equations on moving domains. *J. Comput. Phys.*, 417, 2020.

[39] P. Houston, C. Schwab, and E. Süli. Discontinuous *hp*-finite element methods for advection-diffusion-reaction problems. *SIAM J. Numer. Anal.*, 39(6):2133–2163, 2002.

[40] T. J. R. Hughes and G. M. Hulbert. Space-time finite element methods for elasto-dynamics: Formulations and error estimates. *Comput. Methods Appl. Mech. Engrg.*, 66(3):339–363, 1988.

[41] P. Jamet. Galerkin-type approximations which are discontinuous in time for parabolic equations in a variable domain. *SIAM J. Numer. Anal.*, 15(5):912–928, 1978.

[42] V. John, A. Linke, C. Merdon, M. Neilan, and L. G. Rebholz. On the divergence constraint in mixed finite element methods for incompressible flows. *SIAM Rev.*, 59(3):492–544, 2017.

[43] R. S. Johnson. *A Modern Introduction to the Mathematical Theory of Water Waves*. Cambridge University Press, 1997.

[44] R. M. Kirby, S. J. Sherwin, and B. Cockburn. To CG or to HDG: A comparative study. *J. Sci. Comput.*, 51(1):183–212, 2012.

[45] K. L. A. Kirk, T. L. Horvath, A. Cesmelioglu, and S. Rhebergen. Analysis of a space-time hybridizable discontinuous Galerkin method for the advection-diffusion problem on time-dependent domains. *SIAM J. Numer. Anal.,*, 57(4):1677–1696, 2019.

[46] K. L. A. Kirk and S. Rhebergen. Analysis of a pressure-robust hybridized discontinuous Galerkin method for the stationary Navier–Stokes equations. *J. Sci. Comput.*, 81(2):881–897, 2019.

[47] C. M. Klaij, J. J. W. van der Vegt, and H. van der Ven. Space-time discontinuous Galerkin method for the compressible Navier–Stokes equations. *J. Comput. Phys.*, 217:589–611, 2006.

[48] R. J. Labeur and G. N. Wells. Interface stabilised finite element method for moving domains and free surface flows. *Comput. Methods Appl. Mech. Engrg.*, 198:615–630, 2009.

[49] L. D. Landau and E. M. Lifshitz. *Fluid Mechanics*, volume 6. Pergamon Press, 1987.

[50] C. Lehrenfeld and J. Schöberl. High order exactly divergence-free hybrid discontinuous Galerkin methods for unsteady incompressible flows. *Comput. Methods Appl. Mech. Engrg.*, 307:339–361, 2016.

[51] M. Lesoinne and C. Farhat. Geometric conservation laws for flow problems with moving boundaries and deformable meshes, and their impact on aeroelastic computations. *Comput. Methods Appl. Mech. Engrg.*, 134:71–90, 1996.

[52] Z. Li. The immersed interface method using a finite element formulation. *Appl. Numer. Math.*, 27(3):253–267, 1998.

[53] C. Lin, H. Lee, T. Lee, and L. J. Weber. A level set characteristic Galerkin finite element method for free surface flows. *Int. J. Numer. Meth. Fluids*, 49:521–547, 2005.

[54] E. Marchandise and J.-F. Remacle. A stabilized finite element method using a discontinuous level set approach for solving two phase incompressible flows. *J. Comput. Phys.*, 219:780–800, 2006.

[55] A. Masud and T. Hughes. A space-time Galerkin/least-squares finite element formulation of the Navier–Stokes equations for moving domain problems. *Comput. Methods Appl. Mech. Engrg.*, 146(1-2):91–126, 1997.

[56] A. Masuda and T. J. R. Hughes. A space-time Galerkin/least–squares finite element formulation of the Navier–Stokes equations for moving domain problems. *Comput. Methods Appl. Mech. Engrg.*, 146:91–126, 1997.

[57] D. N'dri, A. Garon, and A. Fortin. A new stable space–time formulation for two-dimensional and three-dimensional incompressible viscous flow. *Int. J. Numer. Meth. Fluids*, 37(8):865–884, 2001.

[58] D. N'dri, A. Garon, and A. Fortin. Incompressible Navier–Stokes computations with stable and stabilized space–time formulations: a comparative study. *Commun. Numer. Meth. En.*, 18(7):495–512, 2002.

[59] M. Neunteufel and J. Schöberl. Fluid-structure interaction with h(div)-conforming finite elements. *arXiv preprint arXiv:2005.06360*, 2020.

[60] N. C. Nguyen, J. Peraire, and B. Cockburn. An implicit high-order hybridizable discontinuous Galerkin method for linear convection-diffusion equations. *J. Comput. Phys.*, 228:3232–3254, 2009.

[61] N. C. Nguyen, J. Peraire, and B. Cockburn. High-order implicit hybridizable discontinuous Galerkin methods for acoustics and elastodynamics. *J. Comput. Phys.*, 230:3695–3718, 2011.

[62] S. Osher and J. A. Sethian. Fronts propagating with curvature-dependent speed: Algorithms based on Hamilton–Jacobi formulations. *J. Comput. Phys.*, 79:12–49, 1988.

[63] S. Rhebergen, O. Bokhove, and J. J. W. van der Vegt. Discontinuous Galerkin finite element method for shallow two-phase flows. *Comput. Methods Appl. Mech. Engrg.*, 198(5–8):819–830, 2009.

[64] S. Rhebergen and B. Cockburn. A space-time hybridizable discontinuous Galerkin method for incompressible flows on deforming domains. *J. Comput. Phys.*, 231:4185–4204, 2012.

[65] S. Rhebergen and B. Cockburn. Space-time hybridizable discontinuous Galerkin method for the advection-diffusion equation on moving and deforming meshes. In C.A. de Moura and C.S. Kubrusly, editors, *The Courant–Friedrichs–Lewy (CFL) condition, 80 years after its discovery*, pages 45–63. , Birkhäuser Science, 2013.

[66] S. Rhebergen, B. Cockburn, and J. J. W. van der Vegt. A space-time discontinuous Galerkin method for the incompressible Navier–Stokes equations. *J. Comput. Phys.*, 233:339–358, 2013.

[67] S. Rhebergen and G. N. Wells. A hybridizable discontinuous Galerkin method for the Navier-Stokes equations with pointwise divergence-free velocity field. *J. Sci. Comput.*, 76:1484–1501, 2018.

[68] B. Rivière. *Discontinuous Galerkin Methods for Solving Elliptic and Parabolic Equations*, volume 35 of *Frontiers in Applied Mathematics*. Society for Industrial and Applied Mathematics, Philadelphia, 2008.

[69] I. Robertson and S. Sherwin. Free-surface flow simulation using hp/spectral elements. *J. Comput. Phys.*, 155:26–53, 1999.

[70] C. Schwab. *p- and hp- Finite Element Methods: Theory and Applications to Solid and Fluid Mechanics*. Oxford University Press, 1999.

[71] W. E. H. Sollie, O. Bokhove, and J. J. W. van der Vegt. Space–time discontinuous Galerkin finite element method for two–fluid flows. *J. Comput. Phys.*, 230:789–817, 2011.

[72] G. Sosa Jones, J. J. Lee, and S. Rhebergen. A space-time hybridizable discontinuous Galerkin method for linear free-surface waves. 2019. Submitted.

[73] M. Stanglmeier, N. C. Nguyen, J. Peraire, and B. Cockburn. An explicit hybridizable discontinuous Galerkin method for the acoustic wave equation. *Comput. Methods Appl. Mech. Engrg.*, 300:748–769, 2016.

[74] J. J. Sudirham, J. J. W. van der Vegt, and R. J. van Damme. *Space-time discontinuous Galerkin method for advection-diffusion problems on time-dependent domains*. PhD thesis, University of Twente, 2005.

[75] J. J. Sudirham, J. J. W. van der Vegt, and R. J. van Damme. Space-time discontinuous Galerkin method for advection-diffusion problems on time-dependent domains. *Appl. Numer. Math.*, 56:1491–1518, 2006.

[76] M. Sussman, P. Smereka, and S. Osher. A level set approach for computing solutions to incompressible two-phase flow. *J. Comput. Phys.*, 114:146–159, 1994.

[77] M. Tavelli and M. Dumbser. A staggered space-time discontinuous Galerkin method for the incompressible Navier–Stokes equations on two-dimensional triangular meshes. *Comput. Fluids*, 119:235–249, 2015.

[78] M. Tavelli and M. Dumbser. A staggered space-time discontinuous Galerkin method for the three-dimensional incompressible Navier–Stokes equations on unstructured tetrahedral meshes. *J. Comput. Phys.*, 319:294–323, 2016.

[79] T. E. Tezduyar, M. Behr, S. Mittal, and J. Liou. A new strategy for finite element computations involving moving boundaries and interfaces—the deforming-spatial-domain/space-time procedure: II. Computation of free-surface flows, two-liquid flows, and flows with drifting cylinders. *Comput. Methods Appl. Mech. Engrg.*, 94(3):353–371, 1992.

[80] S.K. Tomar and J. J. W. van der Vegt. A Runge–Kutta discontinuous Galerkin method for linear free–surface gravity waves using high order velocity recovery. *Comput. Methods Appl. Mech. Engrg.*, 196:1984–1996, 2007.

[81] J. J. W. van der Vegt and J. J. Sudirham. A space-time discontinuous Galerkin method for the time-dependent Oseen equations. *Appl. Numer. Math.*, 58:1892–1917, 2008.

[82] J. J. W. van der Vegt and S. K. Tomar. Discontinuous Galerkin method for linear free-surface gravity waves. *J. Sci. Comput.*, 22:531–567, 2005.

[83] J. J. W. van der Vegt and H. van der Ven. Space-time discontinuous Galerkin finite element method with dynamic grid motion for inviscid compressible flows. i. General formulation. *J. Comput. Phys.*, 182:546–585, 2002.

[84] J. J. W. van der Vegt and Y. Xu. Space-time discontinuous Galerkin method for nonlinear water waves. *J. Comput. Phys.*, 224:17–39, 2007.

[85] E. Walhorn, A. Kölke, B. Hübner, and D. Dinkler. Fluid–structure coupling within a monolithic model involving free surface flows. *Comput. Struct.*, 83(25-26):2100–2111, 2005.

[86] D. Wang, R. Tezaur, and C. Farhat. A hybrid discontinuous in space and time Galerkin method for wave propagation problems. *Int. J. Numer. Meth. Fluids*, 99:263–289, 2014.

[87] G. N. Wells. Analysis of an interface stabilized finite element method: the advection-diffusion-reaction equation. *SIAM J. Numer. Anal.*, 49(1):87–109, 2011.

[88] J. H. Westhuis. *The numerical simulation of nonlinear waves in a hydrodynamic model test basin*. PhD thesis, University of Twente, 2001.

[89] G. X. Wu and R. Eatock Taylor and D. M. Greaves. The effect of viscosity on the transient free-surface waves in a two-dimensional tank. *J. Eng. Math.*, 40:77–90, 2001.

[90] S. Yakovlev, D. Moxey, R. M. Kirby, and S. J. Sherwin. To CG or to HDG: A comparative study in 3D. *J. Sci. Comput.*, 67(1):192–220, 2016.

[91] O. Zanotti, F. Fambri, M. Dumbser, and A. Hidalgo. Space–time adaptive ADER discontinuous Galerkin finite element schemes with a posteriori sub-cell finite volume limiting. *Computers & Fluids*, 118:204–224, 2015.

[92] L. Zhang, A. Gerstenberger, X. Wang, and W. K. Liu. Immersed finite element method. *Comput. Methods Appl. Mech. Engrg.*, 193(21–22):2051–2067, 2004.